2007

Development of a high performance parallel computing platform and its use in the study of nanostructures : clusters, sheets and tubes .

S. Gowtham
Michigan Technological University

DEVELOPMENT OF A HIGH PERFORMANCE PARALLEL COMPUTING PLATFORM AND ITS USE IN THE STUDY OF NANOSTRUCTURES: CLUSTERS, SHEETS AND TUBES

By

S GOWTHAM

A DISSERTATION

Submitted in partial fulfillment of the requirements

for the degree of

DOCTOR OF PHILOSOPHY

(Engineering Physics)

MICHIGAN TECHNOLOGICAL UNIVERSITY

2007

This dissertation, "Development of A High Performance Parallel Computing Platform and Its Use in the Study of Nanostructures: Clusters, Sheets and Tubes", is hereby approved in partial fulfillment of the requirements for the degree of DOCTOR OF PHILOSOPHY in the field of Engineering Physics.

DEPARTMENT:
Physics

Signatures:

Dissertation Advisor _____
Dr. Ravindra Pandey

Committee _____
Dr. Donald R Beck

_____
Dr. Maximilian J Seel

_____
Dr. Gregory M Odegard

Department Chair _____
Dr. Ravindra Pandey

Date _____

Dedication

To My Mother, Teachers and Friends...

ಸಂದೇಹವೀ ಕೃತಿಯೊಳಿನ್ನಿಲ್ಲವೆಂದಲ್ಲ ।
ಇಂದು ನಂಬಿಹುದೆ ಮುಂದೆಂದುಮೆಂದಲ್ಲ ॥
ಕುಂದು ತೋರ್ದಂದದನು ತಿದ್ದಿಕೊಳೆ ಮನಸುಂಟು ।
ಇಂದಿಗೀ ಮತವುಚಿತ – ಮಂಕುತಿಮ್ಮ ॥

Not that there are no doubts in this work
Not that what holds today will hold forever
When pointed out, am willing to accept the mistake
But for now, this feels right – Dim Tim

Mankutimmana Kagga, # 939

Contents

List of Figures

List of Tables

Acknowledgments

The work entailed in this dissertation as well as the experience (academic and co-curricular alike) would have never been possible without help and support from many. I would neither be what I am or where I am except for my mother sacrificing promotions in her professional career (to make sure that I was well fed and that I studied well) and some relatives who kindled the scientific spirit at a very young age by answering my questions.

Sincere thanks to Dr. Ravindra Pandey - my academic advisor - for his understanding of my interests as well as guidance, patience, opportunities, freedom, support and for fulfilling all my wishes without ever asking for them. Members of my advisory committee - Dr. Donald Beck, Dr. Maximilian Seel and Dr. Gregory Odegard (ME-EM), and Dr. Richard Brown (Chemistry), Dr. Jong Lee (MSE) have offered their support and valuable suggestions through out these projects and I am very much grateful to them. Funding from the Dow Corning Foundation, DARPA and Neil V Hakala Endowment Fellowship is acknowledged.

The initial learning curve in research methods would have been lot steeper but for Dr. Aurora Costales and Dr. Miguel Blanco (Universidad de Oviedo, Spain) - my god parents in computational research. Likewise, my thanks to members / graduates of Dr. Pandey's research group (Haiying He, Dr. Huitian Jiang, Dr. Anil Kandalam, Kah Chun Lau, Dr. Ralph Scheicher) as well as collaborators / visiting scholars - Dr. Harish Bahadur (NPL, India), Dr. Dilip Kanhere (University of Pune, India), Dr. Shashi Karna (Army Research Labs/DARPA), Dr. Roberto Orlando (University of Torino, Italy) and Dr. John Vail (University of Manitoba, Canada).

For much of the computational/computer skills I acquired, I must thank Srikanth

Chintala (ME-EM, for teaching HTML); Michael Larsen (Physics, for teaching LaTeX amongst many other things); James Hoel, David Kraus, Patrick Krogel, Christopher Linn (Center for Experimental Computation - for patiently answering all my computer related questions); Jim Oliver and Karen Springsteen (Center for Computer Aided Learning and Instruction); Matthew Buss, Scott Carrol, Kathrine Strojny, Jon W (Distributed Computing Services); Jacob Fugal and Bijunath Patla (Physics, for suggesting corrections and improving my LaTeX templates); Mary Peed (West Engineering Computing Network) and members of Linux/UNIX Users' Group.

Fellow graduate students and faculty/staff members of Physics, Chemical Engineering, Chemistry, Computer Science, DCS/ITS/ETS, ECE, Humanities, Mathematics, ME-EM departments, Graduate School (Dr. Debra Charlesworth and Nancy Byers Sprague), J R V P Library (and their families) have taught me important things along the way. My thanks to each one of them as well as to Pamm Besmer, Pamm Givens, Andrea Lappi, Elizabeth Pollins, Marg Rohrer, Kathy Wollan (Physics); Diane Koskela (Information Technology Services); Dorothy Clairmont, Diane Gilbert, Daniel Rouleau (Facilities); Mary Larson, Ruth Ojala, Darlene Persha, James Schultz, Ginger Sleeman, Robert Wenc (Daniell Heights) for all their help over the years.

My teachers - from grade school through graduate school, at the Bangalore Association for Science Education (BASE) and πoneer Academy - have consistently been a significant part of my motivation to pursue the art and history of science. Although naming all of them individually would be an improbable task, my thanks to each one of them for going out of their way to help me learn, understand and appreciate the process.

Playing in the Michigan Tech GSC/IM softball league (Fiziks, ITS, Humanestry, Grads N' Staff), Church league (Good Shepard Lutheran Church) as well as watching many a sports events live (thanks to the Athletic Dept. & coaching staff - John Barnes,

Kim Cameron, Wes Frahm, Luke Kiss, Kevin Luke, Suzanne Sanregret; athletes, their families) and sports related documentaries (*Beyond The Glory* series by Fox Sports Net) helped a great deal in learning and appreciating the aspects of team effort. While members/supporters of these teams as well as several from opposing teams showed classic sportsmanship traits and provided more than enough motivation during down times off the field, the experience gained from almost every game served as a microcosm of life in general. Thanks to Evan Dixon, for answering my barrage of questions and helping me understand the technicalities and appreciate professional sports even better.

My advisor's advise to do something other than research one day a week coupled with photography related discussions and expeditions with many a friends - David Archembeau, Steve Bailey, Josie Balmes, Scott Blake, Michelle Borkowski, Tim Carmean, Bharat Choudhary, Lynn Czarnecki, Adam Johnson, Luke Johnson, Santosh Karre, Matthew King, Karen Koethe, Amy Krause, Adam Manty, Ravish Mehta, Tim Obermann, David Otokpa, Nagesh Saligrama, Katie Schalk, Kyle Schneider, Michael Schupe, William Slough, Kalyan Varma, Jill Witt, Kevin Zeits and Changgong Zhou - have helped to keep the sanity and improve the performance of work week.

I would not have come to Michigan Tech but for Dr. Sharath Ananthamurthy, Dr. B N Meera, Dr. M K Raghavendra, Dr. C R Ramaswamy, Dr. A R Usha Devi, Dr. A S Vytheeshwaran (Bangalore University); K M Raghavendran, Dr. M Sathyakrishna, Dr. J Vishwanath (MES College); Dr. K N Sreenivasa Rao (Mysore University); H R Madhusudana, Dr. B S Shylaja, Dr. C V Vishweshwara (Bangalore Association for Science Education); S Vishwanath (& family, Gandhinagar Higher Secondary School); N S Manorama (Malleshwaram Ladies' Association); Dr. Pushpalatha Murthy (MTU Chemistry), Owen (& Susan) Mills (MTU MSE). Neither would my stay here have been complete without constant support/encouragement from David Bezotte, Cindy Blake, Phyllis Boutilier, Mark Hoffmann, Marcus Johnson, Phillip Kelm, Mark Oliver,

Kristin Peterson, Daniel Sayen, Art Weaver, Victoria & George Williams and rest of this wonderful local community.

And last, but certainly not the least, support and encouragement from many a friends from across the Atlantic ocean - Balaji, Chandrashekhar, Deepti, Giridhar, Govind, Lakshmi, Padmalekha, Pramod, Prashanth, Raghavendra, Rashmi, Rithesh, Santosh, Shivakumar, Soumya, Srilatha, Srimatha, Srivathsa, Sumana, Surya and more - their (and their parents') belief in me has gone a long way in sustaining my varied interests. Like a timeless composition by a timeless composer goes....

endaro mahaanubhaavulu andariki mana vandanamulu

There are very many great souls and my thanks to every one of them

Abstract

Small clusters of gallium oxide, technologically important high temperature ceramic, together with interaction of nucleic acid bases with graphene and small-diameter carbon nanotube are focus of *first principles* calculations in this work. A high performance parallel computing platform is also developed to perform these calculations at Michigan Tech. *First principles* calculations are based on density functional theory employing either local density or gradient-corrected approximation together with plane wave and Gaussian basis sets.

The bulk Ga_2O_3 is known to be a very good candidate for fabricating electronic devices that operate at high temperatures. To explore the properties of Ga_2O_3 at nanoscale, we have performed a systematic theoretical study on the small polyatomic gallium oxide clusters. The calculated results find that all lowest energy isomers of Ga_mO_n clusters are dominated by the Ga–O bonds over the metal-metal or the oxygen-oxygen bonds. Analysis of atomic charges suggest the clusters to be highly ionic similar to the case of bulk Ga_2O_3. In the study of sequential oxidation of these clusters starting from Ga_3O, it is found that the most stable isomers display up to four different backbones of constituent atoms. Furthermore, the predicted configuration of the ground state of Ga_2O is recently confirmed by the experimental results of Neumark's group.

Guided by the results of calculations the study of gallium oxide clusters, performance related challenge of computational simulations, *of producing high performance computers/platforms*, has been addressed. Several engineering aspects were thoroughly studied during the design, development and implementation of the high performance parallel computing platform, *rāma*, at Michigan Tech. In an attempt to stay true to the principles of Beowulf revolution, the *rāma* cluster was extensively customized to

make it easy to understand, and use - for administrators as well as end-users. Following the results of benchmark calculations and to keep up with the complexity of systems under study, *rāma* has been expanded to a total of sixty four processors.

Interest in the non-covalent interaction of DNA with carbon nanotubes has steadily increased during past several years. This hybrid system, at the junction of the biological regime and the nanomaterials world, possesses features which makes it very attractive for a wide range of applications. Using the in-house computational power available, we have studied details of the interaction between nucleic acid bases with graphene sheet as well as high-curvature small-diameter carbon nanotube. The calculated results find that the nucleic acid bases exhibited significantly different interaction strengths when physisorbed on graphene or carbon nanotube. The calculated trend in the binding energies strongly suggests that the polarizability of the base molecules determines the interaction strength of the nucleic acid bases with graphene. When comparing the results obtained here for physisorption on the small diameter nanotube considered with those from the study on graphene, it is observed that the interaction strength of nucleic acid bases is smaller for the tube. Thus, these results show that the effect of introducing curvature is to reduce the binding energy. The binding energies for the two extreme cases of negligible curvature (i.e. flat graphene sheet) and of very high curvature (i.e. small diameter nanotube) may be considered as upper and lower bounds. This finding represents an important step towards a better understanding of experimentally observed sequence-dependent interaction of DNA with carbon nanotubes.

Chapter 1

Introduction

Notations

AFM	Atomic Force Microscope
CNT	Carbon NanoTube
IC	Integrated Circuit
STM	Scanning Tunneling Microscope

The story of nanotechnology began in the 1950s and 1960s, when most scientists and engineers were thinking big, not small. This was the era of big automobiles, big aircraft and big plans for sending human beings into outer space. Landmark skyscrapers were built in the major cities around the world. The world's largest cruise ships, oil tankers, bridges, highways and power plants are all products of this era. Around the same time, the electronics industry began its ongoing affair with making things smaller. The invention of the transistor in 1947 and the first Integrated Circuit (IC) in 1959 launched an era of electronics miniaturization. Somewhat ironically, it was these small devices that made large devices possible. For the next few decades, as computing applications and demands grew, transistors and ICs shrank, so that by the 1980s engineers already predicted a limit to this miniaturization and began looking for an entirely new approach.

As electronics engineers focused on making things smaller, engineers and scientists from an array of other fields turned their focus to small things - atoms and molecules. After successfully splitting the atom in the years before World War II, physicists struggled to understand more about the particles from which atoms were made, and the forces that kept them together. At the same time, chemists worked to combine atoms into new kinds of molecules. Meanwhile biologists discovered that genetic information is stored in our cells on long, complex molecules called DNA. This and other work led to a greater understanding of molecules, which, by the 1980s, suggested entirely new lines of engineering research.

So, the roots of nanotechnology lie in the merging of three lines of thinking - atomic physics, chemistry, and electronics. Only in the 1980s did this new field of study get a name - *nanotechnology*. E. Drexler, who popularized this term, pointed out that nanotechnology had been predicted much earlier [1, 2]. It was R. P. Feynamn who proposed the idea of building machines and mechanical devices out of individual atoms during his 1959 lecture to the American Physical Society called *There's Plenty of Room at the Bottom*. The resulting machines would actually be artificial molecules, built atom by atom. While the resulting molecule might itself be larger than a nanometer, it was the idea of manipulating things at the atomic level that was the essence of nanotechnology. Not only was this kind of manipulation impossible at the time, but few people had any idea why it would be useful to pursue it! With all the new research, however, Drexler revived Feynman's vision and helped introduce the general public to the basic concepts of nanotechnology.

As such, nanotechnology allows scientists and engineers to manipulate individual atoms and molecules, making it possible to build tiny machines - with dimensions of the order of a few nanometers.

While engineers thought about practical uses for fullerenes another discovery in search of an application was being made. In 1981 G. K. Binnig and H. Rohrer invented the Scanning Tunneling Microscope (STM), which has a tiny tip so sensitive that it can in effect "feel" the surface of a single atom. It then sends information about the surface

to a computer that reconstructs an image of the atomic surface on a display screen. Researchers discovered a little later that the tip of the STM could actually move atoms around. Researchers believed they had a tool, the Atomic Force Microscope (AFM), that could build things atom-by-atom.

The development of tools such as AFM coincided with the introduction of powerful computers and software thus opening up a new yet complimentary (to Theory and Experiment) approach. Computational Science is *Doing Science* by means of computational methods. The essential point in computational science is not the use of machines, but the systematic application of numerical techniques in place of, and sometimes in addition to, analytical methods, in order to render mathematical description as large a part of physical reality as possible. A number of fundamental techniques of this approach were introduced by Newton, Gauss, Jacobi, etc. who lived quite a while before the invention of calculating machines.

What makes computational methods so important in science? One primary reason is that most of analytical tools are well suited to analyze linear problems. However, not many natural phenomena are linear and as such, are extremely sensitive to small changes in variables. The challenges invloved in computational simulations are threefold:

† Performance: Producing high-performance computers.

† Programming: Programming for high-performance computers.

† Prediction: Development of truly predictive application codes.

As naive a question as *How can I formulate the problem on a computer?* has led to new formulations of scientific laws as rules for a computer. Theory underlying the computational methods used in this work are presented in Chapter 2.

Nanostructured materials can contain a few to few thousands of atoms, and may extend to the larger microscopic size prior to approaching the bulk matter [3, 4]. These atomic aggregates or clusters, in which the surface plays a paramount role, respond to external stimuli such as light, mechanical stress, and electromagnetic fields quite differently from the bulk matter. In many instances, at sufficiently small sizes (usually in nanoscopic regime), dependence of the material property on the system size becomes non-scalable. Thus, the exhibited behavior is characteristic of the assembly of particles rather than being a property of the individual constituents. Hence, identification and understanding of these series of microscopic origins and phenomena associated with nanostructures, are of fundamental importance [5].

As a particular example, motivated by the dearth of theoretical and experimental studies on gallium oxide at cluster level, a systematic study of properties was initiated. Small clusters were the focus of an initial study as they were expected to provide useful prototypes to understand the physics and chemistry of surfaces and nanostructures.

The smaller size of the clusters makes it possible to obtain a detailed geometric, electronic, and bonding information, that can also be used to benchmark theoretical methods to be used in the larger structural elements. Chapter 3 provides a very detailed description of computational methods used as well as the analysis of results obtained from these calculations. Apart from the scientific values, this project hinted at an hitherto unexpected result: *need for better computational facility to carry out studies on larger/complex systems.*

Upon development of a high performance parallel computing platform from ground zero, which by itself was a project, the facility was used to study, amongst other projects, the interaction between carbon nanotubes and biological molecules. As a hybrid at the junction of the biological regime and the nanomaterials world, this system possesses features which makes it very attractive for a wide range of applications. Chapter 5 describes in detail the computational methods used along with the analysis of results obtained from these calculations.

Chapter 2

Theoretical Details

Notations

AO	Atomic Orbital
BSSE	Basis Set Superposition Error
GGA	Generalized Density Approximation
GTO	Gaussian Type Orbital
LCAO	Linear Combination of Atomic Orbitals
LDA	Local Density Approximation
MD	Molecular Dynamics
MO	Molecular Orbital
SCF	Self-Consistent Field
STO	Slater Type Orbital
VASP	Vienna Ab-initio Simulation Program

2.1 Introduction

The word *quantum* (meaning "how much" in Latin) in quantum mechanics refers to a discrete unit assigned to certain physical quantities. The discovery that waves have discrete energy packets (called *quanta*) that behave in a manner similar to particles led to the branch of physics that deals with atomic and sub-atomic systems, which has come to be known as quantum mechanics. It is the underlying mathematical framework of many fields of physics and chemistry, including condensed matter physics, solid state physics, atomic physics, molecular physics, computational chemistry, particle physics and nuclear physics.

The effects of quantum mechanics are not observable on macroscopic scales, but become evident at the atomic and subatomic level. Quantum theory generalizes all classical theories, including mechanics and electromagnetism, except general relativity, and provides accurate descriptions for many previously unexplained phenomena in physics.

The starting point for most quantum mechanical calculations is the non-relativistic Schrödinger equation [6]

$$\hat{H}\,\Phi \;=\; E\,\Phi \tag{2.1}$$

where, $\hat{H}$ is Hamiltonian operator and properties of the system under study can be

obtained by appropriately tapping the wave function, Φ. For a system with A nuclei and N electrons, the hamiltonian in the above expression takes the form:

$$\hat{H} = -\sum_{i} \frac{\hbar^2}{2m} \nabla_{\mathrm{i}}^2 + \frac{1}{2} \sum_{i \neq j} \frac{e^2}{|\mathbf{r}_{\mathrm{i}} - \mathbf{r}_{\mathrm{j}}|} - \sum_{i,\,\alpha} \frac{Z_\alpha\, e}{|\mathbf{r}_{\mathrm{i}} - \mathbf{R}_\alpha|} - \sum_{\alpha} \frac{\hbar^2}{2M_\alpha} \nabla_\alpha^2 + \frac{1}{2} \sum_{\alpha \neq \beta} \frac{Z_\alpha\, Z_\beta\, e^2}{|\mathbf{R}_\alpha - \mathbf{R}_\beta|}$$

Here, $\hbar$ is the reduced Planck's constant; m is the electronic mass; e is the electronic charge; $\mathbf{r}_i$ are the electronic positions; M_α is the nuclear mass; Z_α is the nuclear charge; and $\mathbf{R}_\alpha$ are the nuclear positions.

The first two terms correspond to kinetic energy of the electrons and inter-electron Coulombic interaction respectively; the third term represents electron-nuclei Coulombic interaction and can be regarded as an external potential, V_{ext}; the last two terms correspond to the kinetic energy of nuclei and inter-nuclear Coulombic interaction. For simple systems, such as atoms and small molecules, Schrödinger equation can be solved in a numerical manner. However, the electronic structure studies of larger systems are computationally quite expensive, and hence demand simplified schema.

This problem is simplified by adopting the *Born-Oppenheimer Approximation* [7]. Since the nuclei are much heavier than electrons and move very slowly compared to the electrons, the electrons can rapidly adjust their distributions with the nuclear

positions. As such, one can reasonably assume that the electron distribution depends only on the instantaneous positions of the nuclei and thus, the nuclear motion in a molecule can be decoupled from the motion of electrons. With this being the case, it can be shown that the total energy of the system is the sum of electronic and nuclear energies, and that the total wave function of a molecule is the product of electronic and nuclear wave functions:

$$\Phi\left(\mathbf{r},\mathbf{R}\right) \;=\; \Phi_{\mathrm{e}}\left(\mathbf{r},\mathbf{R}\right)\,\Psi\left(\mathbf{R}\right) \tag{2.2}$$

where, function $\Phi_{\mathrm{e}}\left(\mathbf{r},\mathbf{R}\right)$ is the electronic wave function, and function $\Psi\left(\mathbf{R}\right)$ is the nuclear wave function. Hamiltonian describing the electronic problem, in the field of fixed nuclei, can be written as

$$\hat{H}_{\mathrm{e}} \;=\; -\sum_{i}\frac{\hbar^2}{2m}\,\nabla_{\mathrm{i}}^2 \;+\; \frac{1}{2}\sum_{i\neq j}\frac{e^2}{|\mathbf{r}_{\mathrm{i}} \;-\; \mathbf{r}_{\mathrm{j}}|} \;-\; \sum_{i,\,\alpha}\frac{Z_\alpha\, e}{|\mathbf{r}_{\mathrm{i}} \;-\; \mathbf{R}_\alpha|} \tag{2.3}$$

$$\hat{H}_{\mathrm{e}}\,\Phi_{\mathrm{e}}\left(\mathbf{r},\mathbf{R}\right) \;=\; E_{\mathrm{e}}\,\Phi_{\mathrm{e}}\left(\mathbf{r},\mathbf{R}\right) \tag{2.4}$$

Although simplified, the electronic Hamiltonian still depends on the coordinates of every electron and presents itself as still a quite complicated problem.

2.2 The Hartree Approximation

In early 1920s, Bohr [8] suggested that an electron in a penetrating orbit moves all the way from the outer to the inner part of an atom and that the field through which it moves can be represented by a static distribution of other electrons. Following Bohr's suggestion, Hartree [9] developed an intuitive method of including electron repulsions in the Schrödinger equation Eqn. (2.1). Also known as the *independent particle approximation*, the total wave function in this approach is represented as a product of single particle wave functions.

$$\Phi\left(\mathbf{r}_1, \mathbf{r}_2, ..., \mathbf{r}_{\mathrm{N}}\right) \;=\; \prod_i \phi_{\mathrm{i}}\left(\mathbf{r}_{\mathrm{i}}\right) \tag{2.5}$$

This approximation results in a set of non-linear equations

$$\left[-\frac{\hbar^2}{2m}\,\nabla_{\mathrm{i}}^2 \;+\; V_{\mathbf{ext}} \;+\; V_{\mathbf{sp}}\left(\mathbf{r}_{\mathrm{i}}\right)\right]\,\phi_{\mathrm{i}}\left(\mathbf{r}_{\mathrm{i}}\right) \;=\; \epsilon_{\mathrm{i}}\,\phi_{\mathrm{i}}\left(\mathbf{r}_{\mathrm{i}}\right) \tag{2.6}$$

[$V_{\mathrm{sp}}\left(\mathbf{r}_{\mathrm{i}}\right)$ being the average single particle potential] that need to be solved in a SCF manner. However, the wave function so obtained is not antisymmetric with respect to the interchange of electron coordinates and thus does not satisfy the Pauli's *Exclusion Principle* [10].

2.3 The Hartree-Fock Approximation

By incorporating the Pauli's *Exclusion Principle*, Fock [11] represented the wave function Φ - describing the ground state of an N electron system - with a single Slater determinant of orthonormal one-electron orbitals or single particle wave functions $\phi_{\mathrm{i}}(\mathbf{r})$:

$$\Phi = \frac{1}{\sqrt{N}} \begin{vmatrix} \phi_1(\mathbf{r}_1) & \phi_2(\mathbf{r}_1) & \cdots & \phi_{\mathrm{N}}(\mathbf{r}_1) \\ \phi_1(\mathbf{r}_2) & \phi_2(\mathbf{r}_2) & \cdots & \phi_{\mathrm{N}}(\mathbf{r}_2) \\ \vdots & \vdots & & \vdots \\ \phi_1(\mathbf{r}_{\mathrm{N}}) & \phi_2(\mathbf{r}_{\mathrm{N}}) & \cdots & \phi_{\mathrm{N}}(\mathbf{r}_{\mathrm{N}}) \end{vmatrix} \tag{2.7}$$

The Hartree-Fock equation, to be solved in a SCF way, is given by

$$\left[-\frac{\hbar^2}{2m} \nabla_{\mathrm{i}}^2 + V_{\mathrm{ext}} + V_{\mathrm{sp}}(\mathbf{r}_{\mathrm{i}}) \right] \phi_{\mathrm{i}}(\mathbf{r}_{\mathrm{i}}) - \sum_j \int \frac{e^2}{|\mathbf{r} - \mathbf{r}'|} \phi_{\mathrm{j}}^*(\mathbf{r}') \phi_{\mathrm{i}}(\mathbf{r}') \phi_{\mathrm{j}}(\mathbf{r}) \delta_{\mathrm{s_i}} \delta_{\mathrm{s_j}} d\mathbf{r}' = \epsilon_{\mathrm{i}} \phi_{\mathrm{i}}(\mathbf{r}_{\mathrm{i}})$$

This approach introduces *exchange energy*, an additional non-local term (last term on LHS of the above expression) and it only operates between electrons with the same spin. However, the Hartree-Fock approximation does not take into account the correlation interaction between the electrons and as such, the correlation energy can be thought of as the difference between the *exact* energy and the Hartree-Fock energy.

2.4 Density Functional Theory

Density Functional Theory (DFT) is based on the two fundamental theorems introduced by Hohenberg and Kohn [12], and extended later by Kohn and Sham [13].

Theorem 1: The ground state energy, $E_\circ$, of a many electron system is a unique functional of the ground state electron density, $\eta(\mathbf{r})$.

Theorem 2: For any trial density $\tilde{\eta}\,(\mathbf{r})) \;\geq\; 0$, the ground state energy, $E_\circ$ is less than or equal to E $[\tilde{\eta}\,(\mathbf{r})]$. Symbolically put,

$$E_\circ \leq E\,[\tilde{\eta}(\mathbf{r})] \quad \text{for} \quad \tilde{\eta}\,(\mathbf{r}) \;\geq\; 0 \quad \text{and} \int \tilde{\eta}\,(\mathbf{r})\,d\mathbf{r} \;=\; N \tag{2.8}$$

While Hohenberg-Kohn theorems only provide the proof of existence of the functionals, Kohn and Sham provided a way of constructing them. Underlying method is to map the original problem of interacting electrons to a non-interacting electrons moving in an effective potential. This can be achieved by splitting up the total energy functional as

$$E\,[\eta(\mathbf{r})] \;=\; T\,[\eta(\mathbf{r})] \;+\; \frac{1}{2}\int\int \frac{\eta(\mathbf{r})\;\eta(\mathbf{r}')}{|\mathbf{r} \;-\; \mathbf{r}'|}\,d\mathbf{r}\,d\mathbf{r}' \;+\; \int V_{\text{ext}}\,(\mathbf{r})\;\eta(\mathbf{r})\,d\mathbf{r} \;+\; E_{\text{xc}}\,[\eta(\mathbf{r})]$$

Here, the first term is the kinetic energy functional of a non-interacting electron gas, the second term is the electrostatic energy (or the Hartree energy), the third term is the external energy due to the nuclei, and the last term is the *Exchange-Correlation energy* (which contains all the remaining contribution to the energy). By varying the above expression with respect to the density, one can get a set of single electron Schrödinger-like equations - known as the *Kohn-Sham Equations*.

$$\left[-\frac{1}{2}\nabla^2 + V_{\text{eff}}(\mathbf{r})\right]\phi_{\text{n}}(\mathbf{r}) = \epsilon_{\text{n}}\phi_{\text{n}}(\mathbf{r}) \tag{2.9}$$

where $\phi_{\text{n}}(\mathbf{r})$ are the Kohn-Sham orbitals, ϵ_{n} are the Kohn-Sham eigen values and the effective potential, V_{eff} is given by

$$V_{\text{eff}}(\mathbf{r}) = V_{\text{ext}}(\mathbf{r}) + \frac{1}{2}\int \frac{\eta(\mathbf{r}')}{|\mathbf{r} - \mathbf{r}'|}\, d\mathbf{r}' + V_{\text{xc}}(\mathbf{r}) \tag{2.10}$$

and the exchange-correlation potential, V_{xc}, is given by

$$V_{\text{xc}}(\mathbf{r}) = \frac{\delta E_{\text{xc}}[\eta]}{\delta \eta(\mathbf{r})} \tag{2.11}$$

Once the $\phi_{\mathrm{n}}(\mathbf{r})$ are known, the electron density can be constructed using

$$\eta(\mathbf{r}) = \sum_{i}^{N} |\phi_{\mathrm{n}}(\mathbf{r})|^2 \tag{2.12}$$

For numerical calculations, one starts from initial charge density (such as the atomic charge density), then calculates the effective potential and in turn solves the Kohn-Sham equations [Eqns. (2.10) - (2.12)] in a self-consistent manner.

The exchange-correlation energy, E_{xc}, plays a significant role in DFT as it is used to describe all the many-body effects. However, neither exchange nor correlation interactions can be described exactly within the DFT and as such, one has to rely on approximations for E_{xc}.

2.4.1 Local Density Approximation

A simple, yet surprisingly efficient approach to model the exchange-correlation potential is to treat it as the potential of a homogeneous but interacting electron gas. Known as the *Local Density Approximation* (LDA), it is one of the most commonly employed approximation and works best if the density of the system under study

varies only slowly. Mathematically, it can be defined as

$$E_{\rm xc}^{\rm LDA} \;=\; \int d\mathbf{r}\, \eta(\mathbf{r})\, \epsilon_{\rm xc}^{\rm LDA}\, [\eta(\mathbf{r})] \tag{2.13}$$

where $\epsilon_{\rm xc}^{\rm LDA}$ is the exchange-correlation energy per particle of a homogeneous electron gas. Although the general form of $\epsilon_{\rm xc}$ is unknown, the low and high density limits can be calculated analytically and, one uses a suitable interpolation scheme for intermediate values. For simple molecules, LDA gives good results for bond lengths, electron densities, vibrational frequencies, ionization potentials, etc. For open shell systems, LDA tends to over-estimate the ground state energy and bond dissociation energy when compared with experimental values and with Hartree-Fock approximation. As the LDA is similar to that of the Thomas-Fermi model, it works well in the regions with oscillatory electron waves (core), but fails to represent the exchange-correlation effect in asymptotic regions. The self-interaction effects also play a role. This leads to inaccurate results for anions, chemical bonding, and calculations of surface energies. The fact that the molecules are far from resembling the homogeneous electron gas also adds to the failure of LDA in certain systems.

2.4.2 Generalized Gradient Approximation

An improvement over the LDA, the *Generalized Gradient Approximation* (GGA), describes the exchange-correlation energy in terms of the densities as well as its local gradients.

$$E_{\rm xc}^{\rm GGA} \;=\; \int d\mathbf{r}\; \eta(\mathbf{r})\; \epsilon_{\rm xc}^{\rm GGA}\; [\eta(\mathbf{r}),\; \nabla\eta(\mathbf{r})] \tag{2.14}$$

$\epsilon_{\rm xc}^{\rm GGA}$ is not uniquely defined and its construction makes use of sum rules, general scaling properties, asymptotic behavior of effective potentials and so on. Strength of GGA lies in the significant improvement it gives over LDA in estimation of bond dissociation energies, etc. However, one should note that using GGA - which makes use of more information about electron density compared to LDA - does not always increase the accuracy of results.

2.5 Basis Sets

In the Kohn-Sham equations [Eqns. (2.10) - (2.12)], the orbitals ϕ_i are represented as linear combinations of a finite set of pre-defined N one-electron functions, known as basis functions, ξ_μ.

$$\phi_{\mathrm{i}} \;=\; \sum_{\mu=1}^{N} C_{\mu \mathrm{i}}\, \xi_\mu \tag{2.15}$$

where $\mathrm{C}_{\mu \mathrm{i}}$ are the molecular orbital expansion coefficients. Under the LCAO approximation, atomic orbitals of constituent atoms are used as basis functions. However, any set of appropriately defined functions may be used for the basis set expansion. These basis functions can be either analytic in nature or numerical functions. There are two types of analytic basis functions commonly used in the electronic structure calculations. They are Slater Type Orbitals (STO) [14] and Gaussian Type Orbitals (GTO) [15]. STOs are given as:

$$\xi(r, \theta_1, \theta_2) \;=\; N\, r^{\mathrm{n}-1}\, \exp\left[-\zeta\, r\right]\, Y_{\mathrm{l,m}}\left(\theta_1, \theta_2\right) \tag{2.16}$$

where $Y_{\mathrm{l,m}}$ are the conventional spherical harmonics. The exponential dependence on the distance between the nucleus and the electron is given accurately in these functions. When the radial wave function passes through zero, such regions are described as radial nodes, or spherical radial nodes since this describes their shape.

However, due to the nature of exponential radial part, they do not have any radial nodes. The radial nodes are included by using a linear combination of STOs. The advantages of using STOs is that they represent well the electron wave functions for smaller values of r. However, evaluating the three- and four- centered integrals in the SCF calculations with STOs is extremely expensive. As such, STOs are only used in the calculations of atomic and linear systems.

The immediate solution to the above mentioned problems with STOs is using GTOs, instead of STOs as basis functions. GTOs can be written, in terms of polar coordinates, as :

$$\xi(r, \theta_1, \theta_2) \;=\; N\, Y_{\mathrm{l,m}}(\theta_1, \theta_2)\, r^{2\mathrm{n}-2-\mathrm{l}}\, \exp\left[-\zeta\, r^2\right] \tag{2.17}$$

$$\xi(x, y, z) \;=\; N\, x^{\mathrm{lx}}\, y^{\mathrm{ly}}\, z^{\mathrm{lz}}\, \exp\left[-\zeta\, r^2\right] \tag{2.18}$$

where the sum of l_{x}, l_{y} and l_{z} determines the angular part of the orbital, ζ represents the radial extent of the function.

With the introduction of GTOs, the evaluation of the three- and four- center integrals of the two-electron integrals, are reduced to two-center integrals. This is due to the fact that the product of two GTOs, each on two different centers can be written as a GTO centered between the two centers. Though the use of GTOs reduces the

computational cost, they have certain drawbacks. The e^{-r^2} dependence in GTO, results in a zero slope at nucleus, instead of a cusp. Moreover, the e^{-r^2} dependence also results in a poor representation of the tail of the orbitals. Hence, a single GTO cannot properly describe the behavior of an AO. To circumvent this problem, each basis function is represented as a linear combination of a set of at least two per STO Gaussian functions.

However, due to a large number of Gaussian basis functions going into describing each of the atomic orbitals, it sometimes become computationally very expensive in molecular calculations. Moreover, the core electrons are chemically not active, hence are less prone to the changes due to the formation of a molecule. Hence, the MO coefficients for these basis functions also change very little during the SCF calculations. This fact lead to the *contracted* basis sets. In these basis sets, the variational coefficients of inner basis functions are are kept constant during SCF calculations, thereby reducing the computational cost with little effect on the accuracy.

In addition to localized basis sets, plane wave basis sets can also be used in quantum mechanical calculations. Following Bloch's Theorem [16], the electronic wave function, $\Phi_e(\mathbf{r})$, can be written as a product of cell periodic part, f_j, and a wavelike part [17]:

$$\Phi_e(\mathbf{r}) = f_j \exp[i\,\mathbf{k}\cdot\mathbf{r}] \tag{2.19}$$

As stated by Bloch's theorem, the electronic wave functions at each k-point can be expanded in terms of a discrete plane wave basis sets. When plane waves are used as a basis set for the electronic wave function, $\Phi_{\mathrm{i}}(\mathbf{r})$, the Kohn-Sham equations take the following form [16]:

$$\varepsilon_{\mathrm{i}}\, c_{\mathrm{i,\,k+G}} \;=\; \sum_{G'} \left[\frac{\hbar^2}{2m} \left|k+G\right|^2 \delta_{GG'} \;+\; V_{\mathrm{ion}}\left(G-G'\right) \;+\; V_{\mathrm{H}}\left(G-G'\right) \;+\; V_{\mathrm{XC}}\left(G-G'\right) \right] c_{i,\,k+G'}$$

In this secular equation, the kinetic energy is diagonal, and the various potentials can be described in terms of their Fourier transforms. Then, the solution of this equation can be obtained by the diagonalization of a Hamiltonian matrix whose matrix elements, $H_{\mathrm{k+G,\,k+G'}}$ are defined by the terms in the brackets in the equation above. Together with the introduction of an energy cutoff to the discrete plane waves basis set, it produces a finite basis set. As a result, this truncation of the plane wave basis set will lead to an error in computed total energy. Although in principle, it is possible to reduce the magnitude of this error by increasing the value of cutoff energy, in practice, this comes at the expense of computational time in the diagonalization of a huge matrix, since the dimension of the matrix, $H_{\mathrm{k+G,\,k+G'}}$ is determined by the choice of the cutoff energy $(\hbar^2/2m)\ |k+G|^2$.

From a computational view point, certain integrals and operations are much easier

to code and carry out with plane wave basis functions, than with their localized counterparts. Furthermore, as all functions in the basis are mutually orthogonal, plane wave basis sets do not exhibit basis set superposition error [18].[†]

[†]Calculations of interaction energies, performed using finite basis sets, are susceptible to basis set superposition error (BSSE). As the atoms of interacting molecules (or of different parts of the same molecule) or two molecules approach one another, their basis functions overlap. Each monomer borrows functions from other nearby components, effectively increasing its basis set and improving the calculation of derived properties such as energy. If the total energy is minimized as a function of the system geometry, the short-range energies from the mixed basis sets must be compared with the long-range energies from the unmixed sets, and this mismatch introduces an error.

2.6 Computational Packages

2.6.1 Gaussian

GAUSSIAN [19, 20] is an electronic structure program, from the Gaussian Inc. Designed to model a broad range of molecular systems under a variety of conditions, it performs its computations starting from the basic laws of quantum mechanics. GAUSSIAN is used by chemists, physicists and engineers for research in established and emerging areas of chemical interest, studying molecules and reactions of definite or potential interest, including both stable species and compounds which are difficult or impossible to observe experimentally: short-lived intermediates, transition structures and the like.

GAUSSIAN can predict energies, molecular structures, vibrational frequencies along with numerous molecular properties that are derived from these three basic computation types - for systems in the gas phase and in solution, and it can model them in both their ground state and excited states. Chemists apply these fundamental results to their own investigations, using GAUSSIAN to explore chemical phenomena like substituent effects, reaction mechanisms, and electronic transitions.

This package was primarily employed in performing calculations for results discussed in Chapter 3 as well as for some additional calculations in Chapter 5.

2.6.2 VASP

VASP [21, 22, 23, 24] is a package for performing *ab initio* Quantum Mechanical Molecular Dynamics (MD) simulations using Pseudo Potentials (PP) or the Projector-Augmented Wave (PAW) method and a plane wave basis set. The approach implemented in VASP is based on the (finite temperature) Local Density Approximation (LDA) with the free energy as variational quantity and an exact evaluation of the instantaneous electronic ground state at each MD time step.

VASP uses efficient matrix diagonalization schemes and an efficient Pulay/Broyden charge density mixing. These techniques avoid all problems possibly occurring in the original Car-Parrinello method, which is based on the simultaneous integration of electronic and ionic equations of motion. The interaction between ions and electrons is described by Ultra Soft Vanderbilt Pseudo Potentials (US-PP) [25, 26] or by PAW method. US-PP (and the PAW method) allow for a considerable reduction of the number of plane waves per atom for transition metals and first row elements. Forces and the full stress tensor can be calculated with VASP and used to relax atoms into their instantaneous ground-state.

This was the primary package employed in performing calculations for results discussed in Chapter 5.

Chapter 3

Metal Oxide Nanoclusters

Notations

AEA	Adiabatic Electron Affinity
AIMPAC	Atoms In Molecules PACkage
AIP	Adiabatic Ionization Potential
BE	Binding Energy
CI	Configuration Interaction
DFT	Density Functional Theory
EA	Electron Affinity
HF	Hartree-Fock
HOMO	Highest Occupied Molecular Orbital
IP	Ionization Potential
LUMO	Lowest Unoccupied Molecular Orbital
MP	Möller-Plesset
QTAM	Quantum Theory of Atoms in Molecules
SCF	Self-Consistent Field
VAE	Vertical Attachment Energy

VDE	Vertical Detachment Energy
VEA	Vertical Electron Affinity
VIP	Vertical Ionization Potential

3.1 Introduction

Coined by F. A. Cotton in the early 1960s, the term *cluster* refers to a collection of atoms or molecules, ranging from a few to a few thousands of atoms and these are classified, albeit weakly, depending on the number of atoms or molecules. A small cluster can have as many atoms, but no more than a thousand of them; whereas a larger cluster would consist of a few thousand atoms. However, a meaningful and distinct classification was given by Berry and Haberland [27]. This classification was based on the unique property of the clusters, namely the size- and shape-dependent variations in the properties of clusters. In small clusters, though the properties vary with the size, no smooth variation with size and shape can be observed; in the medium-sized clusters the properties vary smoothly with the size. In larger clusters, however, the properties are more similar to that of the bulk and are almost independent of the size. The larger clusters usually fall into nanometer dimensions. Hence, the cluster size may vary from a molecule to almost bulk-like and have become a subject of interest in studying the emergence of bulk-like crystalline properties starting from molecules.

The study of clusters is usually based on the composition and the type of chemical bonding between the atoms forming the cluster. Clusters of a given composition may have a large number of stable structures, referred to as local minima. Likewise, there are homogeneous and heterogeneous clusters, based on the kind of atoms making up the clusters. Heterogeneous clusters can exist in two forms, namely, stoichiometric and

non-stoichiometric clusters. The stoichiometric clusters have the same composition as that of the corresponding bulk but exhibit properties which may be different from that of the crystal. The nature of bonding in these clusters is quite different in each case and can vary from ionic [$(NaCl)_n$ clusters] to covalent (C_{60}) to van der Waals (rare gas clusters). Clusters of water molecules are held together by hydrogen bonds. Moreover, for a given cluster, the nature of the chemical bond can vary with the cluster size. For example, in Hg_n clusters the nature of the chemical bonds in small clusters is van der Waals, whereas for larger clusters the chemical bonds exhibit metallic character [28].

One of the interesting features of clusters is that the atoms have a high surface to volume ratio, i.e., majority of the atoms are surface atoms. Hence, clusters can offer new insights into surface reactions such as chemical catalysis. Large clusters can sometime act as a bulk surface, and thus can serve as *model surfaces* in the chemisorption reactions studies. Smalley *et al.*, reported the production of semiconductor and metallic clusters, which behaved like a nano-surface [29]. However, using these model surfaces in chemisorption studies works well only when adsorbate bonding to the model surface is a local phenomenon. Clusters are also expected to offer ways to develop new kinds of materials. With the advances in the experimental techniques, the size and the properties of the clusters can be controlled precisely and are used to develop cluster assembled materials such as C_{60}. From a theoretical stand point, the study of clusters is expected to provide interesting avenues leading to the

prediction and development of novel materials, whose properties can be varied at the nano-scale to create the desired chemical properties. It also allows us to study the emergence of material properties with variations in the size of the cluster.

Gallium oxide low dimensional nanostructures have been created by physical evaporation [30] and arc-discharge [31, 32] methods, thus opening up a new research area with promising applications. Gallium oxide is a ceramic material with high melting point of about 1900°C. Owing to its wide band gap (4.80 eV) [33], it behaves like an insulator at room temperature and as a semi-conductor above 800°C. These characteristics have made Ga_2O_3 a very good candidate for fabricating electronic devices that operate at high temperatures. Also, at high temperatures, gallium oxide thin films have shown significant conductance response to oxygen gas concentrations and at low temperatures the sensitivity switches to reducing gases such as carbon monoxide, methane, and ammonia. In the form of low-dimensional nanostructures such as nanowires, nanosheets and nanoribbons, it shows a very high surface to volume ratio, which provides a larger reaction surface using only very small amounts of the oxide material. This simultaneously increases gas-sensing reaction times while reducing power requirements associated with heating the sensors. These attributes provide great advantages in gas-sensing over gallium oxide thin films and can provide a means by which gallium oxide based systems can effectively solve problems associated with conventional tin oxide sensors.

Small clusters of gallium oxide are expected to provide useful prototypes to understand the physics and chemistry of surfaces and nanostructures. The smaller size of the clusters makes it possible to obtain a detailed geometric, electronic, and bonding information, that can also be used to benchmark theoretical methods to be used in the larger structural elements. However, there is a dearth of both theoretical and experimental work on gallium oxide at the cluster level. A few scattered studies have been reported on diatomic GaO and triatomic Ga_2O, and GaO_2. For example, the vibrational spectrum of the GaO molecule [34] is well known. Structural and vibrational properties of neutral GaO_2 have also been reported earlier [35, 36]. In neutral Ga_2O, both experimental studies [37, 38, 39, 40, 41, 42, 43, 44, 45] and *ab initio* calculations [46] were carried out to settle the controversy of its ground state configuration.

The results and discussions are split into three sections. Section 3.3.1 deals with the structure, bonding, vibrational, and electronic properties of small clusters of gallium oxide, Ga_mO_n (m,n = 1,2) are studied here with a focus on the changes induced by the addition or removal of an electron from the neutral species. Section 3.3.2 discusses the next level of calculations on Ga_3O_3, for which both metal-excess and oxygen-excess fragments have been considered while investigating the effect of the oxygen/metal ratio on their structural and electronic properties. Of specific interest is the investigation of changes induced by the sequential oxidation of Ga_3 to Ga_3O_3, and then the sequential removal of metal atoms up to O_3. Section 3.3.3 deals with

calculations on the oxygen-rich gallium oxide clusters performed with an aim to study the changes in structural and electronic properties of gallium oxide clusters as a result of their sequential oxidation starting from Ga_3O_4 to Ga_3O_8. Of particular interest is to see if the stability of the oxygen-rich gallium oxide clusters is governed by the formation of the O-O bonds.

3.2 Computational Methodology

Electronic structure calculations were performed on neutral and singly ionized clusters of gallium oxide by solving the Kohn-Sham equations in the framework of Density Functional Theory, using the GAUSSIAN 98 [19] suite of programs. Gradient Corrected Becke's 3-parameter hybrid exchange functional [47] and Lee, Yang and Parr correlation functional [48] were employed in these calculations. It is to be noted that the choice of DFT-B3LYP methodology together with the 6-31+G** basis set is based on the equilibrium between the quality of results and the available computational resources. Table 3.1 includes the results on the GaO molecule showing the convergence of the bond length and frequency with respect to the basis sets.

All of the isomers in this study have been fully optimized. The convergence criteria for the energy 10^{-9} hartree and for the gradient was 10^{-4} hartree/Å. The stability of the lowest energy configurations (neutral, anionic, and cationic) was checked by computing the vibrational frequencies under harmonic approximation, with analytical force constants. The atomic and bonding properties were studied under the QTAM [49]. In order to perform this analysis, AIMPAC95 package [50] was used with the Promega algorithm for integration of the atomic properties and the error in the total charge was less than $10^{-3}e$.

3.3 Results and Discussion

3.3.1 Ga_mO_n $(m, n = 1, 2)$

Discussions will begin with the results for diatomic GaO in neutral and singly ionized charged states. Those for the triatomic and dimer clusters will be follow subsequently.

The electronic states together with the structural properties for the neutral, anionic, and cationic gallium oxide are given in Table 3.1. The dissociation energies are computed with respect to the atoms in their ground states using the same theoretical scheme. However, in the case of GaO^- and GaO^+ dissociation products, the electron added or removed was assigned to oxygen and gallium atoms respectively, in accordance with Pauling's electronegativity values (Ga 1.6 and O 3.5). The electronic state for the neutral GaO is predicted to be a $^2\Sigma$, in agreement with the experimental observation [34]. For GaO^- and GaO^+, calculations find the state to be $^1\Sigma$ and $^3\Sigma$, respectively. Calculations show that the inclusion of a diffuse function in the basis set produces a variation of about 1% in bond length, 2% in dissociation energy and 2% in frequency. In subsequent calculations, the diffuse function was therefore included for optimum quality, while noting that the diffuse function could have been ignored for larger clusters without losing too much precision.

The anionic GaO was found to be more stable than the neutral GaO with nearly

	$^{2S+1}\Lambda$	R_e (Å)	D_e (eV)	ω_e (cm^{-1})
GaO				
Experiment [34]	$^2\Sigma$	1.74		767
This work				
6-31G**	$^2\Sigma$	1.73	4.25	708
6-31+G**	$^2\Sigma$	1.74	4.29	696
6-311G**	$^2\Sigma$	1.72	4.43	739
6-311+G**	$^2\Sigma$	1.72	4.35	726
GaO				
6-31+G**	$^2\Sigma$	1.74	4.29	696
GaO^-				
6-31+G**	$^1\Sigma$	1.74	5.22	775
GaO^+				
6-31+G**	$^3\Sigma$	1.94	0.43	410

Table 3.1: Electronic state, bond length (Å), dissociation energy (eV), and vibrational frequency (cm^{-1}) of neutral and ionized GaO.

the same value for the bond length and a higher stretching frequency (775 cm^{-1}) indicating that the Ga-O bond is stronger than that in neutral GaO. This is consistent with the picture given by the molecular orbitals. The added electron to the neutral GaO occupies the LUMO which has a σ bonding character. The anionic GaO therefore completes a molecular orbital stabilizing the system. For the cationic case, the ionized electron comes out from a σ bonding orbital of the neutral GaO. It therefore results in the less stable configuration with a larger bond length and a smaller vibrational frequency.

Table 3.2 presents the results for both linear and bent isomers of GaO_2 (Fig. 3.1) which are found to be in doublet electronic state. The lowest energy isomer of the neutral GaO_2 is a bent configuration with C_{2v} symmetry in which R_{Ga-O} is 20%

larger than that of GaO. The O–O bond is also 12% larger than the diatomic oxygen molecule and the O–Ga–O angle is 38°. Analysis of the normal modes of vibration (Table 3.3) finds the lowest frequency mode to be the Ga–O asymmetric stretching, the next one to be Ga–O symmetric stretching and the highest frequency mode to be stretching of the O-O bond.

In GaO_2^- isomers, the singlet electronic state is lower in energy than the triplet. The ground state is a linear $D_{\infty h}$ structure (i.e. O-Ga-O) in which the first vibrational

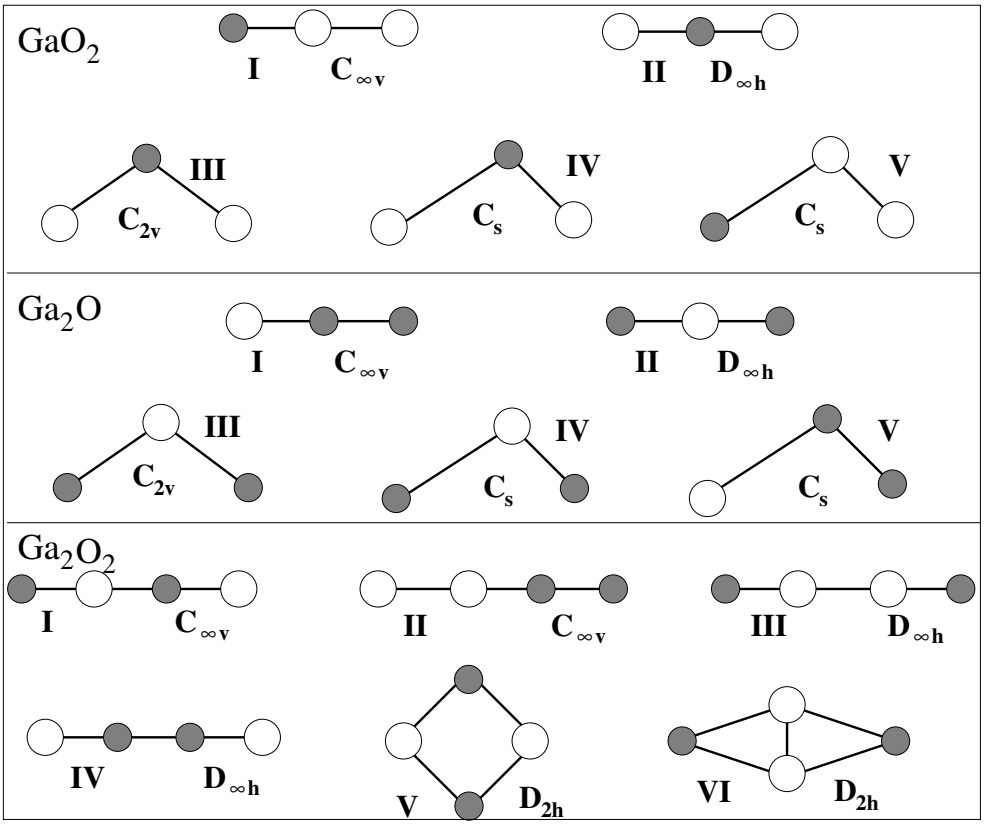

Figure 3.1: Schematic representation of GaO_2, Ga_2O and Ga_2O_2 cluster configurations. The filled and empty circles represent gallium and oxygen atoms respectively.

Isomer	I ($C_{\infty v}$)	II ($D_{\infty h}$)	III (C_{2v})	IV (C_s)	V (C_s)
GaO_2					
ΔE	0.62	0.12	0.00	Str II	Str III
R_{Ga-O}	1.90	1.71	2.08		
$\overline{BE}$	2.33	2.58	2.54		
GaO_2^-					
ΔE	2.93	0.00	Str II	Str II	1.92
R_{Ga-O}	1.78	1.71			1.92
$\overline{BE}$	2.26	3.24			2.60
GaO_2^+					
ΔE	0.00	3.27	Str II	Str II	Str I
R_{Ga-O}	2.70	1.74			
$\overline{BE}$	1.82	0.73			
Ga_2O					
ΔE	2.76	0.00	Str II	0.56	Str II
R_{Ga-O}	1.69	1.83		1.85, 1.95	
$\overline{BE}$	2.23	3.15		2.96	
Ga_2O^-					
ΔE	3.51	0.03	0.00	Str III	Str II
R_{Ga-O}	1.72	1.84	1.86		
$\overline{BE}$	1.45	2.61	2.62		
Ga_2O^+					
ΔE	1.21	0.00	Str II	Str II	Str II
R_{Ga-O}	1.71	1.82			
$\overline{BE}$	2.00	2.40			

Table 3.2: Isomeric configurations of GaO_2 and Ga_2O. ΔE is energy (eV) relative to the most stable isomer, R_{Ga-O} is the bond length (Å) and $\overline{BE}$ is the binding energy per atom (eV). *Str X* represents the case where the optimization leads to the configuration X.

mode corresponds to out-of-plane bending. The next two modes involve symmetric and asymmetric stretching of the Ga–O bonds respectively. These vibrational frequency values (Table 3.3) bracket the diatomic anion value (Table 3.1) in agreement with the coupling of two similar bonds.

Cationic isomers of GaO_2 were found to be lower in energy in the triplet electronic

state than the singlet, a different behavior compared to the anionic clusters. The ground state is $C_{\infty v}$ linear configuration (i.e. Ga-O-O) formed by a diatomic oxygen molecule weakly bonded to a gallium cation. The O-O bond length is exactly the same as in the diatomic oxygen molecule, the Ga–O internuclear distance (2.70 Å) is quite larger than 1.74 Å of GaO. Analyzing the vibrational modes presented in Table 3.3, one finds that the lowest frequency mode corresponds to the stretching movement of the Ga–O bond. The value is small, indicating a weak bond between this pair of atoms. The π mode represents bending out-of-plane of the molecule. The highest frequency mode involves only the stretching of the O-O bond and its value is quite close to that of the O_2 molecule (1642 cm^{-1}).

In neutral Ga_2O, singlet electronic state is found to be lower in energy than the triplet one. The ground state is the $D_{\infty h}$ symmetric linear structure (i.e. Ga-O-Ga). The optimization of the bent configurations (Fig. 3.1) always lead to the linear configuration. Since the asymmetric linear structure $C_{\infty v}$ is about 3 eV higher in energy, a preference for metal-oxygen bond over metal-metal bond can be observed in the neutral Ga_2O. This is consistent with the computed binding energy of 1.47 eV and 4.27 eV for the Ga–Ga and Ga–O bonds respectively.

For the neutral Ga_2O, the high temperature electron diffraction results suggest it to be in the C_{2v} configuration with apex angle of 140° and bond length of 1.84 Å [38]. Later, a re-assessment of the electron diffraction data suggested that the molecule to

be linear [39]. Since then, few more experimental studies on Ga_2O were not able to provide a unique assignment for its ground state [41, 42, 43, 44]. On the other hand, *ab initio* calculations at HF, MP2 and CISD levels [46] yielded a linear structure in agreement with the more recent experiments [45, 37]. Results of this DFT-B3LYP study also predict a symmetric linear structure as a global minimum.

Cationic and anionic Ga_2O have been found to be in the doublet spin electronic state. In both cases, the ground state is governed by the relative strengths of bond energies that favor Ga–O over Ga–Ga bonds. In Ga_2O^-, it is an angular structure (C_{2v}) with angle of 110° followed by the linear symmetric configuration (ΔE=0.03 eV). On the other hand, Ga_2O^+ maintains linear symmetric structure, as is the case with neutral Ga_2O.

In Ga_2O^-, the lowest frequency vibrational mode corresponds to the flexion movement, and the next two modes to the symmetric and asymmetric stretching of the two Ga–O bonds respectively. In both neutral and cationic Ga_2O, the degenerate modes represent (out-of-plane) bending movements, and the last two σ modes correspond to symmetric and asymmetric stretching of the Ga–O bonds respectively. For neutral Ga_2O, the frequency values are in good agreement with the MP2 frequencies obtained by Leszczýnski *et al.* (52, 300, and 854 cm^{-1}) [46].

In neutral Ga_2O, a very good agreement was found with the experimental value of asymmetric stretching mode (ν_3), 823 cm^{-1} [35]. The calculated DFT-B3LYP value

System	Symmetry	Frequency (mode)
GaO		
Q=0	$C_{\infty v}$	696 (σ)
Q=-1	$C_{\infty v}$	775 (σ)
Q=+1	$C_{\infty v}$	410 (σ)
GaO_2		
Q=0	C_{2v}	319 (b_2), 416 (a_1), 1166 (a_1)
Q=-1	$D_{\infty h}$	213 (π_u), 738 (σ_g), 879 (σ_u)
Q=+1	$C_{\infty v}$	80 (σ), 108 (π), 1645 (σ)
Ga_2O		
Q=0	$D_{\infty h}$	98 (π_u), 285 (σ_g), 812 (σ_u)
Q=-1	C_{2v}	79 (a_1), 491 (a_1), 536 (b_2)
Q=+1	$D_{\infty h}$	149 (π_u), 275 (σ_g), 625 (σ_u)
Ga_2O_2		
Q=0	$C_{\infty v}$	75 (π), 201 (π), 282 (σ), 832 (σ), 941 (σ)
Q=-1	D_{2h}	197 (b_{3u}), 276 (a_g), 450 (b_{1u}), 464 (b_{3g}), 559 (b_{2u}), 629 (a_g)
Q=+1	$C_{\infty v}$	80 (π), 210 (π), 242 (σ), 653 (σ), 896 (σ)

Table 3.3: Frequency values (ω) in cm^{-1} of the normal modes of vibration for the neutral, anionic and cationic Ga_mO_n $(m, n = 1, 2)$ clusters.

of ν_3 is 812 cm^{-1} (Table 3.3). A recent theoretical study by Jones *et. al.* [51] reported asymmetric and symmetric stretch modes of Ga_2O to be 806 and 300 cm^{-1} respectively and calculations in this study found them to be 812 and 285 cm^{-1}. Hinchcliffe *et. al.* [43] argued that heavier sub-oxides should have a bending mode below 100 cm^{-1} and our calculations found this to be 98 cm^{-1}.

Figure 3.1 shows different isomeric configurations of Ga_2O_2 considered in this study. The results find singlet states to be lower in energy than the triplet ones. The optimal values of the bond lengths and the energies relative to the most stable isomer are presented in Table 3.4.

Isomer	I ($C_{\infty v}$) *	II ($C_{\infty v}$)	III ($D_{\infty h}$)	IV ($D_{\infty h}$)	V (D_{2h})	VI (D_{2h})
$\mathbf{Ga_2O_2}$						
ΔE	0.00	5.09	2.50	1.93	0.21	1.30
$R_{\mathrm{Ga-O}}$	1.74	1.77	1.83	1.66	1.86	2.03
$\overline{BE}$	3.20	1.93	2.58	2.72	3.15	2.88
$\mathbf{Ga_2O_2^-}$						
ΔE	1.58	5.55	4.67	2.30	0.00	1.00
$R_{\mathrm{Ga-O}}$	1.92	1.76	1.84	1.73	1.90	1.94
$\overline{BE}$	2.99	1.99	2.21	2.95	3.38	3.13
$\mathbf{Ga_2O_2^+}$						
ΔE	0.00	2.44	0.97	2.93	0.29	1.14
$R_{\mathrm{Ga-O}}$	1.70	1.80	2.07	1.71	1.85	1.99
$\overline{BE}$	2.45	1.84	2.21	1.72	2.38	2.17

Table 3.4: Isomeric configurations of Ga_2O_2. ΔE is energy (eV) relative to the most stable isomer, $R_{\mathrm{Ga-O}}$ is the bond length (Å) and $\overline{BE}$ is the binding energy per atom (eV). [*: Other two values of $R_{\mathrm{Ga-O}}$ are 1.84, 1.67 (neutral), 1.79, 1.75 (anion) and 1.96, 1.79 (cation)]

The relative stability of the various isomers of Ga_2O_2 can be interpreted in terms of the bond energies which are calculated to be 4.29, 1.47 and 5.83 eV for the Ga–O, Ga–Ga and O–O bonds respectively. The calculated results find the most stable configuration to be the linear structure, I-$C_{\infty v}$. Based on the bond energetics, the isomer III-$D_{\infty h}$ is expected to be the lowest energy isomer of the neutral Ga_2O_2. However, it is 2.50 eV higher in energy due to the charge transfer from Ga to O atoms resulting in a 12% increase of $R_{\mathrm{O-O}}$ when compared to the O_2 molecule. On the other hand, the V-D_{2h} rhombic structure consists of higher number of Ga–O bonds than in I-$C_{\infty v}$ isomer, but $R_{\mathrm{Ga-O}}$ is larger than those in the diatomic molecule. This is a consequence of the electrostatic repulsion between equal atoms making the bond angles close to 90°. The competing factors, electrostatic repulsion and higher number of Ga–O bonds, make this isomer only 0.21 eV higher in energy with respect

to the lowest I-$C_{\infty v}$ isomer.

In anionic Ga_2O_2, the presence of an extra electron makes the ground state to be the V-D_{2h} structure. This is due to the fact that the LUMO of the ground state (I-$C_{\infty v}$) of the of the neutral Ga_2O_2 has an antibonding character. This fact results in the increase of interatomic distances, upon accommodation of the extra electron. On the other hand, the LUMO in the neutral rhombus structure of Ga_2O_2 has a bonding character in the Ga–O bonds.

The ground state of the cationic Ga_2O_2 does not show any change in the cluster configuration. The ionized electron comes out from an antibonding molecular orbital of neutral Ga_2O_2. The resulting cationic dimer has a partially filled antibonding molecular orbital.

The relative ordering in terms of energy of the cationic and anionic isomers is similar to that in the neutral case, only with the following difference: the III-$D_{\infty h}$ is stabilized in the cationic and is destabilized in the anionic cluster. This may be due to the HOMO of cationic cluster - a bonding orbital mainly localized over the O–O bond resulting in the 7% contraction of O–O interatomic distance relative to that in the neutral Ga_2O_2. This O–O bond has highest binding energy and determines the stability of the cluster. Also, it is important to notice that the II-$C_{\infty v}$ is higher in energy in both neutral and anionic clusters relative to that in the cationic state. The stabilization in the cationic state may be due to the elongation of the Ga–Ga bond, making it

to be almost a disconnected cluster in which a Ga atom is weakly bonded to the O–O–Ga unit. The IV-$D_{\infty h}$ anionic isomer is also almost disconnected, because the Ga–Ga interatomic distance is very large and two GaO molecules are weakly bonded by means of a weak Ga–Ga interaction.

Due to the lack of experimental and theoretical studies on the gallium oxide dimers, calculated results are compared with the values reported for the aluminum oxide dimers. Early semi-empirical and *ab initio* calculations performed on Al_2O_2 suggested that there were two stable isomers, one was a square cyclic structure (D_{2h}) and the other was a linear configuration less stable than the square [52]. Later SCF and MP2 calculations determined that there were two minima, one almost square and the other a rhombus [52, 53, 54, 55, 56]. The linear and cyclic structures were also found to be the minima for Ga_2O_2 but two striking differences with Al_2O_2 were noticed: the linear structure is the lowest in energy followed very closely in energy by the square cyclic D_{2h}.

The values of the normal vibration frequencies are presented in Table 3.3 for the neutral, cationic and anionic Ga_2O_2 in their ground states. In the neutral and cationic cases, two low degenerate modes present the bending out-of-plane movements, the first π vibration corresponds to the bending of the Ga–O–Ga angle and the second one is associated with the bending of both O–Ga–O and Ga–O–Ga angles. The rest of the normal modes correspond to the stretching movements of the cluster. The

lower mode is a symmetric stretching of both Ga and the outer O atoms without any participation of the central oxygen in the movement. The next two frequencies are associated with the asymmetric and symmetric stretching of the oxygen atoms respectively. The oxygen atoms are moving in-phase whereas the central gallium is out-of-phase. In anionic Ga_2O_2 cluster, the out-of-plane bending of the cluster is associated with the lowest frequency b_{3u} mode. The a_g mode involves the bending of the four angles leading to a rhombic distortion. Next, b_{1u}, and b_{3g} modes show a quasi-degeneracy due to the fact that they correspond to a ring torsion where the movement of two oxygen atoms is in-phase and out-of-phase respectively. The b_{2u} mode represents O–O symmetric stretching. Lastly, the a_g is a breathing mode of the O–O pair in anionic Ga_2O_2.

The QTAM approach is used for determining the character of the chemical bond in these clusters. The atomic charges were computed to study the effect of addition or removal of an electron in these systems. It is to be noted here that the topological atomic charges are mostly independent of the computation method and are calculated by the integration of the electron density over the atomic basin [49].

The topological structures of neutral and ionized Ga_mO_n (m,n=1,2) clusters considered in this work are almost the same as drawn in Fig. 3.1, with the only exception of the neutral GaO_2, in which two oxygen atoms are bonded, resulting in a closed triangle structure. The ground state configurations of the clusters considered here

Monomer			Triatomic			
	Q_{Ga}	Q_O		Q_{Ga}	Q_O	
GaO	0.889	-0.888	GaO_2	0.719	-0.359	
GaO^-	0.304	-1.303	GaO_2^{-*}	1.444	-1.221	
GaO^+	1.254	-0.254	GaO_2^{+*}	0.992	(-1.226	1.303)
			Ga_2O	0.673	-1.345	
			Ga_2O^{-*}	0.255	-1.337	
			Ga_2O^+	1.084	-1.167	
Dimer						
	Q_{Ga_1}	Q_{Ga_2}	Q_{O_1}	Q_{O_2}		
Ga_2O_2	0.751	1.594	-1.303	-1.041		
$Ga_2O_2^{-*}$	0.772		-1.270			
$Ga_2O_2^+$	0.904	1.758	-1.185	-0.477		

Table 3.5: Topological charges for oxygen and gallium atoms in the most stable neutral and ionized isomers of Ga_mO_n $(m, n = 1, 2)$ clusters. In dimers, Ga_1 and O_2 are the terminal atoms. (* : Error in total charge is greater than $10^{-3}e$.)

contain two different kinds of bonds: Ga–O and O–O. Both ρ and $\nabla^2\rho$ at the bond critical points follow an exponential relationship with the distance for a given pair of atoms [57]. In this way, the short bonds have a higher density, indicating a stronger bond. In all cases, Ga–O bond shows a positive $\nabla^2\rho$ value indicating a non-sharing ionic-like interaction. On the other hand, O-O bonds show a negative $\nabla^2\rho$ value indicating a sharing covalent-like interaction.

The topological charges for the monomer, triatomic, and dimer in their lowest energy isomers are collected in Table 3.5. In neutral GaO, there is a considerable charge transfer (about $0.9e$) from gallium to oxygen, in accordance with the chemical intuition and Pauling electronegativities for Ga (1.6) and O (3.5). The Ga–O bond has, therefore, a high ionic character. In other neutral clusters, charge transfer tends to

decrease for terminal atoms (O in GaO_2, Ga in Ga_2O, Ga_1 and O_2 in Ga_2O_2), whereas it tends to increase in higher coordinated atoms (Ga in GaO_2, O in Ga_2O, Ga_2 and O_2 in Ga_2O_2). The addition or removal of an electron in the monomer is shared more or less equally among the atoms in the cluster.

GaO_2 is a cluster with a partial ionic character, though the anionic cluster is more ionic. The extra electron is localized over oxygen atoms and moreover, the formation of linear symmetric structure induces a higher charge transfer from the gallium atom to the oxygen ones. The cationic cluster, GaO_2^+, presents an important feature. Its structure, as described previously, is formed by an oxygen diatomic molecule weakly bonded to the gallium atom. The topological charges indicate that the O_2 unit is almost neutral, but highly polarized by the positive charge of the Ga atom: the outer O possesses a $1.3e$ charge, while the inner O has a negative charge, $-1.2e$. Comparing with the neutral case, the ionized electron comes mainly from the O_2 unit; thus, GaO_2^+ attains the triplet character as in a neutral isolated O_2 molecule.

The loss of an electron from the Ga_2O to reach the cationic structure comes mainly from the gallium atoms, and only about 10% is provided by the oxygen atom. The topological analysis in the anionic Ga_2O reveals that the total charge for the predicted ground state is $-0.8e$, instead of $-1.0e$. This discrepancy is not due to any numerical error, but is attributed to a complex shape of the oxygen atomic basin [58]. Several electronic states other than $^2A_1$ for Ga_2O^- have also been explored, but

all of them were at a higher total energy than that of $^2A_1$. All these considerations lead one to believe that Ga_2O^- is an electronically unstable cluster. In a photoelectron spectroscopy study of aluminum oxide clusters, Al_2O^- was not observed, despite numerous attempts to produce it at various source conditions.

The neutral Ga_2O_2 consists of two atoms different by symmetry for each type. The inner oxygen atom receives charge from the two gallium atoms while the terminal one receives charge only from the inner gallium. This effect is also present in the cationic Ga_2O_2. All atoms of the cluster contribute to the loss of the electron but not to the same extent. The larger contribution, about 56%, is from the terminal oxygen atom. The remaining percentage is contributed almost equally by the three atoms. On the other hand, the anionic Ga_2O_2 can be formed by closing the neutral Ga_2O_2. In this way all atoms in the cluster have the same coordination index. The extra electron is then assigned mostly to the former inner gallium atom in the neutral cluster; thus making both metallic atoms to have the same atomic charge. The oxygen atoms in the anionic cluster present an average charge between the terminal and the inner oxygen atoms from the neutral dimer.

Both adiabatic and vertical EA and IP have been computed for the monomer, triatomics and dimer of gallium oxide clusters. The values are listed in Table 3.6. The

definition of these properties employed in this work is as follows:

$$\text{EA} = E_{\text{Q=0}} - E_{\text{Q=-1}} \qquad \text{and} \qquad \text{IP} = E_{\text{Q=1}} - E_{\text{Q=0}} \tag{3.1}$$

In this way, VEA or VDE [59] can be defined as the energy difference between the anionic and neutral clusters when both are at the optimized geometry of the anionic cluster, while the AEA is defined as the energy difference between the anionic and neutral clusters at their respective optimized geometries. VAE, which is defined as the energy difference between the neutral and anionic clusters with both at the optimized geometry of the neutral cluster, was calculated. Although this is not attainable through any experiment, it provides a lower bound to the AEA in the same way that the VDE is an upper bound [59]. VIP can be defined as the energy difference between the cationic and neutral clusters with both at the optimized geometry of the neutral cluster, while the AIP is defined as the energy difference between the cationic and neutral clusters at their respective optimized geometries.

For all cases, the anionic clusters are more stable than the neutral ones. It is to be noted that in Ga_2O, anionic and neutral clusters are almost degenerate in energy, thereby confirming the instability of the anionic Ga_2O cluster.

Due to the lack of experimental studies on GaO clusters, the calculated values for the EA were compared with the experimental results of the photoelectron spectroscopy

	O/Ga	VEA	AEA	VIP	AIP	H-L
GaO	1	2.56	2.56	9.84	9.89	2.85
GaO_2	2	3.85	3.72	9.78	8.20	3.70
Ga_2O	1/2	0.44	0.03	7.89	8.27	4.83
Ga_2O_2	1	2.59	2.33	9.16	9.04	4.99

Table 3.6: Vertical and adiabatic values of the EA and IP as well as HOMO-LUMO gap for the Ga_mO_n $(m, n = 1, 2)$ clusters. Values in eV.

on AlO clusters [60]. The values measured by Desai *et al.* are 2.60, 4.23 and 1.88 for the AlO, AlO_2 and Al_2O_2 respectively. In both cases, aluminum and gallium oxide clusters, one can observe a significant increase in the EA when progressing from MO to MO_2 (M = Al, Ga). In these calculations, a decrease in the EA values can be observed when a gallium atom is added to form Ga_2O. The explanation of this behavior is that clusters that have excess of oxygen atoms are electron deficient and thus present high EA values.

The adiabatic and vertical values for the EA in the monomer are almost the same, while in rest of the cases, adiabatic values are smaller than the vertical ones. This is because the internuclear distance does not change when an electron is added to the neutral monomer. However, the addition of one electron in triatomic and dimer clusters produces larger changes in the structural parameters, resulting in lower values of AEA.

The HOMO-LUMO gaps have been computed for the most stable isomers in gallium oxide clusters under study, and are listed in Table 3.6. As a general trend, there is

an increase in the gap values when the cluster size increases for the neutral cases. The experimental band gap energy value for the bulk Ga_2O_3 at room temperature is 4.8 eV [33]. It appears that the bulk value has been reached for the dimer, but small oscillations in the HOMO-LUMO gap are expected before convergence is attained.

3.3.2 Ga_3O_n $(n = 1 - 3)$ & Ga_mO_3 $(m = 1, 2)$

Some of the initial configurations were taken from previous studies on small alumina clusters [60, 61, 62, 63, 64]. Table 3.7 presents the electronic and structural properties, namely total energy, electronic state, symmetry and interatomic distances of the lowest energy isomers of neutral, anionic, and cationic gallium oxide clusters. The lowest energy isomers in all cases prefer planar arrangements. They also display the lowest possible spin state, with Ga_2O_3, $Ga_3O_3^+$ and GaO_3^+ being exceptions where the spin state is triplet. The ground state configuration of a given cluster always prefers to maximize the heteroatomic, Ga-O (ionic-like), interactions as compared to the homodiatomic, Ga-Ga and O-O, interactions.

Figure 3.2 shows the calculated ground state and some of the low lying structures of the hyper-metallic Ga_3O. Based on the fact that the ground state of Ga_3 is predicted to be the C_{2v} isosceles triangle [65], several structural possibilities for Ga_3O have been investigated including the D_{3h} structure with oxygen at the center of the triangle. The optimization of the D_{3h} configuration leads to lowering of the energy due to Jahn-Teller distortion where competing T or Y type geometries are expected. The T-type $^2B_2$ state is the lowest energy configuration with R_{Ga-Ga} of 2.96 Å, base R_{Ga-O} of 1.93 Å, and an apex R_{Ga-O} of 2.05 Å. In Ga_3O, gallium atoms prefer a triangular arrangement instead of the linear atomic arrangement, bonding the extra gallium directly to the oxygen atom. This makes the number of Ga-O bonds increase

	E	$^{2S+1}\Lambda$	Sym.	$R_{\mathrm{Ga-Ga}}$	$R_{\mathrm{O-O}}$	$R_{\mathrm{Ga-O}}$
Ga_3O						
Q=0	-5844.10116	$^2B_2$	C_{2v}	2.96	-	1.93, 2.05
Q=-1	-5844.13361	$^1A_1$	C_{2v}	2.74	-	1.93, 2.07
Q=1	-5843.90282	$^1A_1'$	D_{3h}	3.46	-	1.99
Ga_3O_2						
Q=0	-5919.36477	$^2B_2$	C_{2v}	2.83	2.62	1.85, 1.88, 2.00
Q=-1	-5919.44125	$^1A'$	C_s	2.96	2.64	1.80, 1.87, 2.11
Q=1	-5919.13182	$^1\Sigma_g$	$D_{\infty h}$	3.64	3.42	1.71, 1.93
Ga_3O_3						
Q=0	-5994.59951	$^2B_2$	C_{2v}	2.69	2.69	1.77, 1.93, 1.96, 1.97
Q=-1	-5994.70775	$^1A_1$	C_{2v}	2.72	2.70	1.77, 1.90, 1.99, 2.01
Q=1	-5994.30412	$^3B_2$	C_{2v}	2.68	2.40	1.70, 1.78, 1.87, 1.92
Ga_2O_3						
Q=0	-4071.52564	$^3B_2$	C_{2v}	2.55	2.69	1.81, 1.84, 1.87
Q=-1	-4071.64062	$^2A_1$	C_{2v}	2.61	2.70	1.71, 1.84, 1.92
Q=1	-4071.18050	$^2B_2$	C_{2v}	2.49	2.74	1.79, 1.80, 1.91
GaO_3						
Q=0	-2148.43918	$^2A_2$	C_{2v}	-	1.37	1.67, 1.97
Q=-1	-2148.54844	$^1A_1$	C_{2v}	-	1.61	1.70, 1.86
Q=1	-2148.08216	$^3B_1$	C_{2v}	-	1.39	1.77, 1.90

Table 3.7: Total energy (hartree), electronic state, symmetry, and interatomic distance (Å) of the most stable configurations of Ga_3O_n ($n = 1-3$) & Ga_mO_3 ($m = 1, 2$) clusters.

compared to Ga-Ga bonds.

Addition of an electron is found to stabilize the metallic Ga_3^- configuration with D_{3h} symmetry [65]. When oxygen is added to Ga_3^-, the resulting ground state of Ga_3O^- is the T-type structure in $^1A_1$ state with C_{2v} symmetry where the base $R_{\mathrm{Ga-O}}$ remains almost the same as in the neutral case, but $R_{\mathrm{Ga-Ga}}$ decreases by 7% because the base atoms are moved towards the apex one closing the angle. This fact finds its explanation in the analysis of molecular orbitals. The LUMO in the neutral cluster shows a bonding contribution between the gallium atoms. In this way, the extra

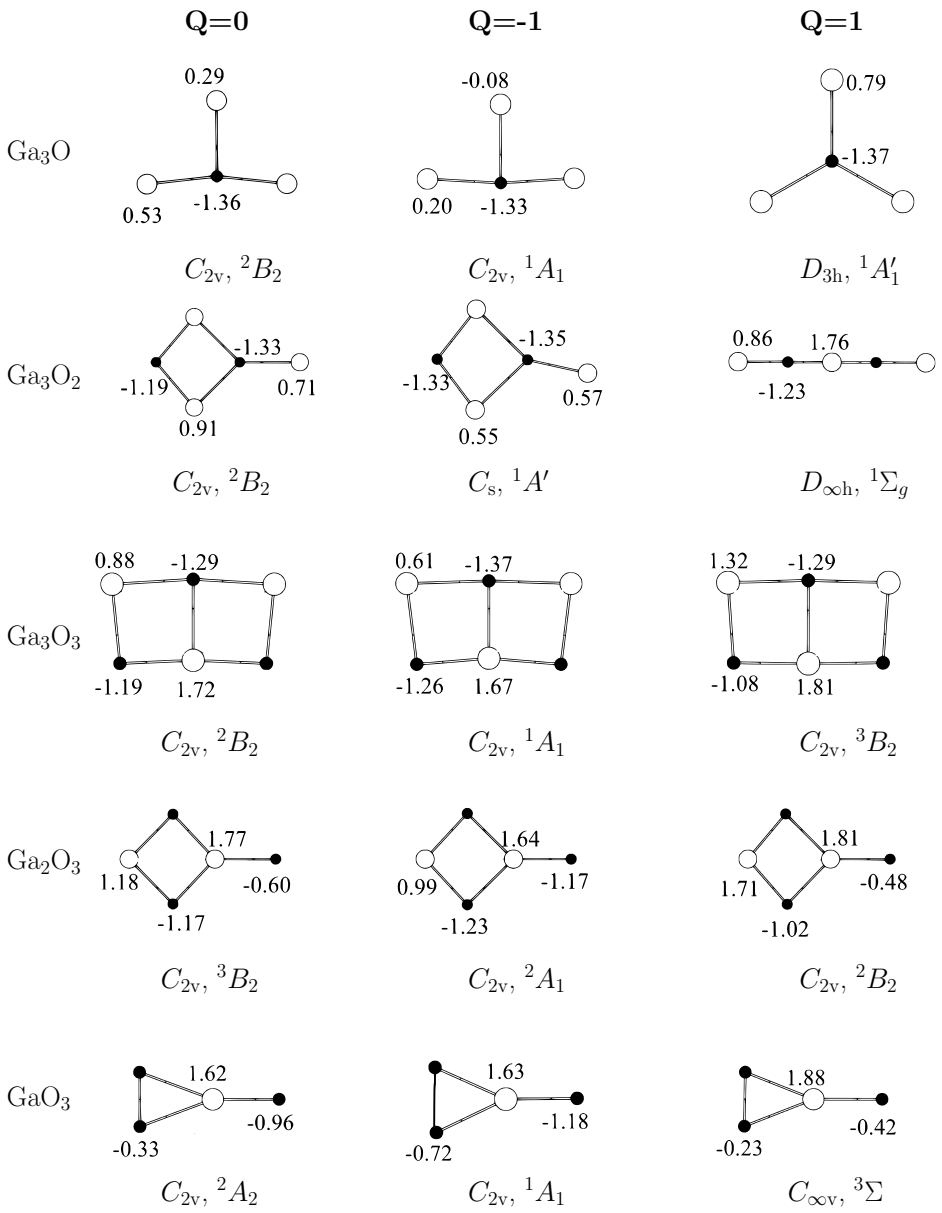

Figure 3.2: Schematic representation of most stable Ga_3O_n (n = 1 − 3) & Ga_mO_3 (m = 1, 2) clusters. Oxygen is represented by a smaller circle, while the larger one represents gallium. Numbers alongside the isomers denote the Bader charge associated with that atom.

electron in the anion cluster is localized on this orbital and this leads to the bent structure. On the other hand, removal of an electron leads to the ground state of the ionized Ga_3O cluster being an equilateral triangle with D_{3h} symmetry and R_{Ga-O} of 1.99 Å and R_{Ga-Ga} of 3.46 Å. As compared to the bond length in the neutral Ga_3O, R_{Ga-O} remained nearly the same while R_{Ga-Ga} is increased by 17%. The molecular orbital picture shows that the HOMO in the cation cluster exhibits symmetrical bonding contributions along all the three Ga-O bonds.

The topological QTAM charge analysis for the neutral and ionized lowest energy configurations provides a clue in explaining the predicted changes in the neutral ground state upon addition or removal of an electron. The oxygen charge is maintained almost constant during the ionization process. The added electron goes mainly to the gallium atoms, oxygen receiving only 3% of its charge. The distribution of the electron between gallium atoms is not equivalent, with the apex one accumulating more charge (37%) than the others (33%). In the cation cluster, the removed electron comes from the gallium atoms, leaving the oxygen atom unchanged. Employing QTAM, the molecular graphs of these clusters have been analyzed, finding that there are no Ga-Ga bonds, even in favorable situations like Ga_3O^- with a relatively short distance between the gallium atoms. This indicates a strong tendency to form Ga-O bonds. All these bonds have a positive value of the Laplacian of the electron density, indicating their ionic-like character.

Addition of an oxygen to Ga_3O leads to changes in the structural arrangement, and the lowest energy configuration comes out to be a planar rhombus-like configuration in which the extra oxygen can be seen as attached between two gallium atoms of the Ga_3O cluster. In this configuration, the minimum R_{Ga-O} is 1.85 Å, while R_{Ga-Ga} is 2.83 Å, is larger than the Ga_2 dimer bond length (2.40 Å). There is a manifestation of the preference to maximize the number of Ga-O bonds in these clusters.

$Ga_3O_2^-$ does not show any significant change in the lowest energy configuration relative to that of the neutral structure. The addition of an electron relaxes the structure slightly, breaking the symmetry and with a marginal increase in the average R_{Ga-O} in the ring and a considerable decrease of the terminal Ga-O bond distance. This is in agreement with the picture exhibited by the molecular orbitals. The neutral LUMO presents a strong bonding interaction for the terminal Ga-O that makes the anionic cluster show a shorter distance for this bond.

The removal of an electron induces significant changes in the ground state of neutral Ga_3O_2. The ground state of cationic Ga_3O_2 is a linear chain with alternate Ga-O bonds. The formation of this chain can be explained using the molecular orbitals. Since the removed electron comes from the $\alpha-$HOMO orbital which presents a bonding interaction between the ring Ga-O bonds, the ring bonding interactions decrease, and hence a linear structure is preferred for the cation.

In neutral Ga_3O_2, QTAM charges reflect the expected behavior: greater coordina-

tion index leads to greater atomic charge. The oxygen charges are relatively higher indicating an ionic nature in these bonds. In the anionic configuration, the added electron is shared mostly by the gallium atoms, although 14% is localized over the bi-coordinated oxygen. The tri-coordinated oxygen receives negligible charge. In cationic Ga_3O_2, this leads to the same average electron density charge over the oxygen atoms as that in the neutral species. The total charge over the gallium atoms is one electron less than in the neutral cluster, while the total charge over the oxygens is the same in both clusters. As happened in case of Ga_3O, a topological analysis of the electron density reveals that these clusters do not have Ga-Ga bonds. All bonds show an ionic character as Laplacian of the electron density values are positive.

The calculated ground state geometry of Ga_3O_3 is the planar window-pane C_{2v} structure with a doublet electronic state (Figure 3.2). Addition of an oxygen to Ga_3O_2 leads to a new structure containing two more Ga-O bonds. Again, one can observe a strong tendency to maximize the number of Ga-O bonds in the lowest energy isomer. In the window-pane structure, the coordination number of the inner Ga and O atoms is 3, while in the hexagonal cyclic structure, the coordination number for all atoms is 2. On the other hand, the coordination numbers of Ga atoms in the competing rhombus-like C_s structure are 3, 2 and 1. This evolutionary trend shows that maximization of the coordination number for Ga atoms appears to play an increasing role in the stability of the gallium oxide clusters.

The calculated ground state of $Ga_3O_3^-$ is similar to the one predicted for neutral Ga_3O_3. Addition of an electron to the neutral cluster relaxes the structure with an increase of 3% in the average R_{Ga-O}. The geometrical features of the ground state are also preserved in going from neutral to cation, although the electronic state becomes triplet. Overall, the energy difference between planar and non-planar structures is very high in neutral as well as in the charged configurations. The molecular orbitals picture explains the spin multiplicities of the ionized clusters. In the neutral cluster, the HOMO (b_2) is semi-occupied and the HOMO-1 (a_1) is filled and are close in energy. Removing an electron from the HOMO-1 leaves this orbital semi-occupied, leading to the final electronic state of the cluster as $^3B_2$. In the anionic case, the extra electron fills the HOMO (b_2), making the final cation electronic state $^1A_1$.

The QTAM charges for the neutral cluster show a very high value for the tri-coordinated gallium, being almost twice that of bi-coordinated gallium atoms. However, the difference in the atomic charges between tri- and bi-coordinated oxygen atoms is much smaller. In $Ga_3O_3^-$, 75% of the added electron goes to bi-coordinated gallium atoms. The extra 25% is shared more or less equally among the oxygen atoms and the tri-coordinated gallium atom. In the cationic cluster, the electron comes mainly from the external gallium atoms, giving them 68% of the added charge. One can notice that the tri-coordinated oxygen atom maintains its charge unaltered with respect to its counterpart in the neutral cluster.

Figure 3.2 shows the low lying configurations of neutral and ionic Ga_2O_3. The ground state of Ga_2O_3 is the rhombus-like C_{2v} configuration in triplet electronic state. The structure is similar to the one in Ga_3O_2 and can be viewed as a rhombus Ga_2O_2 configuration plus an oxygen atom attached to one of the Ga atoms. As compared to Ga_3O_3, the average R_{Ga-O} distance decreases from 1.92 Å to 1.85 Å.

Neither addition nor removal of an electron seems to be affecting the geometry of the lowest energy configuration of the neutral Ga_2O_3. The most stable structure of $Ga_2O_3^-$ is the doublet state. The structural features in the ground state of cationic Ga_2O_3 are similar to those calculated for the neutral case, but the removal of an electron alters the sequence of other low lying structures. The ionization process maintains the average Ga-O bond distance. In the anionic case, the extra electron goes into the neutral β-LUMO which exhibits a certain antibonding character over the Ga-O bonds linked to the terminal oxygen. This increases these Ga-O distances, while decreasing all the other Ga-O bond distances. In the cationic cluster, the electron comes from the neutral α-HOMO which presented an antibonding contribution for the bi-coordinated Ga-O bond and bonding interactions for the tri-coordinated bonds. This explains the distance changes when the electron is removed.

QTAM charge analysis shows that the extra electron is localized mainly (60%) over the external oxygen atom. The remaining electron is distributed over the rhombus, with the gallium atoms taking majority of it. In the cationic case, 50% of the electron

comes from the bi-coordinated gallium atom, while the other 50% is contributed equally by the three oxygen atoms. The Ga-O bonds are the only ones present in these structures. All of them have a positive value of the Laplacian of the electron density indicating an ionic character.

The lowest energy configuration of this oxygen-rich, GaO_3, cluster is a Y-type structure which can be considered as a GaO molecule attached to an O_2 molecule. In this configuration, the terminal R_{Ga-O} bond distance is 1.67 Å, shorter than the GaO molecule. The inner R_{Ga-O} bond distances are 1.97 Å, indicating a weak interaction with the O_2 unit. The O-O bond is much longer than the O_2 molecule (1.37 Å *versus* 1.21 Å).

Addition or removal of an electron does not significantly alter the geometry of the lowest energy neutral isomer. In the anionic case, R_{O-O} is 0.23 Å longer than that in the neutral case, but the inner R_{Ga-O} bond distances decrease significantly, making these interactions stronger than in the neutral cluster. The molecular orbital analysis allows us to interpret this as follows: the extra electron goes to the α-HOMO, partially filled in the neutral cluster, which has an antibonding character between the oxygens and a slightly antibonding character between the terminal Ga-O. The electron density localized over the O-O bond in the neutral cluster is moved in the anionic cluster towards the inner Ga-O bonds. In this way, the latter distance decreases as compared to the neutral case, the O-O distance increases and the terminal Ga-O bond decreases

marginally. Also, complete filling the α-HOMO makes the electronic state in this cluster a singlet.

In cationic GaO_3, the most stable isomer is found to be in triplet state with a triplet-singlet energy difference of 2.32 eV. The formation of this triplet can be explained by noting that the α and β-HOMO in the neutral cluster are almost degenerate. The removed electron comes from β-HOMO leaving two molecular orbitals semi-occupied. The O-O bond distance is very similar to that in the neutral case, but the inner Ga-O bond distances decrease due to the bonding character that the neutral β-HOMO had in these interactions. The terminal distance increases due to the antibonding character of these bonds.

In the neutral cluster, the QTAM charge of Ga is $1.62e$ while that of the terminal oxygen atom is -0.96e. The oxygen atoms forming the O-O bond are associated with a charge of -0.33e each. In GaO_3^-, the atomic charges show us that the extra electron is shared among the three oxygen atoms. In cationic GaO_3, 50% of the removed electron comes from the external oxygen atom, and 25% from the gallium. The topological analysis of the electron density reveals in these systems one important feature exhibited by the neutral, anionic, and cationic lowest energy isomers: the existence of the O-O bond. However, this bond presents a different character in the three clusters. In the neutral and cationic, the Laplacian of the electron density has a negative value, indicating a covalent bond or shared shell interaction. However, in

the anionic cluster, with a larger interatomic distance than the others, the Laplacian of the electron density has a positive value, prototypical of the ionic bonds or closed shell interactions. It is seen that the interatomic distance is the parameter controlling the bonding regimes [57].

Since aluminum and gallium are isovalent elements, similarities between structures of small oxide clusters of aluminum and gallium are expected. In the bulk phase, however, Al_2O_3 occurs in the α phase while Ga_2O_3 occurs in the β phase. If one follows a comparison of same size and composition gallium oxide and aluminum oxide clusters, it is found that both prefer planar structures [60, 61, 62, 63, 64]. The subtle differences in structural features can be explained by the fact that the Al-O bond is relatively stronger than the Ga-O bond. The binding energy of the AlO molecule is 2.48 eV/atom while that of the GaO molecule is 2.14 eV/atom.

Summarizing Ga_3O_n $(n = 1 - 3)$ & Ga_mO_3 $(m = 1, 2)$ clusters, it is seen that these systems have a clear preference to form the highest number of Ga-O interactions. There is no Ga-Ga bond in these clusters. Some O-O interactions in the GaO_3 family were found but no Ga-Ga interactions were noticed in the hyper-metallic Ga_3O family.

A general trend in these clusters is that they prefer low spin electronic state over the higher ones, Ga_2O_3, and the cationic $Ga_3O_3^+$ and GaO_3^+ being the exceptions. In the cationic cases, the HOMO is an semi-occupied orbital and the HOMO-1 is filled, but both orbitals are almost degenerate in energy. The removed electron comes from the

HOMO-1 instead the HOMO giving rise to a triplet electronic state.

In the metal rich clusters, the extra (removed) electron always is shared by (comes from) the gallium atoms. However, in the oxygen rich clusters, the extra electron is shared by the oxygen atoms.

The average charge over the oxygens follows a decreasing trend when the O/Ga ratio increases (-1.36, -1.26, -1.22, -0.98 and -0.54 for Ga_3O, Ga_3O_2, Ga_3O_3, Ga_2O_3 and GaO_3 respectively), while the opposite is true for the average gallium charge (0.45, 0.84, 1.22, 1.47 and 1.62), as expected. Interestingly, when the total charge transfer is divided by the number of Ga-O bonds present in the cluster (average charge transfer per bond), the values are fairly constant (0.45, 0.50, 0.52, 0.59 and 0.54). The maximum value corresponds to the stoichiometric compound, Ga_2O_3, which exhibits the highest ionicity in the series.

	O/Ga	VAE	VDE	AEA	VIP	AIP	η	H-L
Ga_3O	1/3	0.74	0.98 (1.68)	0.88 (1.57)	5.95	5.40	2.49	2.31
Ga_3O_2	2/3	1.91	2.25 (2.29)	2.08 (2.18)	7.67	6.34	2.71	2.34
Ga_3O_3	3/3	2.88	3.06 (2.96)	2.95 (2.80)	8.10	8.04	2.52	1.55
Ga_2O_3	3/2	2.87	3.40 (3.71)	3.13	9.59	9.39	3.10	2.71
GaO_3	3/1	2.13	3.61	2.97	10.22	9.71	3.31	2.55

Table 3.8: Vertical Attachment Energy, Vertical Detachment Energy, Adiabatic Electron Affinity, Adiabatic Ionization Potential, Chemical Hardness and HOMO-LUMO gap (eV) of Ga_3O_n ($n = 1 - 3$) & Ga_mO_3 ($m = 1, 2$) clusters. Values given in parenthesis for VEA and AEA correspond to aluminum oxide clusters.

Table 3.8 presents the calculated values of VAE, VDE, AEA, IP and chemical hardness

(η) for the clusters considered. The electron affinity results show an increasing trend of these values when the number of oxygen atoms in the cluster increases. The explanation of this behavior is that the clusters that have an excess of oxygen atoms are electron deficient and thus present high electron affinity values. In this way, it is important to notice that the addition of oxygen in Ga_3 significantly reduces the EA from 1.68 [65] to 0.98. This fact seems to go against the previously observed trend, but one should note that there is a noticeable change in the nature of bond when the Ga_3 (metallic) cluster is oxidized to form three Ga-O bonds (ionic). The IP values increase with a increasing oxygen-gallium ratio. Again, the electron deficient oxygen rich clusters offer a strong resistance to removed an electron.

The calculated values are compared with those reported in the photoelectron spectroscopy experiments on small aluminum oxide clusters [60, 61]. EA values increase gradually in going from M_3O to M_2O_3 (where M = Al, Ga). In accordance with the periodic group evolution of this property, the values for alumina are higher than those predicted in this study for the gallium clusters. A quantification of the concept of chemical hardness [66] for a particular system is defined as

$$\eta \approx \frac{\text{IP} - \text{EA}}{2} \approx \frac{\text{HOMO} - \text{LUMO}}{2} \tag{3.2}$$

where IP and EA are the first vertical ionization energy and electron affinity of the

chemical species. Thus, the increase in the oxygen to metal ratio is found to increase the chemical hardness of the clusters considered here. This can also be observed in the HOMO-LUMO gap of these clusters (Table 3.8).

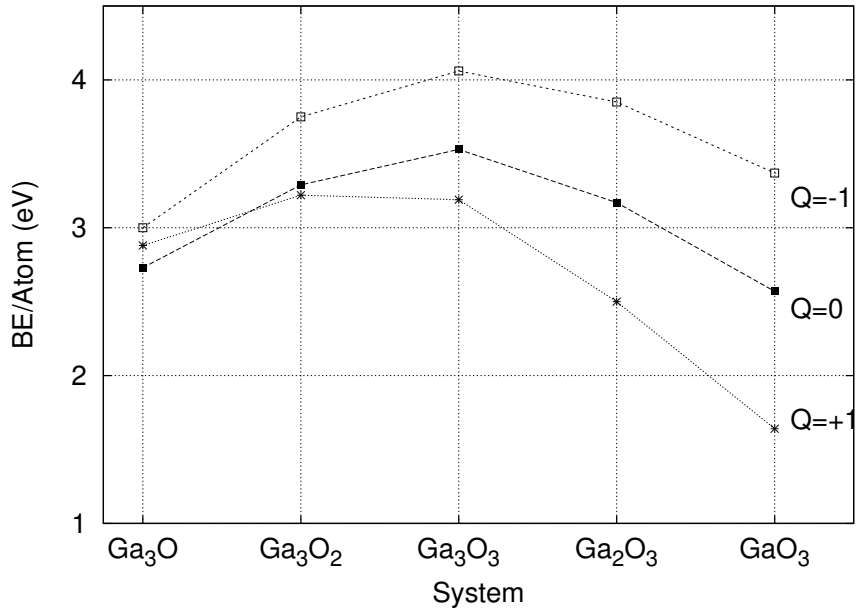

Figure 3.3: Binding energy per atom of the most stable neutral and ionic Ga_3O_n $(n = 1 - 3)$ & Ga_mO_3 $(m = 1, 2)$ clusters.

The HOMO-LUMO gap for the neutral configurations varies from 1.55 to 2.71 eV. The band gap value in the bulk monoclinic Ga_2O_3 is 4.80 eV [33], whereas in the neutral cluster configurations the highest value is 2.71 eV. Due to differences in the structural configuration, a trend in the energy gap is not seen with the increase in the oxygen to metal ratio in these clusters.

The stability of neutral and charged gallium oxide clusters with respect to their constituent atoms can be characterized by the binding energy. Figure 3.3 shows the

binding energy per atom, which first increases with the oxygen/metal ratio and attains maximum at Ga_3O_3. It then decreases in the oxygen-excess clusters, being lowest for GaO_3. Anionic clusters are relatively more stable with respect to both neutral and cationic clusters. For the neutral cluster, the curve is more or less symmetric with respect to the maximum at Ga_3O_3. One can observe that the metal rich clusters are slightly more stable than their oxygen rich counterparts. This trend is maintained for the cationic cluster with the Ga-excess linear Ga_3O_2 cluster being the most stable, but the oxygen excess anions are more stable than the metal excess anions. This behavior can be explained as follows: when an electron is added to the neutral system, it tends to stabilize over the more electronegative oxygen atoms in the oxygen rich clusters. A part of this electron has to be shared by the Ga atoms in the metal rich clusters, which is a less favorable situation. However, the removed electron comes mainly from the Ga atoms. As a result, the metal rich clusters are more stable in the ionization process. The average coordination indices for these clusters are 0.75, 1, 1.16, 1 and 1 for Ga_3O, Ga_3O_2, Ga_3O_3, Ga_2O_3 and GaO_3 respectively. The behavior of these curves can be explained using this magnitude: Ga_3O_3 is the most stable cluster because it has the highest average coordination index.

The results on the relative stability of the neutral and singly ionized clusters with respect to their fragmentation into atoms or clusters are also presented. Only the lowest energy configuration for each of the clusters involved was considered, neglecting contributions from the zero point vibration energy. Table 3.9 presents the energy

	Neutral			Anion			Cation		
	O	O_2	GaO	O	O_2	GaO	O	O_2	GaO
Ga_3O	-7.2		-5.2	-6.5		-4.8	-8.2		-6.8
Ga_3O_2	-5.5	-7.3	-2.8	-6.7	-7.8	-5.0	-4.6	-7.4	-4.7
Ga_3O_3	-4.7	-4.9	-4.2	-5.6	-6.9	-4.9	-3.0	-2.2	-5.0
Ga_2O_3	-3.1	-1.1	-4.1	-4.0	-4.3	-3.9	-2.7	-1.1*	-4.3
GaO_3	-2.7	-0.6	-0.6	-2.3	-1.3	-2.8	-2.6	-0.7	-3.5

Table 3.9: Fragmentation energies (eV) of Ga_3O_n ($n = 1 - 3$) and Ga_mO_3 ($m = 1, 2$) clusters via loss of oxygen atom, oxygen molecule, and GaO molecule. [*: Geometry of Ga_2O^+ is taken to be the first (linear) in Fig. 3.1]

associated with the fragmentation channels via loss of O, O_2 and GaO (the total energies in hartree of O, O_2 and GaO are -75.06062, -150.32004 and -1998.09669 respectively). The fragmentation energy is defined as:

$$E_{\text{Fragmentation}} = E_{\text{Cluster}} - E_{\text{Fragment1}} - E_{\text{Fragment2}} \tag{3.3}$$

Thus, the cluster is said to be stable with respect to the particular fragments if the fragmentation energy is negative. In this case, the fragment 2 is either O, O_2, or GaO. It is found that all clusters are stable against fragmentation by the channels considered in this study. One finds that neutral and anionic clusters tend to favor the GaO channel, while the cationic ones favor the O_2 channel in general. The preference of the O_2 channel over the O channel for the loss of oxygen is greater in oxygen rich clusters, while the opposite is true for the metal rich clusters.

The configurational stability of the ground state of the neutral and ionic clusters

considered has further been investigated by computing their vibrational frequencies under the harmonic approximation. Table 3.10 presents the vibrational frequencies of the lowest energy isomer for the neutral, anionic and cationic clusters.

Ga_3O^-	Ga_3O	Ga_3O^+	$Ga_3O_2^-$	Ga_3O_2	$Ga_3O_2^+$	$Ga_3O_3^-$	Ga_3O_3	$Ga_3O_3^+$
123	86	78	34	33	36	102	107	110
137	93	78	72	85	36	130	132	144
153	126	169	129	185	112	138	154	170
231	243	232	182	203	112	246	189	255
417	384	484	238	272	196	252	258	257
597	577	484	270	276	213	266	272	283
			567	522	213	380	451	507
			641	576	319	461	494	508
			723	705	819	568	498	568
					924	570	544	659
						686	672	701
						785	767	751

(a) Ga_3O, Ga_3O_2 and Ga_3O_3

$Ga_2O_3^-$	Ga_2O_3	$Ga_2O_3^+$	GaO_3^-	GaO_3	GaO_3^+
137	131	133	175	59	86
162	145	140	182	138	122
243	248	255	510	278	412
272	281	289	550	503	537
459	516	467	790	888	712
555	587	538	880	1123	1070
611	625	674			
667	643	705			
839	724	735			

(b) Ga_2O_3 and GaO_3

Table 3.10: Vibrational frequencies of the most stable neutral, anionic and cationic Ga_3O_n ($n = 1 - 3$) and Ga_mO_3 ($m = 1, 2$) clusters. The frequency values are given in cm^{-1}.

In the hyper-metallic family, Ga_3O, Ga_3O^-, and Ga_3O^+, the first three modes are

related to the bending movement (both in plane and out of plane) of all bonds. In the neutral Ga_3O, the sequence is: bending in plane of the apex Ga-O bond, bending in plane of the other two Ga-O bonds, and bending out of plane of the oxygen atom. In the cationic cluster all the bonds are equivalent by symmetry and the first two degenerate modes involve the bending in plane of all Ga-O bonds, and the next non-degenerate one is related to the out of plane bending of the oxygen atom. For the anionic cluster, there is a different relative ordering, as displayed by the symmetry labels. For neutral and anionic clusters, the three higher frequency modes correspond to the symmetric stretching of the equivalent Ga-O bonds, the asymmetric stretching of the apex Ga-O bond, and the asymmetric stretching of the equivalent Ga-O bonds. For the cationic cluster, the degenerate mode involves the asymmetric movement of all bonds and the a_1' reflects the symmetric displacement. A correlation between the interatomic distance and the vibrational frequency trends can be observed..

Although their symmetry is different Ga_3O_2 and $Ga_3O_2^-$ present very similar structures. The first three modes correspond to the in plane bending of the ring, and the asymmetric and symmetric bending out of plane of the oxygen atoms. The remaining vibrational frequencies are stretching modes: the lowest one displays a symmetric stretching of Ga-O bonds in the ring closer to the Ga-O terminal bond, the next one is related to the symmetric stretching of the ring Ga-O bonds, followed by the asymmetric stretching of Ga-O bonds in the ring closer to the Ga-O terminal bond, the next two modes correspond to the symmetric and asymmetric movement of the

terminal Ga-O bond, and the last mode presents the symmetric stretching of all Ga-O bonds: ring and terminal. Since the structure for the cationic cluster is linear, it has an extra vibrational mode, and we present a separate description of its normal vibrational modes. Briefly, the two first degenerate modes correspond to the asymmetric out of plane bending of the oxygen and gallium atoms, respectively. The following movement with σ_g symmetry corresponds to the symmetric stretching of terminal Ga-O bonds. The π_u degenerate normal mode shows the symmetric bending out of plane of the oxygen atoms. The last three modes represent stretching movements: the first is the stretching of all bonds in the cluster, the next two are the symmetric and asymmetric stretching of the oxygen atoms. A clear relationship between the interatomic distances and the frequency values is observed.

Ga_3O_3 and the corresponding charged clusters belong to the same symmetry point group, and as can be seen in Table 3.10 they follow the same ordering of the vibrational modes for the neutral, anion and cation. The only exception is $Ga_3O_3^+$, where the 9^{th} and the 11^{th} mode are interchanged. The lower frequency modes correspond to the bending and torsion movements: first one corresponds to the out of plane bending of the central oxygen; the next one displays the asymmetric bending out of plane of the terminal oxygen atoms, followed by the asymmetric in plane bending of the gallium atoms. The fourth mode is the torsion of the ring, generated by the movement of gallium atoms, and the last bending mode corresponds to the symmetric out of plane displacement of all oxygen atoms. The remaining modes are stretching movements.

A brief description of them follows: the first one is an asymmetric stretching of the two Ga-O bonds with the tri-coordinated oxygen atom; the next mode shows the asymmetric stretching of the two Ga-O bonds perpendicular to the previous mode. The third stretching mode exhibits the movement of inner Ga-O bond. The next one is equivalent to the first stretching mode but the stretching is symmetric. The 10^{th} and 11^{th} modes reflect the symmetric and asymmetric stretching of all Ga-O bonds, and the last one indicates the symmetric displacement of all Ga-O bonds except the inner one.

Neutral, anionic and cationic Ga_2O_3 again exhibit the same symmetry in their lowest energy isomer and in Table 3.10 one can notice the same ordering of their normal vibrational modes. As expected, the lower frequency modes are related to the bending vibrations: the first one is the out of plane bending of the terminal Ga-O bond, followed by the bending in plane of this bond, and the last bending mode corresponds to the out of plane displacement of the ring Ga-O bonds. The first stretching mode shows the asymmetric movement of ring gallium atoms. The next two modes represent the symmetric and asymmetric torsion movements of the ring oxygen atoms. The next mode corresponds to the stretching of the ring oxygen atoms. The two highest frequency values are related to the symmetric and asymmetric stretching of all oxygen atoms, respectively.

Finally, all clusters in the GaO_3 family also belong to the same point group and they

will be discussed together. As is the case with other clusters, the lower vibrational frequencies are related to the bending movements. In this case, the first one corresponds to the asymmetric in plane bending of the oxygen atoms. The second one is the bending out of plane of the terminal oxygen atom. The third mode corresponds to the torsion of the O-O bond. The next one is the asymmetric stretching of the two ring Ga-O bonds. The last two modes represent different movements in the neutral and ionic clusters: the first one is stretching of the terminal Ga-O bond and the last one is stretching of the O-O bond. Due to the weakness of the bonds between the Ga bridge and the O-O group, the terminal Ga-O group is very similar to the free GaO molecule ($R_{\mathrm{Ga-O}}$ 1.74 Å experimental value [34]). The O-O group is similar to the O_2 molecule (1.21 Å experimental value [34]) but with a larger distance (1.38 Å, and 1.39 Å for the GaO_3 and GaO_3^+, respectively). Accordingly, the Ga-O stretching is larger than that of GaO molecule (767 cm^{-1}, experimental value [34]) for the neutral cluster and a little bit smaller for the cationic one, while the O-O stretching is smaller than the O_2 frequency (1581 cm^{-1} experimental value [34]) in both clusters. The two remaining modes in the anionic cluster represent a different behavior with respect to these modes in their in neutral and cationic counterparts. Larger interatomic distance of O-O group along with the shortening of the bond length between this group and the Ga bridge explains this different behavior. In this way, the vibrational movements are coupled, contrary to what was observed in the neutral and cationic clusters. These modes involve the symmetric and asymmetric stretching of all bonds in the cluster.

3.3.3 Ga_3O_n $(n = 4 - 8)$

An extensive search for the ground state of Ga_3O_n clusters was performed which included several two- and three-dimensional configurations. For example, some of the initial structures for Ga_3O_4 are schematically represented in Fig. 3.4 which are based on an addition of GaO_2 to Ga_2O_2, an addition of O_2 to Ga_3O_2, and an addition of O to Ga_3O_3. Linear structures considered in this study were found to have higher energies compared to ground state structures. Other structures, not shown in Fig. 3.4, can be obtained by appropriately interchanging gallium and oxygen atoms. Since the neutral Ga_3O_n clusters have an odd number of electrons, calculations were carried out in doublet and quartet spin states for neutral, and singlet and triplet spin states in singly charged clusters, all of them within the unrestricted spin scheme. In order to verify the stability of the lowest energy configurations, vibrational frequencies were computed under the harmonic approximation, with analytical force constants.

Table 3.11 presents the total energy, electronic state, symmetry, Ga-O (R_{Ga-O}) and O-O (R_{O-O}) bond distances corresponding to the most stable isomers of neutral and ionic oxide clusters. Lowest energy isomers in the case of neutral clusters were found in doublet electronic state whereas charged clusters displayed triplet spin states, except for $Ga_3O_4^-$, $Ga_3O_4^+$ and $Ga_3O_5^-$, which were singlets.

In neutral Ga_3O_4 (Fig. 3.5), the lowest energy isomer is found to consist of two

	E	$^{2S+1}\Lambda$	Sym.	$R_{\mathrm{Ga-O}}$	$R_{\mathrm{O-O}}$
Ga_3O_4					
Q=0	-6069.80494	$^2B_2$	C_{3v}	1.86, 1.95	-
Q=-1	-6069.92380	$^1A'$	C_s	1.70, 1.77, 1.78, 1.90, 1.93, 1.99	-
Q=1	-6069.50239	$^1A_1$	C_{3v}	1.85, 1.93	-
Ga_3O_5					
Q=0	-6144.99150	$^2A''$	C_s	1.79, 1.82, 1.86, 1.92, 1.93, 2.00	-
Q=-1	-6145.12939	$^1A_1$	C_{2v}	1.69, 1.77, 1.90, 1.93	-
Q=1	-6144.67329	$^3B_2$	C_{2v}	1.78, 1.79, 1.84, 1.87, 1.99	-
Ga_3O_6					
Q=0	-6220.15670	$^2A_1$	D_{3h}	1.80, 1.82	-
Q=-1	-6220.31820	$^3A''$	C_s	1.79, 1.84, 1.86, 1.92, 1.95, 1.98	-
Q=1	-6219.85077	$^3A''$	C_s	1.78, 1.79, 1.84, 1.85, 1.87, 1.92	1.39
Ga_3O_7					
Q=0	-6295.34003	$^2B_1$	C_{2v}	1.80, 1.82, 1.96	1.37
Q=-1	-6295.48407	$^3B_1$	C_{2v}	1.80, 1.81, 1.82, 1.90, 1.91, 1.99	1.37
Q=1	-6295.02820	$^3B_2$	C_{2v}	1.78, 1.85, 1.86, 2.00	1.39
Ga_3O_8					
Q=0	-6370.52323	$^2A_1$	C_{2v}	1.80, 1.81, 1.82, 1.96	1.37
Q=-1	-6370.67418	^3A	C_1	1.80, 1.85, 1.90, 1.93, 1.94, 2.00	1.37
Q=1	-6370.17319	$^3B_2$	C_{2v}	1.77, 1.80, 1.83, 1.96	1.27

Table 3.11: Total energy (hartree), electronic state, symmetry and interatomic distance (Å) of the most stable configurations of Ga_3O_n ($n = 6 - 8$) clusters.

equilateral triangles, one of oxygen atoms and another one of gallium atoms on its top, with the fourth oxygen above the gallium triangle. Alternatively, this C_{3v} structure can be visualized as an oxygen tetrahedron intercepted by a gallium triangle. The bond distance between any gallium atom to an oxygen atom at the base of the tetrahedron is 1.86 Å while that to the apical oxygen is 1.95 Å.

Upon addition of an electron, window-pane structure becomes the lowest energy isomer in anionic Ga_3O_4. In the anionic window-pane cluster, $R_{\mathrm{Ga-O}}$ varies between 1.70 - 2.03 Å. Based on Mulliken population analysis, the three gallium atoms ac-

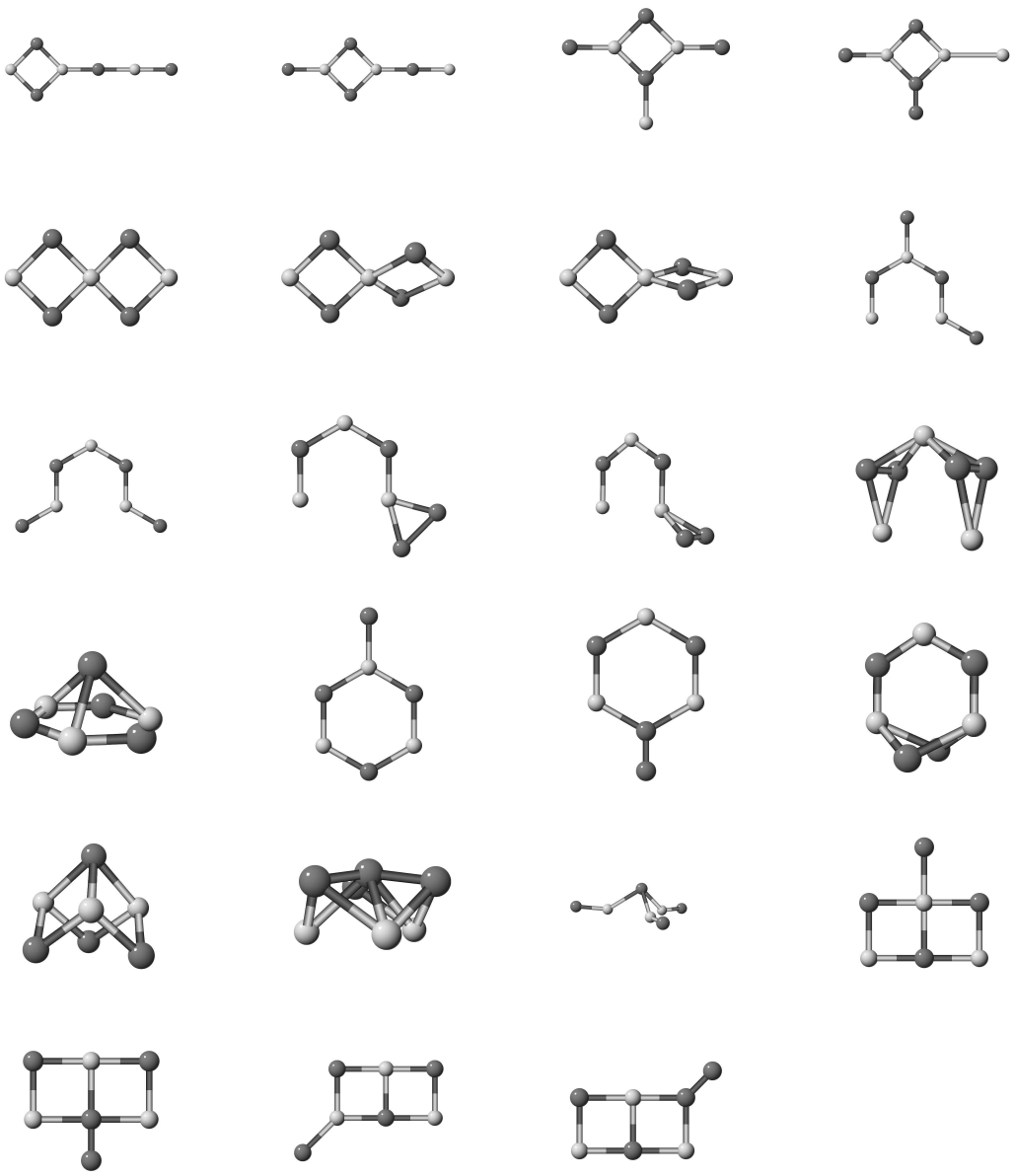

Figure 3.4: Schematic representation of initial structures considered for Ga_3O_4. Smaller (lighter shade) spheres represent gallium atoms while while larger (darker shade) ones represent oxygen atoms.

count for most of the added electron (63%) to the neutral cluster. Removal of an electron, however, has almost no effect on the structural parameters. In the lowest energy cationic isomer, the electron mainly comes out of gallium atoms.

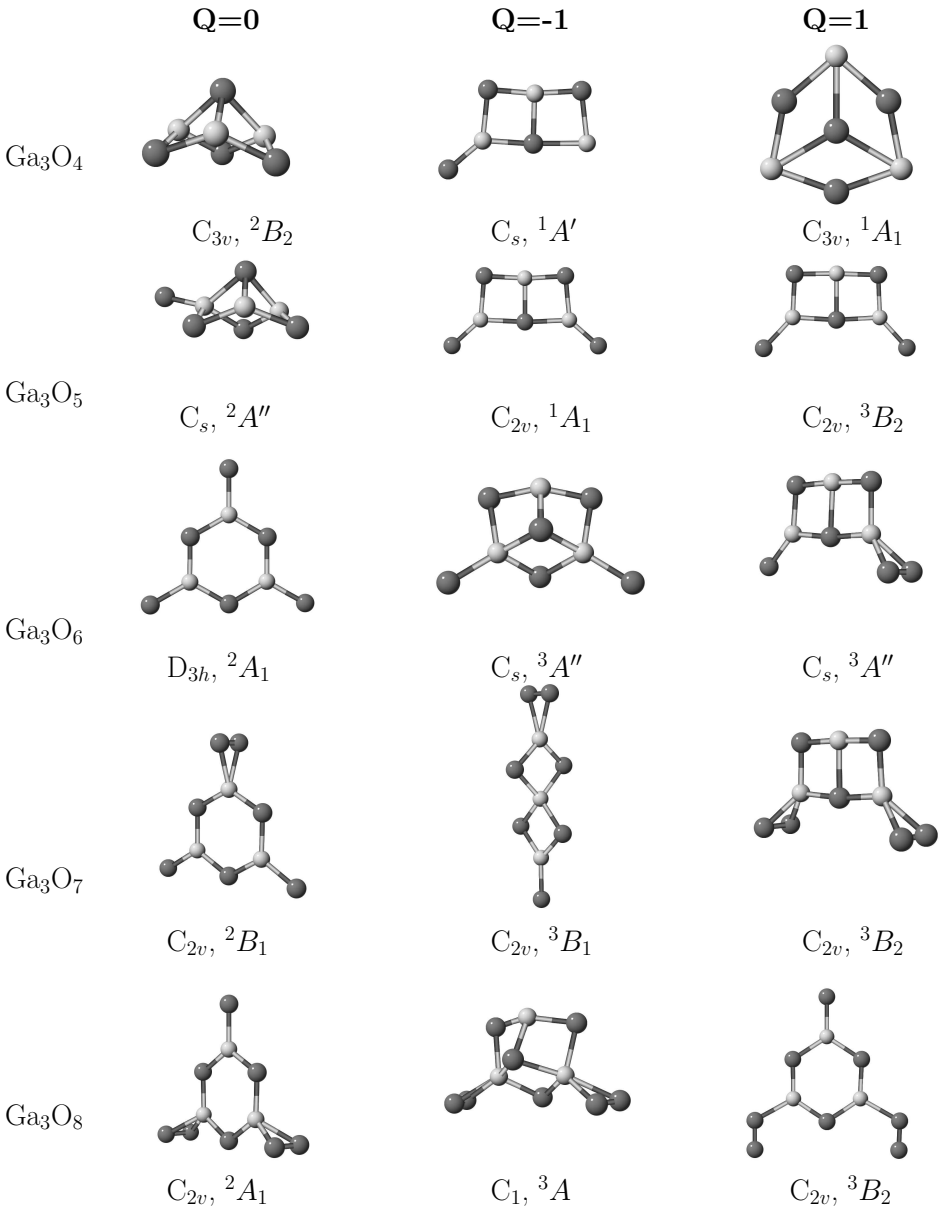

Figure 3.5: Most stable structures of neutral and ionic Ga_3O_n (n = 4 − 8). Smaller (lighter shade) spheres represent gallium atoms while while larger (darker shade) ones represent oxygen atoms.

In the case of Ga_3O_5 (Fig. 3.5), the most stable structure is an extension of the corresponding structure in Ga_3O_4, with an additional oxygen attached to one of the

gallium atoms leading to C_{2v} symmetry for the isomer. Similar to Ga_3O_4, the anionic cluster has a window-pane C_{2v} geometry as the lowest energy isomer, and the added electron is shared by the gallium and the terminal oxygen atoms. Unlike neutral Ga_3O_4, removal of an electron leads to a significant change in the geometry of the lowest energy isomer of cationic Ga_3O_5. The structure appears very much similar to the corresponding anionic isomer but in triplet spin state. Gallium atoms and the terminal oxygen atoms contribute almost equally to the removed electron.

The lowest energy isomer of neutral Ga_3O_6 (Fig. 3.5) has a planar hexagonal arrangement of gallium-oxygen atoms, with three oxygens attached to gallium atoms forming a D_{3h} structure. R_{Ga-O} is 1.80 Å in the ring and 1.82 Å for terminal bonds. The lowest energy isomer in the anionic case is a distorted three-dimensional window-pane C_s structure, with an oxygen cap in the triplet spin state. Removal of an electron also changes the geometrical appearance of the lowest energy isomer - a pyramidical structure in triplet state, with an O_2 bond attached to one of the window-corner gallium atoms. R_{Ga-O} ranges between 1.78 - 1.92 Å and R_{O-O} is about 1.39 Å.

The most stable isomer of neutral Ga_3O_7 (Fig. 3.5) shows a preference for O-O bonds and the structure can be visualized as an extension of Ga_3O_6 - with an extra oxygen atom attached to one of the apical oxygen atoms (C_{2v}). The average R_{Ga-O} remains almost the same as in the previous system (1.84 Å) and R_{O-O} is about 1.37 Å. The lowest energy isomer in the case of $Ga_3O_7^-$ is a twisted rhombic pair in triplet

state with C_{2v} symmetry and two tetrahedrally-coordinated Ga atoms. This isomer exhibits strong Ga-O interactions with R_{Ga-O} ranging between 1.80 - 1.99 Å and the O_2 bond distance is about 1.37 Å. The added electron is shared almost equally by the gallium and terminal oxygen atoms compared to the corresponding neutral isomer. The lowest energy cationic isomer is a window-pane with O_2 units attached to each of the window-corner gallium atoms.

The lowest energy isomer of neutral Ga_3O_8 (Fig. 3.5) can be visualized as an extension of Ga_3O_7 with the extra oxygen attached to another of the terminal oxygens, thus forming a pair of handles (C_{2v}). The lowest energy isomer in anionic case is also a three dimensional structure analogous to neutral Ga_3O_4 with two extra O-O bonds (attached to the gallium atoms at the corner) and an oxygen cap over the gallium triangle. Nearly half of the added electron is shared by the gallium atoms. The lowest energy isomer in $Ga_3O_8^+$ has a hexagonal ring structure similar to the neutral isomer; however, the two O_2 units are bonded asymmetrically (that is, with a Ga-O bond and an O-O bond), whereas in the neutral case they were symmetrically bonded (two Ga-O bonds and an O-O bond).

To understand the structural changes induced by the sequential oxidation as well as the addition (or removal) of an electron, many structural indices may be defined to classify the different structures. They may be grouped into four families. First, pyramid-like structures with terminal O or O_2 units (Ga_3O_4, Ga_3O_5, $Ga_3O_6^-$

and $Ga_3O_8^-$); they can be seen as a non-planar ring Ga_3O_3 structure with an O on top of the Ga, forming an irregular tetrahedron with the other three O atoms. Second, window-pane-like structures ($Ga_3O_4^-$, $Ga_3O_5^-$, $Ga_3O_5^+$, $Ga_3O_6^+$ and $Ga_3O_7^+$), in which the Ga_3O_3 subunit is planar consisting of two bonded squares sharing an edge. Third, hexagonal-like structures ($Ga_3O_4^+$, Ga_3O_6, Ga_3O_7, Ga_3O_8 and $Ga_3O_8^+$), where the Ga_3O_3 unit is a planar, almost regular alternating hexagon. And finally, $Ga_3O_7^-$ displays a chain-like structure with two tetrahedrally co-ordinated Ga and a tri-coordinated Ga. It is to be noted here that the bond length in the the Ga_3O_3 backbones of the first three families remains nearly the same. Based on the choice of $\overline{R}_{\rm BB}$ as the average $R_{\rm Ga-O}$ in the the Ga_3O_3 backbones, one finds $\overline{R}_{\rm BB}$ to be about 1.89 Å in pyramid-like structures, while that for window-pane, it's about 1.86 Å; hexagonal and chain-like structures both have 1.88 Å for $\overline{R}_{\rm BB}$, though there are slight deviations due to positive (or negative) charge states of the clusters.

System	O/Ga	VAE	VDE	AEA	AIP	VIP	η	H-L
Ga_3O	0.33	0.74	0.98	0.88	5.40	5.95	2.49	2.31
Ga_3O_2	0.66	1.91	2.25	2.08	6.34	7.67	2.71	2.34
Ga_3O_3	1.00	2.88	3.06	2.95	8.04	8.10	2.52	1.55
Ga_3O_4	1.33	2.87	6.92	3.23	8.23	8.27	0.68	2.52
Ga_3O_5	1.66	2.94	4.30	3.75	8.66	10.19	2.95	3.25
Ga_3O_6	2.00	1.97	5.54	4.39	8.32	11.23	2.85	3.63
Ga_3O_7	2.33	3.31	5.38	3.92	8.48	13.38	4.00	3.32
Ga_3O_8	2.66	1.93	5.22	4.11	9.53	10.26	2.52	3.34

Table 3.12: Vertical Attachment Energy, Vertical Detachment Energy, Adiabatic Electron Affinity, Vertical Ionization Potential, Adiabatic Ionization Potential, Chemical Hardness (η) and HOMO-LUMO gap of Ga_3O_n ($n = 6 - 8$) clusters. Values are in eV.

Table 3.12 presents AEA, VDE, AIP and VIP values as a function of O/Ga ratio. All these four quantities show an oscillatory trend. As a result, chemical hardness [66] also inherits a similar oscillatory trend. The observed trend can be explained on the basis that oxygen rich clusters have electron efficiency and thus present high EA and IP values. This table also presents VAE, defined as the energy difference between the neutral and anionic clusters, with both at the optimized geometry of the neutral cluster. Though this is unattainable through any experiment, it nevertheless provides a lower limit to AEA, in much the same way that VDE provides an upper limit [59]. Table 3.12 also contains HOMO-LUMO gap values for the most stable neutral isomers. Structural differences between the five systems considered in this study leads to an oscillatory trend of this quantity with the increase in O/Ga ratio.

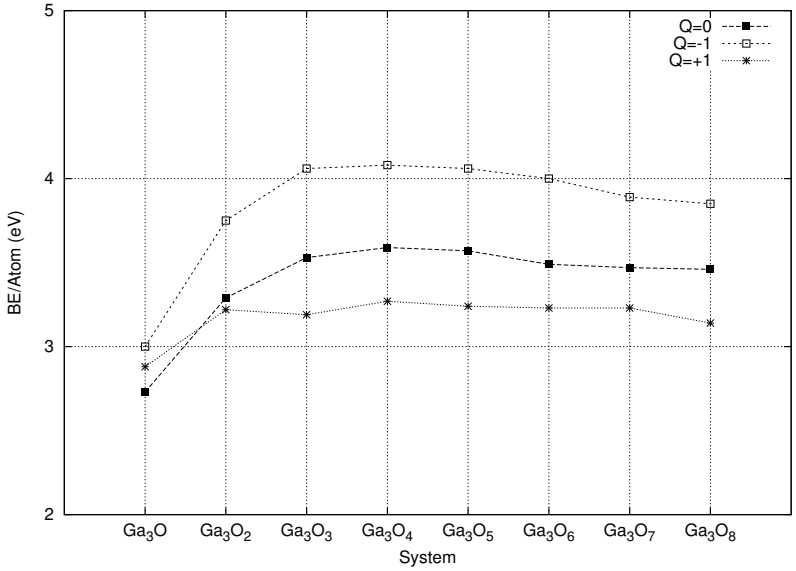

Figure 3.6: Binding energy per atom of the most stable neutral and ionic Ga_3O_n clusters ($n = 1 - 8$).

The calculated results on Ga_3O_n clusters are compared with those on Al_3O_n clusters to gain insight into the chemistry of the oxygen-rich clusters when one goes from aluminum to gallium. It is observed that the lowest energy isomers of neutral Ga_3O_n $(n : 4 - 8)$ resemble the corresponding alumina clusters [67]. Some of the anionic isomers also bear similarity to their alumina counterparts. For neutral Ga_3O_4, the ground state is similar to the one reported for Al_3O_4 by Martinez *et. al.* [68]. The anionic lowest energy isomer is similar to the second lowest energy isomer of $Al_3O_4^-$, reported by Martinez *et. al.* [68]. Al_3O_5 sequence, as reported by Martinez *et.al.* [63], does not have a structure similar in appearance to the lowest energy isomer of Al_3O_4. However, the second lowest energy isomer of $Ga_3O_5^-$ corresponds to the most stable of Al_3O_5 structures. Second and third isomers for $Ga_3O_5^-$ appear exactly as in the $Al_3O_5^-$ case.

VDE values of Ga_3O_n $(n = 4, 5)$ are compared with the results from photo-electron spectroscopy measurements on alumina clusters [60, 61] and these values follow the expected trend. Comparing AEA and VDE values for Ga_3O_n $(n = 4 - 8)$ with corresponding alumina ones [67] the values decrease with an increase in O/Ga ratio, except AEA for Ga_3O_8, similar to alumina clusters.

On a comparative note, the oxygen-rich clusters of alumina and gallia are at a nearly equal footing; they are similar when it comes to tendency to form O-O bonds and trend of electronic properties, yet there are subtle differences when it comes to the

structure of the lowest energy isomers.

The stability of neutral and ionic clusters with respect to the constituent atoms is characterized by the binding energy (BE). Figure 3.6 displays the BE/atom values (in eV) as a function of O/Ga ratio. Here, the values for Ga_3O, Ga_3O_2 and Ga_3O_3 are taken from a previous study [69]. Values for neutral clusters increase with O/Ga ratio up to Ga_3O_4 and tend to remain almost constant with a value of about 3.5 eV. The BE/atom values for ionic clusters follow a trend similar to the neutral cluster exhibiting the expected behavior: anionic ones being more stable and cationic ones less stable, compared to the respective neutral counterparts. While computing the binding energy of ionic clusters, the added electron was assigned to oxygen and the removed electron was assigned to gallium, in accordance with Pauling's electronegativity values (O: 3.5 and Ga: 1.6).

System	O/Ga	$Q = 0$		$Q = -1$		$Q = +1$	
		O	O_2	O	O_2	O	O_2
Ga_3O	0.33	-7.20	–	-6.50	–	-8.20	–
Ga_3O_2	0.66	-5.50	-7.30	-6.70	-7.80	-4.60	-7.40
Ga_3O_3	1.00	-4.70	-4.90	-5.60	-6.90	-3.00	-2.20
Ga_3O_4	1.33	-3.94	-3.27	-4.23	-4.42	-3.75	-1.38
Ga_3O_5	1.66	-3.43	-1.96	-3.95	-2.77	-3.00	-1.37
Ga_3O_6	2.00	-2.85	-0.86	-3.49	-2.02	-3.18	-0.77
Ga_3O_7	2.33	-3.34	-0.78	-2.86	-0.94	-3.18	-0.95
Ga_3O_8	2.66	-3.34	-1.27	-3.52	-0.98	-2.30	-0.07

Table 3.13: Fragmentation energies (eV) of neutral and ionic Ga_3O_n ($n = 1 - 8$) clusters via loss of oxygen atom and oxygen molecule. Negative value of the energy means the cluster is stable.

Presented in Table 3.13 are the fragmentation energies of the most stable neutral and ionic clusters considered in this study via either the loss of an oxygen atom or the oxygen molecule. Zero-point energy vibrational energy contributions have been neglected. The definition given by Eqn. (3.3) was used with fragment 2 being either O or O_2. Neutral and ionic clusters show a preference for the O_2 channel, though from the values in Table 3.13, one finds that all clusters are stable against both fragmentation channels considered. Fragmentation is easier when losing O_2 molecules, except in the smaller clusters: Ga_3O_2, Ga_3O_3 and $Ga_3O_3^-$ and $Ga_3O_4^-$.

Stability of the lowest energy isomers of neutral, anionic and cationic clusters was further investigated by analysis of vibrational frequencies, computed under the harmonic approximation. Almost all modes were found to correspond to Ga-O related displacements and the existence of frequencies corresponding to O-O stretching ($>$ 1000 cm^{-1}) confirmed the tendency of Ga_3O_7, Ga_3O_8 (neutral as well as charged) and $Ga_3O_6^+$ to prefer the formation of O-O bonds.

3.4 Conclusions

It is found that the DFT-B3LYP theoretical scheme and the 6-31G** give very good results for the small polyatomic gallium oxide clusters. The effect of including the diffuse function in the basis set is negligible even for anionic clusters. All clusters are pseudo-ionic and present low spin electronic states. The only exception is GaO_2^+ which was found in a triplet electronic state: formed by a Ga^+ singlet weakly bonded to O_2 triplet. All lowest energy isomers are dominated by the pseudo-ionic Ga–O bonds over the metal-metal or the oxygen-oxygen bonds, with the exception of GaO_2^+. Regarding controversy over the structure of the ground state of Ga_2O, DFT-B3LYP calculations support the linear structure. The atomic charges corroborate the high ionicity picture showing that the charge transfer to a given atom increases with its coordination index. Ga_2O^- is revealed as an unstable system due to the excess of electronic charge. This instability is reflected in the topology of the electronic density, the electron affinity, the orbital energy, and the HOMO-LUMO gap. The electron affinity increases in going from the gallium excess clusters to the oxygen excess clusters as expected.

The results for neutral and ionic Ga_3O_n ($n = 1 - 3$) & Ga_mO_3 ($m = 1, 2$) clusters show a trend similar to that of aluminum oxide. All cluster configurations preferred planar configurations over three dimensional structures with the lowest spin state, with the exception of Ga_2O_3, $Ga_3O_3^+$ and GaO_3^+. The analysis of molecular orbitals indicates that Ga-O interactions play a dominant role in deciding the stability of the cluster.

Except in Ga_3O, anionic clusters are more stable than neutral, and these are more stable than cationic clusters. Binding energy is seen to increase with oxygen content and is maximum at Ga_3O_3, and then decreases with reduction in metal content. These systems do not show any Ga-Ga bonds and a preference to maximize the number of Ga-O bonds is observed. The QTAM analysis allows classification of these kind of clusters as ionic compounds with a high charge transfer from the metal to the oxygen and all the Ga-O bonds are closed shell interactions. Electron affinity and ionization potential values increase from Ga_3O to GaO_3. HOMO-LUMO gap, as predicted in the previous study, continues to exhibit an oscillatory trend in approaching the bulk value of the band gap.

In the study of sequential oxidation of gallium oxide clusters using B3LYP/6-31G(d,p), one finds that the most stable isomers display up to four different backbones of constituent atoms. Also, all neutral isomers, $Ga_3O_4^-$, $Ga_3O_4^+$ and $Ga_3O_5^-$ are found in the respective lowest spin state while all other are found in triplet state. Anionic clusters are found to be more stable than the neutral clusters, and neutral ones are, in turn, more stable than the cationic ones. BE/atom for neutral as well as charged systems stays approximately constant with the increase in oxygen-to-metal ratio. Electron affinity, ionization potential and HOMO-LUMO gap values exhibit an oscillatory trend.

Chapter 4

Development of a High Performance Parallel Computing Platform

Notations

API	Application Program Interface
ATA	AT Attached (Attachment)
BIOS	Basic Input/Output Operating System
BP	Bootstrap Protocol
CAT6	CATegory 6
COW	Cluster Of Workstations
DDR	Double Data Rate
DHCP	Dynamic Host Configuration Protocol
DIMM	Dual In-line Memory Module
FlexLM	Flexible License Manager
FOSS	Free and Open Source Software

GNU	Gnu is Not UNIX
HAC	High Availability Cluster
HPC	High Performance Computing
HPL	High Performance Linpack
IDE	Integrated Development Environment
IP	Internet Protocol
LAN	Local Area Network
M^2COTS	Mass-Market Commodity Off The Shelf
MOSIX	Multicomputer Operating System for UNIX
MPI	Message Passing Interface
NASA	National Aeronautics and Space Administration
NBP	Network Bootstrap Program
NFS	Network File System
NIC	Network Interface Card
NPACI	National Partnership for Advanced Computational Infrastructure
NSF	National Science Foundation
OS	Operating System
PC	Personal Computer
PRAM	Parallel Random Access Machine
PVM	Parallel Virtual Machine
PXE	Pre-boot eXecution Environment
RAID	Redundant Array of Inexpensive (or Independent) Disks
RAM	Random Access Memory
ROM	Read Only Memory
SCSI	Small Computer System Interface
SIESTA	Spanish Initiative for Electronic Simulations with Thousands of Atoms
SMP	Symmetric Multi-Processing
SDSC	San Diego Supercomputer Center
TFTP	Trivial File Transfer Protocol
VASP	Vienna Ab initio Simulation Program
XML	eXtensible Markup Language
1U	1Unit (1.75 inch thickness)

4.1 Introduction

Parallel computing is the simultaneous execution of a combination of multiple instances of programmed instructions and data on multiple processors in order to obtain results faster. The idea is based on the assumption that the problem solving process can usually be divided into smaller tasks, which may be carried out simultaneously and independently, with some coordination.

One way to model parallel computers is via PRAM approach. This model does not take into account the cost of interconnection between the constituent computing units, but nevertheless provides an upper bound on the parallel solvability of many problems. The processors may communicate and cooperate in solving a problem or they may run independently, often under the control of another processor which distributes work to and gathers results from them.

GNU/Linux is a freely (or inexpensively) available OS based on the Linux kernel which was developed by Linus Torvalds. GNU is basically a collection of FOSS implementations of common UNIX utilities and programs written to provide an alternative to expensive commercial UNIX. Since the source code is available, anyone who can code can make modifications to them. This has lead to several implementations of GNU/Linux and clustering is one of them.

4.1.1 What Is A Cluster?

A *cluster* is a group of two or more individual computers (also called nodes) working in conjunction with each other to accomplish a given task. Common end goals for such a set up include a desired increase in reliability, load distribution and performance.

By a practical definition, a cluster must consist of at least two nodes – a front end and a compute node. The front end is the computer that users are most likely to interact with since it usually has a job scheduler running on it. The front end can also participate in computation like the compute nodes do, but it is not required or even recommended in large clusters. The compute nodes are slaves to the front end - they respond to the requests of the front end and in general, do most of the computing.

It is a general understanding that a cluster must at least have a MPI and a job scheduler. MPI works to transmit data among the computers in the cluster. A job scheduler takes job requests from user input (or other means) and schedules them to be run on the number of nodes required in the cluster. However, it is possible to have a cluster without either of these components.

Following is one of the classifications of clusters, based on what they do.

† Load Balancing Clusters

Load balancing clusters distribute network or compute processing load across

multiple nodes. The differentiating factor in that case is the lack of a single parallel program that runs across those nodes. Each node in that type of cluster, in most cases, is an independent system running separate software. However, there is a common relationship between the nodes either in the form of direct communication between the nodes or through a central load balancing server that controls each node's load.

† MOSIX

MOSIX uses a modified kernel to create a process load balanced cluster. Servers and workstations can join (or leave) the cluster increasing (or decreasing) the power of the cluster. Processes can transparently migrate through the system, without user intervention. MOSIX is transparent at the application level. There is no need to recompile or relink with new libraries as everything occurs at the kernel level. In order to participate in the cluster, each node must have the same version of the kernel.

† High Availability Clusters

HACs exist to keep the overall services of the cluster available as much as possible. They provide redundant services across multiple systems, to overcome the loss of service due to hardware failure. When a node fails, another picks up the service, keeping the system environment consistent from the users' point of view. Software and data are replicated across the servers in the cluster, and there is, although temporary, a slight loss of performance when a node fails.

With each of those three basic types of clusters, hybrids and inter-breeding often occur between them. Another classification of clusters is based on how it is built.

† Shared Cluster

A cluster that is built from office machines, which are used for other purposes during day time and become a part of the cluster during nights and weekends. This approach, sometimes, can lead to severe limitations imposed by the requirements of computers' day time jobs.

† Dedicated Cluster

The user, in a sense, owns these computers and this approach provides lot of freedom to configure the individual nodes based on specific needs.

4.1.2 Beowulf Cluster

Beowulf was the legendary 6^{th} century hero who freed the Danes of Heorot by destroying Grendel, an oppressive monster. As a metaphor, the term Beowulf has been applied to a new strategy in HPC that exploits mass-market technologies to overcome the oppressive costs (in time and money) of supercomputing, thus freeing people (scientific & engineering computing community) to devote themselves to their respective disciplines. Thus Beowulf, both in myth and reality, challenges and overcomes a dominant obstacle and in turn, making pathway for further accomplishments.

Originally developed by Thomas Sterling and Donald Becker at NASA, a Beowulf class system is a cluster of M^2COTS PCs interconnected by low cost LAN technology running a FOSS UNIX-like OS and executing parallel applications programmed with an industry standard message passing model and library. Thus, it is not a single program; rather, it's a set of tools and a method for connecting a set of computers together to act as a large parallel computer environment. PCs benefit from the economy of scale of mass production (microprocessors, memory chips, I/O controllers, etc.) as well as the mass production of systems in which these components are used - the ones found in homes, offices, etc. These same PCs are the constituent elements of Beowulf high performance parallel computers. Beowulfs, with no special hardware development costs or lead times, exploit the exceptional cost effectiveness of these complete systems. *Parts By Dawn, Processing By Dusk* is an apt description of Beowulf revolution.

One of the main differences between a Beowulf and a COW is that the Beowulf behaves more like a single machine rather than many workstations. In most cases compute nodes do not have keyboards or monitors, and are accessed via remote login. Beowulf nodes can be thought of as a CPU with a memory package which can be plugged in to the cluster.

4.2 Need For A Cluster

Performance of GAUSSIAN 98 suite of programs [19] on a single processor machine is given in Table 4.1. The data indicates the CPU time required for a fixed geometry (SCF) calculation, for varying number of atoms.

NATOM	CPU time (min:sec)
2	00:09
4	00:18
8	04:11
16	45:40

Table 4.1: GAUSSIAN 98 performance on a single processor Linux PC.

Almost an exponential increase in CPU time is observed as the system size increases. An optimization calculation, on an average, involves several such fixed geometry runs. The aim of these calculations is to scan the potential energy surface (of a given configuration of atoms) and accomplishing this requires running few tens of 50-step calculations, depending on the structural complexity and laws of physics & chemistry (typical of calculations done for obtaining results in Chapter 3). As some of the programs/software suites used for such calculations can be parallelized, a significant reduction in CPU times can be achieved as well as enabling one to study much bigger/complex systems, by using a well designed and implemented Beowulf cluster.

4.3 NPACI Rocks

NPACI Rocks is a FOSS cluster building toolkit developed over the past several years, by SDSC with funding from NSF [70]. Rocks differentiates itself from the majority of system provisioning and management tools in that it manages a system description rather than a bit image of installed software. It manages all software as native OS packages and the selection and configuration of these packages for particular nodes as two distinct entities: the complete OS distribution and the Rocks configuration graph. The OS distribution is the union of all software that could be installed on any particular machine. The configuration graph selects which of these packages will be installed on a particular machine and exactly how to configure that software.

A roll itself is a set of binary packages and a subgraph that is connected to a master graph. The full graph is defined and composed of all rolls selected by the administrator at build time. The binary packages in a roll supply the fundamental building blocks; nodes supplied by the roll describe packages and how to configure them; and graph edges supplied by the roll indicate which nodes should be included for a particular appliance type. This composition of all rolls is automatic and transparent to the end user. In Rocks, even the OS is defined as a roll that contains only packages. This fundamental decomposition of a complete cluster with the ability to recombine these building blocks as a program provides programmatic extensibility of a core system without needing an expert systems administrator for every cluster.

A kickstart file is a text-based description of all the software packages and software configuration to be deployed on a node. The Rocks Kickstart Graph is an XML-based tree structure used to define RedHat Kickstart files. By using a graph, Rocks can efficiently define node types without duplicating shared components.

Rocks controls the provisioning of all appliances from the ground up, meaning a complete OS installation from bare metal state is performed on all machines through the traversal of the configuration graph. Capturing the complete configuration of such varied appliance types has been a major effort for Rocks. Building the OS in this manner allows one to begin with the same initial system state (the empty set) and to end with a predictable final state. This observation is critical to understanding in that this allows both reproducibility and compatibility among appliances in the clustered machine room. The graph is really the source code for a complete set of appliances; installation is then equivalent to compilation of the source code.

At the core of Rocks is extensibility. Adding functionality (e.g. a queuing system) is as simple as inserting the desired queuing system roll at bootstrap time. From there, configuration is automatic and programmatic. All of these processes help break down the clustered machine room into manageable bits that can then be recomposed into new systems.

4.4 Cluster Design & Development

As mentioned in Section 4.1.1, it is necessary to have at least two machines when building a cluster. It is not necessary that these machines have the same levels of performance. Probably the only requirement is that they both are of same make. For instance, the cluster should only consist of all Intel machines or all Apple machines but not a mixture of the two, even though it is possible to mix different makes /by using Java.

To maximize the benefits of a cluster, appropriate hardware must be used. It is generally accepted that for optimal performance, all nodes except the front end must have identical hardware specifications. This is due to the fact that one node which takes longer to do its work can slow the entire cluster down as the rest of the nodes must stop what they are doing and wait for the slow node to catch up. This is not always the case, but it is a consideration that must be made. Having identical hardware specification also simplifies the setup process a great deal as it will allow each hard drive to be imaged from a front end instead of configuring each node individually.

4.4.1 Front End

There are four main considerations when building the front end, as discussed below:

† Processor Speed

This is especially critical if the front end participates in computation. The front end will be handling many more tasks than the compute nodes so a faster processor may be required to keep it from lagging behind. A slow down here can have a huge negative impact on the entire cluster as the compute nodes waste time waiting for their next instruction.

† Disk Speed

Since most work done on the cluster will be saved as files on a hard drive at some time or another, disk speed for the front end is a very important factor - also due to the fact that compute nodes make use of NFS. This means that every node in the cluster will be competing for access of the front end's disk. A fast SCSI drive is recommended, a RAID array of types 5 or 0+1 is ideal, but an IDE drive will work as well.

† Network Speed

This is another critical aspect. Time spent transmitting data is time wasted. The faster the network, the better the performance of the cluster. Fast ethernet is recommended and gigabit ethernet is ideal. While not part of the front end, it

is strongly recommended that a switch be used instead of a hub when designing the cluster network.

† RAM

RAM in the front end plays important role for two reasons. First, the more RAM, the more processes can be run without accessing the disk. Second, the Linux kernel can and will cache its disk-writes to memory and keep them there until they must be written to disk. Both of these increase the speed of the front end which is critical to overall performance of the cluster.

Complying with these requirements, hardware specifications of the front end are as follows:

CPU	Intel Pentium-4 3.0GHz/800FSB (64-bit)
System	Intel SE7221BK1-E Pentium-4 Server Board
Memory	1GB RAM, ECC DDR2 Memory (2-512MB, ECC DDR2/533)
Hard Disk	Seagate 160G SATA Drive 7200RPM/8MB/NCQ with RAID
Network	Dual Intel NIC, 1-10/100 and 1-10/100/1000
Video	Intel Video
Optical Drive	NEC NB-3520A DVD-RW/DL

4.4.2 Compute Nodes

The compute nodes need to accomplish two tasks:

1. Perform the computations assigned to them
2. Send that data back over the network

For this reason, their disk performance is not as critical as compared to front end. It is common to have nodes without hard drives in a cluster. These diskless nodes further reduce the cost of building a cluster and eliminate some of the time required to set a cluster up.

The three important hardware considerations for compute nodes are as follows:

† Processor Speed

Since the primary function of a compute node is computation, the more processing power the better. Multiple processors for each node (i.e. SMP) can be desirable but add another degree of complexity to programming applications for the clusters.

† Network Speed

This affects the compute nodes in exactly the same way that it does the front end.

† RAM

This too affects the compute nodes in the same way that it does the front end.

Complying with these requirements, hardware specifications of the compute nodes are as follows:

Compute nodes 0-15:

CPU	Dual Intel Xeon 2.8GHz/800FSB (EM64T)
System	Intel SE7520JR2ATAD2 Dual Xeon Server Board
Memory	2GB RAM, ECC/Reg-DDR (2x1GB, DDR2-400MHz)
Hard Disk	Seagate 160GB ATA-100 Drive
Network	Dual Intel NICs 2-Pro/1000+

Compute nodes 16-23:

CPU	Dual Intel Xeon Dual Core 1.86GHz/1066FSB (EM64T)
System	Intel SR1500AL Server Platform S5000PAL Server Board
Memory	4GB RAM, FBDIMM/ECC (4x1GB, DDR2/667MHz)
Hard Disk	Seagate 160GB SATA Drive
Network	Dual Intel NICs 2-Pro/1000+

4.4.3 Other Components

As a switch is more desirable than a hub when designing clusters due to the increased speed that it offers, a gigabit switch was chosen for inter nodal communication. Using rack mountable cases when building the cluster reduced space requirements and offered better organization. Cluster with larger number of nodes can produce a significant amount of heat, and affect both the stability of the cluster and comfort of the operator. A properly ventilated facility with *hot-aisle cold-aisle* arrangement was chosen to house the cluster to overcome this issue.

One other important aspect taken into account was the following : setting up a cluster for experimental usage is quite different from setting it up for long term (operational) usage. To that effect, the system was designed and developed such that

† it can be easily understood, maintained and updated/upgraded.

† it is easy enough for end users.

4.4.4 OS Installation & Customization

The front end, in this set up, was a server with two network interfaces. The public interface was attached to the campus network while the private interface was attached

to the cluster. Rocks uses the first interface (eth0) as private interface and second one (eth1) as public. Once the OS installation on front end and the compute nodes was complete, a set of scripts/programs/utilities were written (mostly in BASH, PERL) to accommodate the following tasks:

† Securing the cluster - to prevent unauthorized access.

† Simplifying profile customization for end users - so that they can start using the facility right away.

† Periodic data back up and restoration.

† Monitoring disk usage and emailing users above a certain limit.

† Starting/stopping license daemons for packages that use FlexLM.

† Emailing users upon submission, beginning and termination of a calculation.

Several scientific computation software as well as the associated/required support packages were compiled to facilitate study of complex systems - Crystal [71], DMol [72], Gaussian [19, 20], SIESTA [73], SMEAGOL [74, 75, 76], VASP [21, 22, 23, 24] - just to name a few. Compiling some of these was relatively simple and straightforward whereas couple of them (VASP and SMEAGOL) demanded months of work. Detailed information about the OS installation, customization as well as compilation of every program may be obtained by referring to the cluster manual [77].

4.5 Benchmarks

As discussed in Chapter 2, the properties of a many-particle system can be determined from its wave function Φ, the solution of the non-relativistic Schrödinger equation. given by Eqn. 2.1. Computational Physics/Chemistry packages translate the hamiltonian, $\hat{H}$, into a $N \times N$ matrix before attempting a (numerical) solution. Order of this hamiltonian matrix, N, depends not only on the number of atoms in the system but also on symmetry of the system as well as the basis set/functional form used in the problem. The results obtained for a given system with a certain symmetry using a particular basis set/functional form may not be usable as a benchmark to study other systems. In order to overcome this issue and benchmark a computer/cluster (in terms of CPU time and performance), Linpack benchmark scheme was employed. This scheme provides a performance measure in GFlops (billions of floating point operations per second). Although there are different implementations of this Linpack benchmark, HPL is the most commonly used one.

HPL is a software package that solves a (random) dense linear system in double precision (64 bits) arithmetic on distributed memory computers. It can thus be regarded as a portable implementation of the High Performance Computing Linpack Benchmark. HPL solves an N order system of the form $A\,x = b$ by determining the LU factorization: $A\,b = L\,U\,y$. The solution, x, is computed by $U\,x = y$. Matrix is divided into $NB \times NB$ blocks that are cyclically dealt onto a $P \times Q$ grid with a

block-cyclic layout. Although computational Physics/Chemistry packages do much more than just solving the given hamiltonian, results from HPL runs can be used to estimate a lower bound for the required CPU time.

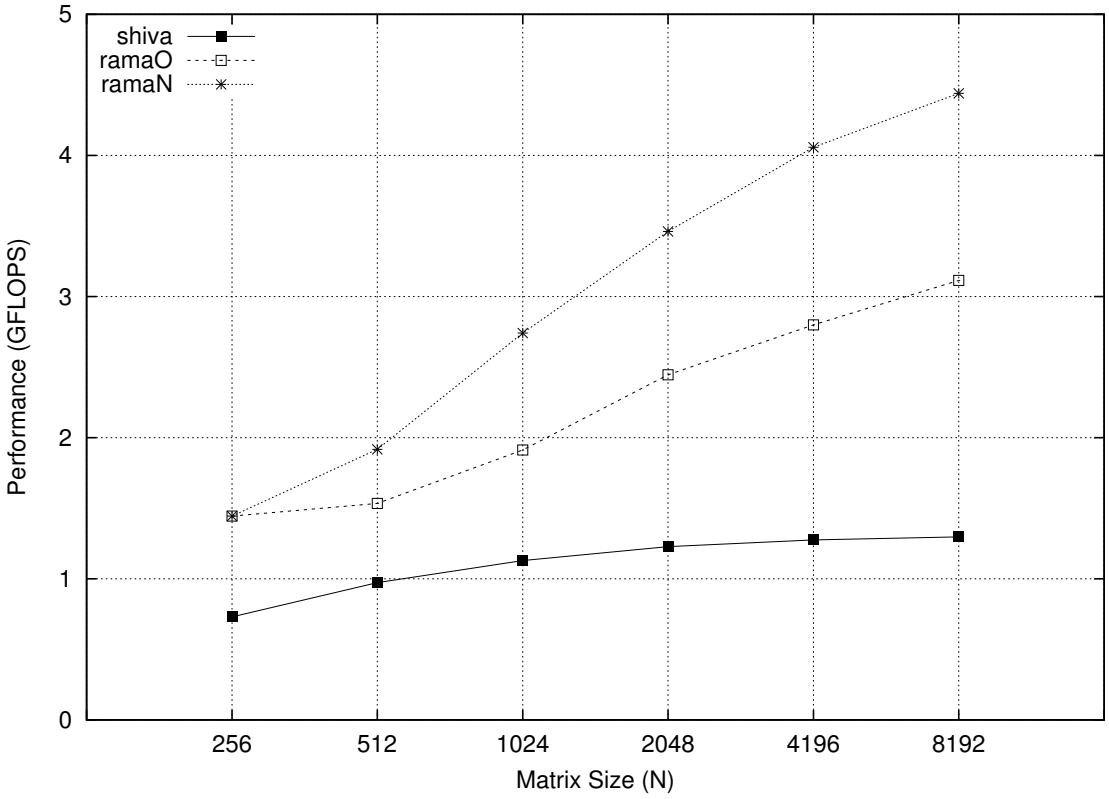

Figure 4.1: High Performance Linpack performance (NPROC: 1 and NB: 32) - a comparison between *shiva* and *rama*. *shiva*: P4 2.80GHz 1GB RAM; *ramaO*: EM64T 3.00GHz 2GB RAM; *ramaN*: EM64T 1.86GHz 4GB RAM

From Fig. 4.1, it is clear that the old nodes of *rama* (ramaO) performed considerably better when compared to *shiva*. Newer nodes (ramaN) show a trend similar to old nodes but provide enhanced performance.

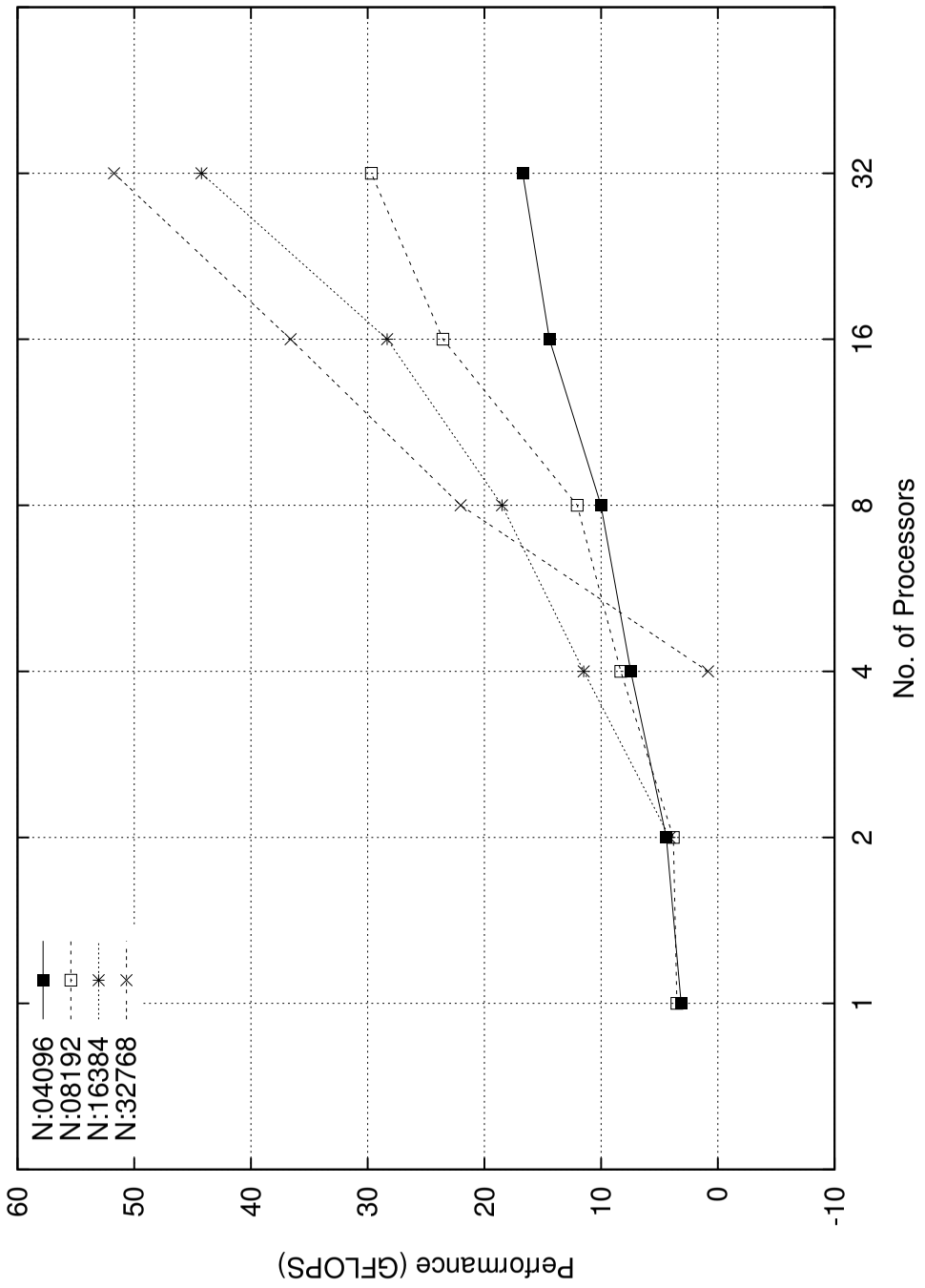

Figure 4.2: High Performance Linpack performance (NB: 64) on old nodes of *rama*: Dual Core EM64T Processors 3.00GHz 2GB RAM

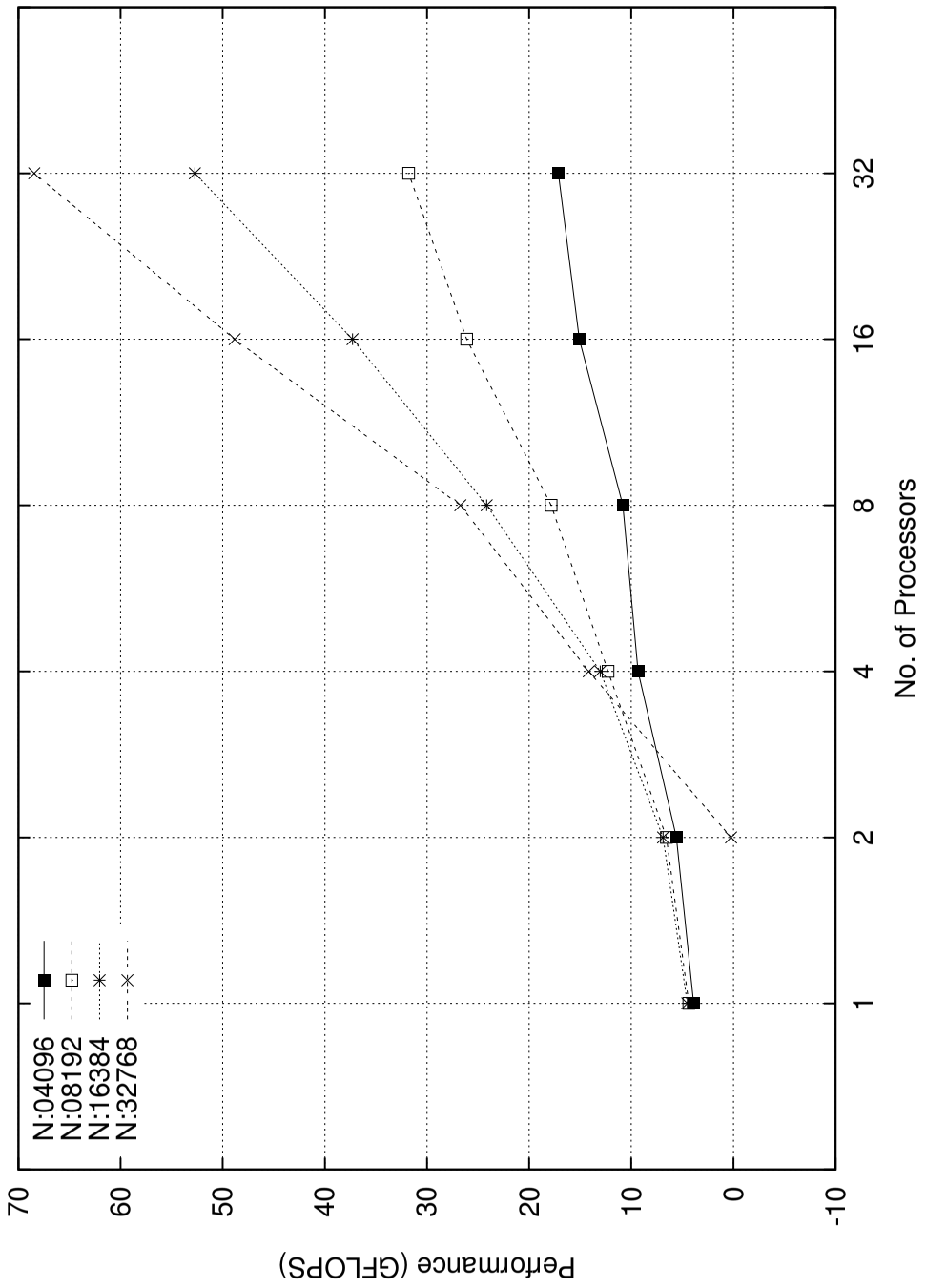

Figure 4.3: High Performance Linpack performance (NB: 64) on new nodes of *rama*: Dual Dual Core EM64T Processors 1.86GHz 4GB RAM

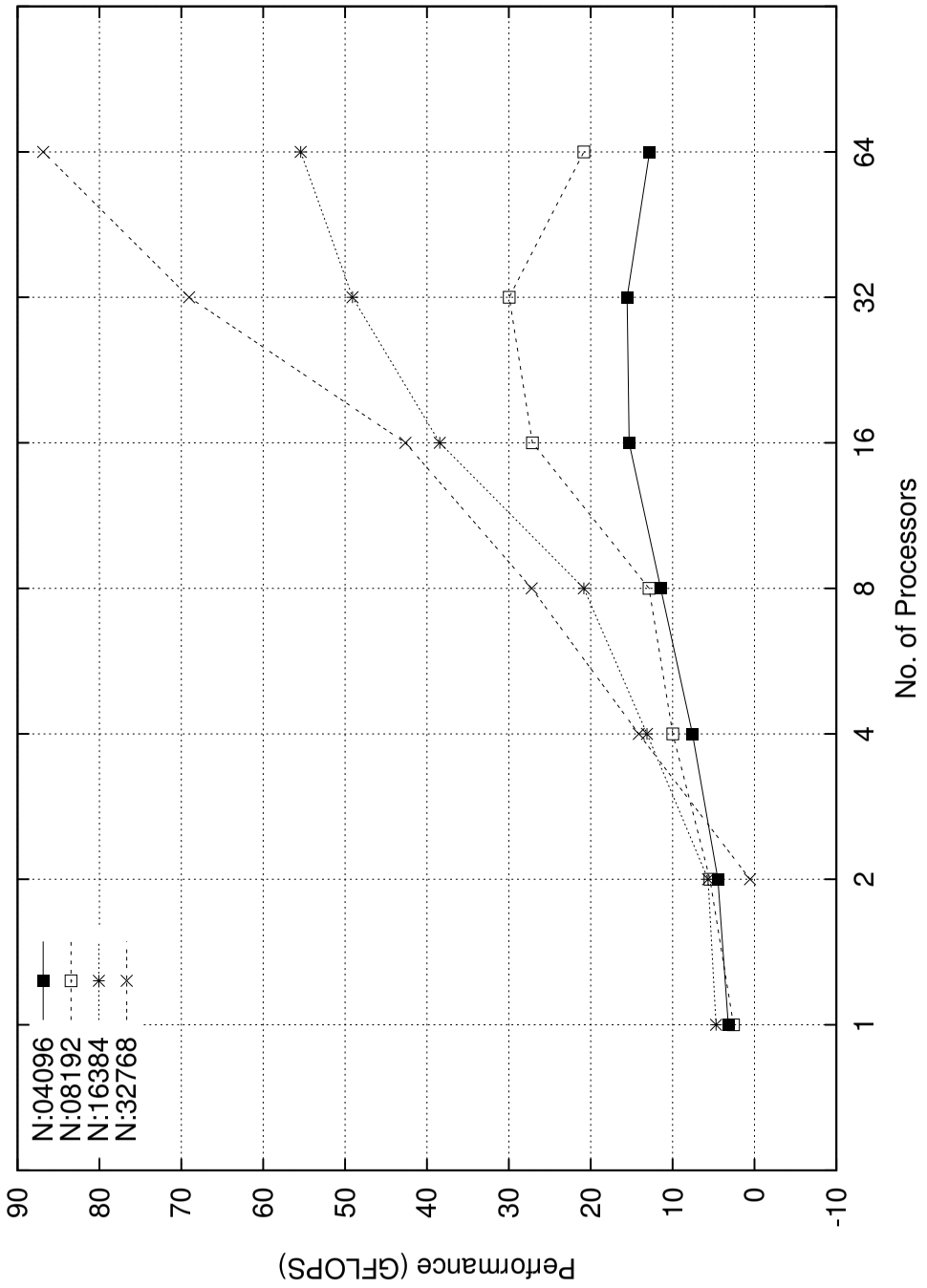

Figure 4.4: High Performance Linpack performance (NB: 64) on *rama* - combination of nodes used in Fig. 4.2 and Fig. 4.3.

Fig. 4.2 and Fig. 4.4 show similar trends - almost linear scaling of performance with respect to the number of processors - in agreement with Fig. 4.1, even when extended to multiple processors. Trend in Fig. 4.4 can be used to estimate the optimum number of processors required for a given matrix size.

4.6 Conclusions

Following the discussions in Chapter 1 and guided by the results of calculations in Chapter 3, performance related challenge of computational simulations, *of producing high performance computers/platforms*, has been addressed. Several engineering aspects - space and power requirements, heat management, etc. were thoroughly studied during the design and implementation of this high performance parallel computing platform. In an attempt to stay true to the principles of Beowulf revolution, the cluster was extensively customized to make it easy to understand, and use - for administrators as well as end-users. Following the results of benchmark calculations and to keep up with the complexity of systems under study, this dedicated cluster has been expanded to a total of 64 processors.

Chapter 5

Interaction of Nanomaterials with Biological Matter

Notations

DOS	Density Of States
DNA	Deoxyribose Nucleic Acid
mwCNT	Multi Walled Carbon NanoTube
RNA	Ribose Nucleic Acid
swCNT	Single Walled Carbon NanoTube
vdW	van der Waals

5.1 Introduction

DNA, with its structure discovered in 1953 [78], is a long polymer made from repeating units called nucleotides [79, 80]. The DNA chain is 2.2 to 2.6 nm wide, and each nucleotide unit is about 0.33 nm long. Although each individual repeating unit is very small, DNA polymers can contain millions of nucleotides. The backbone of the DNA strand is made from alternating phosphate and sugar residues. The DNA double helix is stabilized by hydrogen bonds between the bases attached to the two strands and has four bases: adenine (A), cytosine (C), guanine (G) and thymine (T). Bases are categorized into two types: purines with five- and six-membered rings (A and G) and pyrimidines with six-membered rings (C and T). It should be noted here that uracil (U), is a pyrimidine base and replaces thymine in forming RNA.

Materials at the nanoscale often show significantly different properties paving way for unique applications. Nanotube is one such nanomaterial and is a member of the fullerene structural family. It is cylindrical with at least one end capped with a hemisphere of the buckyball structure. CNTs have sp^2 bonds, with each atom connected to three neighbors as in graphite. This bonding structure, stronger than the sp^3 found in diamond, provides CNTs with their unique strength.

A swCNT is a one-atom thick sheet of graphite rolled up into a seamless cylinder with diameter of the order of a few nm. The length of such a nanostructure is usually

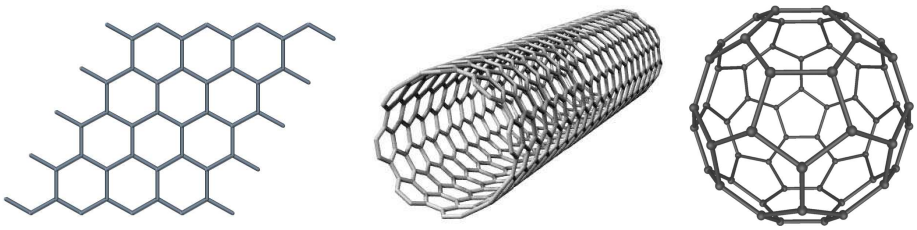

(a) Graphene (b) swCNT (c) Buckyball

Figure 5.1: Schematic representation of graphene, swCNT and buckyball.

several orders of magnitude greater than its diameter. CNTs have novel properties that make them potential candidates for many applications in electronics, optics and nanotechnology.

There has been a steady increase in interest over the past several years in the non-covalent interaction of DNA with CNTs. This hybrid system at the junction of the biological regime and the nanomaterials world possesses features which makes it very attractive for a wide range of applications. The initial focus rested on developing a new way to disperse CNT bundles in aqueous solution [81] and to create a more efficient method to separate CNTs according to their electronic properties [82, 83]. Recently, focus has shifted towards developing applications aimed at electronic sensing of various odors [84] and probing conformational changes in DNA *in vivo* triggered by change in the surrounding ionic concentration [85]. The details of the interaction of DNA with CNTs have not yet fully been understood, though it is generally assumed to be mediated by the π-electron networks of the base parts of DNA and the graphene-like surface of CNTs.

5.2 Computational Methodology

Supercell calculations were performed using the plane-wave pseudopotential approach within the LDA [86] of DFT, as implemented in the VASP [21, 22, 23, 24]. It has been reported that the LDA approximation appears to give a reliable description of dispersive interactions, unlike the GGA [87] for which binding is basically non-existent for vdW bound systems [88, 89]. In a study of the adsorption of the adenine on graphite[90] using LDA and a modified version of the London dispersion formula [91] for vdW interactions in combination with GGA, it was found that LDA, while underbinding the system, does in fact yield a potential energy surface which is almost indistinguishable in its structure from the one obtained via the GGA+vdW approach (cf. Figs. 1a and 1b of Ref. [90]). Furthermore, LDA yields almost the same equilibrium distance of A to graphene as GGA+vdW.

The base molecules were terminated (at the position where they bonded to the sugar ring) with a methyl group in order to generate an electronic environment in the nucleic acid base more closely resembling the situation in DNA and RNA rather than that of just individual isolated bases by themselves. This has the additional benefit that a small magnitude of steric hindrance can be expected from the methyl group, quite similar to the case in which a nucleic acid base with attached sugar and phosphate group would interact with graphene. The cutoff energy for these calculations was set to 850 eV. For k-point sampling of the Brillouin zone, the $1 \times 1 \times 1$ Monkhorst-Pack

grid [92] was used for interaction of nucleic acid bases with graphene, which were found from benchmark calculations.

A 5×5 array of the graphene unit cell in the $x - y$ plane and a separation of 15 Å between adjacent graphene sheets in the z-direction was found to be a suitable choice to represent the supercell. For interaction of nucleic acid bases with CNT, a unit cell of a (5,0) swCNT, consisting of a ring of 20 carbon atoms with a diameter of 3.92 Å, was repeated three times along the tube axis. In the direction perpendicular to the tube axis, a distance of at least 15 Å was maintained between repeated units to avoid interactions between adjacent CNTs. A $1 \times 1 \times 3$ Monkhorst-Pack grid for k-point sampling of the Brillouin zone was used. Geometry optimization process, for each of the five nucleic acid bases, was carried out in following steps:

1. An initial force relaxation calculation step determined the preferred orientation and optimum height of the planar base molecule relative to the graphene sheet (plane of CNT). This configuration was be used in subsequent steps.

2. A slice of the potential energy surface was then explored by translating the relaxed base molecules in a fixed orientation parallel to the graphene plane in steps of 0.246 Å along the lattice vectors of graphene, covering its entire unit cell by a mesh of 10×10 scan points (Figure 5.2).

   A curved slice of the potential energy surface was then explored by translating the relaxed base molecules in a fixed orientation parallel to the CNT surface

covering a surface area 4.26 Å in height, 70° in width and containing a mesh of 230 scan points (Figure 5.7).

3. The determination of the minimum total energy configuration was then followed by a 360° rotation of the base molecules in steps of 5° to probe the dependence of the energy on the orientation of the base molecules with respect to the underlying 2-dimensional graphene sheet.

4. The configuration yielding the minimum total energy was used in the final optimization step in which all atoms in the system were free to relax.

It should be noted here that for all five nucleic acid bases, the eventually determined equilibrium configuration was characterized by a separation between base and graphene sheet that was equal to the optimum height chosen in the previous lateral potential energy surface scan.

An additional set of calculations was performed using the *ab initio* HF approach coupled with MP2 theory as implemented in the GAUSSIAN 03 suite of programs [20]. Due to the use of localized basis sets (rather than plane-wave), the system here consisted of the five nucleic acid bases on top of a patch of nanographene [93, 94], i.e., a finite sheet containing 28 carbon atoms. The LDA optimized configuration and the 6-311++G(d,p) basis sets for C, H, N and O atoms were used for the MP2 calculations.

5.3 Results and Discussions

5.3.1 Interaction With Graphene

The first optimization step involving the initial force relaxation led to a configuration of all five nucleic acid bases in which their planes are likewise oriented almost exactly parallel to the graphene sheet with a separation of about 3.5 Å, characteristic for π–π stacked systems [95, 96]. The interaction of the attached methyl group with the graphene sheet results in a very small tilt of the molecule, with angles less than 5°.

The base is translated 2.461 Å along both graphene lattice unit vectors respectively (maintaining a constant vertical distance of 3.5 Å from the sheet, as determined in the previous step), and rotated 360° in the equilibrium configuration with respect to the configuration obtained after the initial force relaxation step in the optimization procedure. From the optimization steps involving the translational scan of the energy surface, it is apparent that the energy barriers to lateral movement of a given base can range from 0.04 to 0.10 eV (Fig. 5.2), thus considerably affecting the mobility of the adsorbed nucleic acid bases on the graphene sheet at room temperature, and constricting their movement to certain directions. The rotational scans carried out by us found energy barriers of up to 0.10 eV, resulting in severe hindrance of changes in the orientation of the adsorbed nucleic acid base.

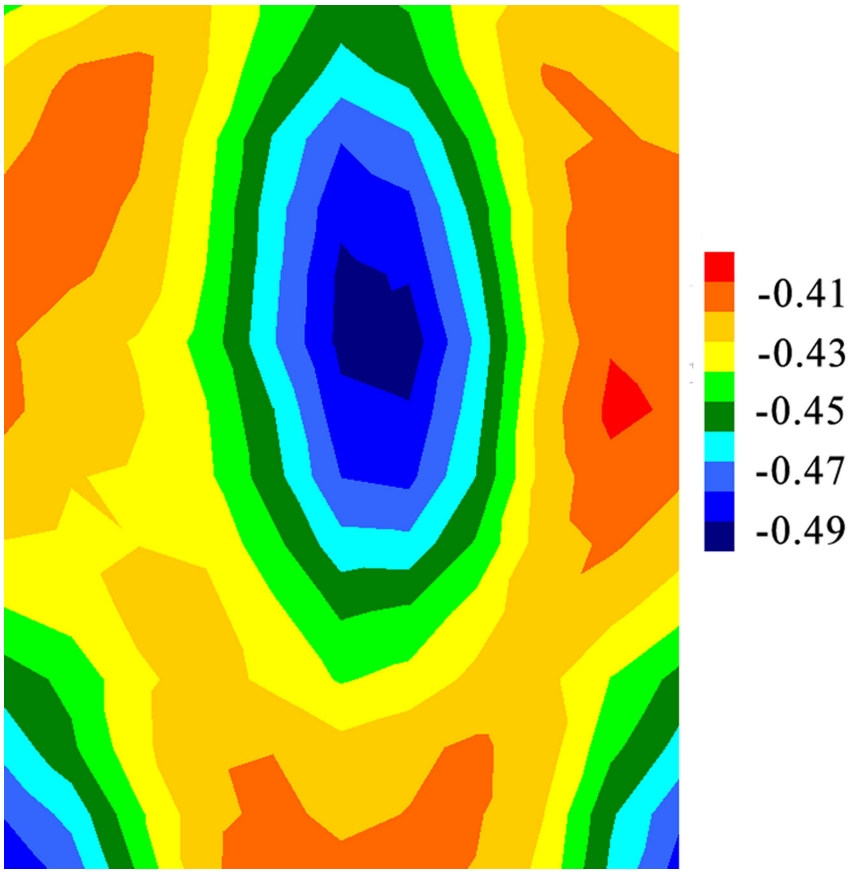

Figure 5.2: Potential energy surface plot (in eV) for guanine on graphene. Approximately a 3 × 3 repetition of the unit cell is shown. The energy difference between peak and valley is approximately 0.10 eV. The energy barriers separating adjacent global minima have heights of about 0.04–0.05 eV, depending on the direction of translocation.

In their equilibrium configuration, three of the five bases tend to position themselves on graphene in a configuration reminiscent of the Bernal's AB stacking of two adjacent graphene layers in graphite (Fig. 5.3). Virtually no changes in the interatomic structure of the nucleic acid bases were found in their equilibrium configurations with respect to the corresponding gas-phase geometries, as it could be expected for a weakly interacting system such as the one studied here. This finding is also in agree-

ment with earlier results reported in the literature for the nucleic acid base adenine [90]. One notable exception is the R_{C-O} in guanine which shows a 10% contraction upon physisorption of the molecule on graphene.

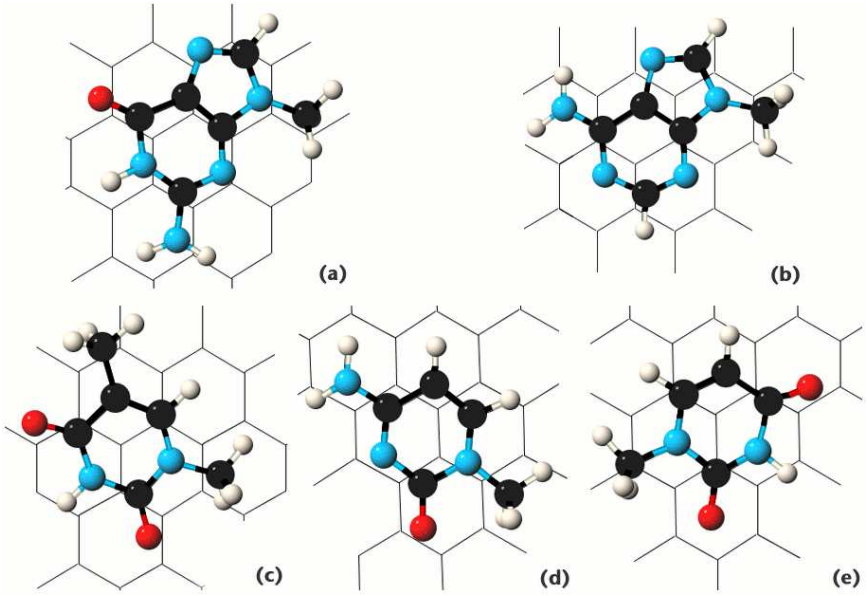

Figure 5.3: Equilibrium geometry of nucleic acid bases on top of graphene: (a) guanine, (b) adenine, (c) thymine, (d) cytosine, and (e) uracil.

The stacking arrangement shown in Fig. 5.3 can be understood from the tendency of the π–orbitals of the nucleic acid bases and graphene to minimize their overlap, in order to lower the repulsive interaction. The geometry deviates from the perfect AB base-stacking as, unlike graphene, the six- and five-membered rings of the bases possess a heterogeneous electronic structure due to the presence of both nitrogen and carbon in the ring systems. In addition, there exist different side groups containing CH_3, NH_2, or O, all of which contribute to the deviation from the perfect AB base-stacking as well. Adenine, thymine and uracil display the least deviation from AB

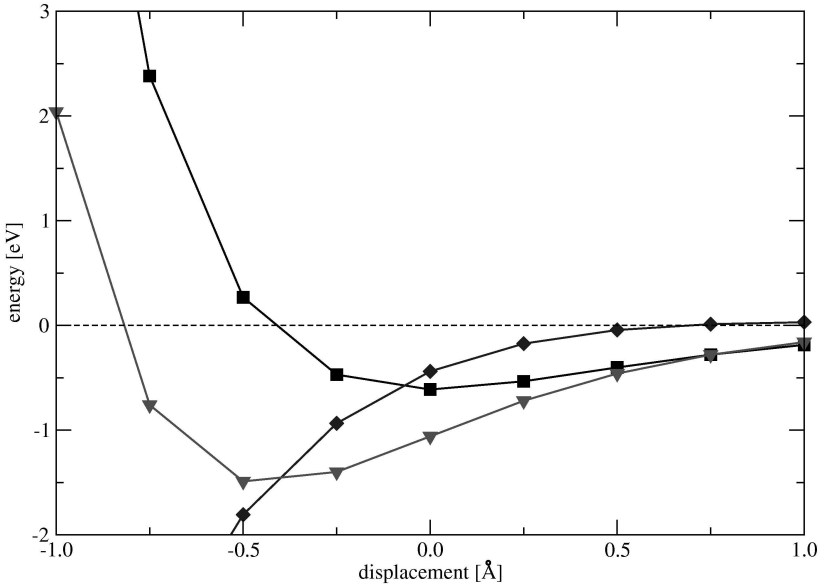

Figure 5.4: Plot of the relative total energy (squares), exchange-correlation energy (diamonds) and kinetic energy (triangles) of guanine adsorbed on graphene calculated as a function of the displacement from its equilibrium position.

stacking (Fig. 5.3) out of the five nucleic acid bases. For guanine and cytosine on the other hand, there is almost no resemblance to the AB stacking configuration recognizable (Fig. 5.3).

Base	LDA E_b (eV)	MP2 E_b (eV)	α $(e^2 a_0^2 E_h^{-1})$
G	0.61	1.07	131.2
A	0.49	0.94	123.7
T	0.49	0.83	111.4
C	0.49	0.80	108.5
U	0.44	0.74	97.6

Table 5.1: Binding energies E_b of the five DNA/RNA nucleic acid bases with graphene as calculated within LDA are compared with binding energies and polarizabilities α obtained from MP2 calculations.

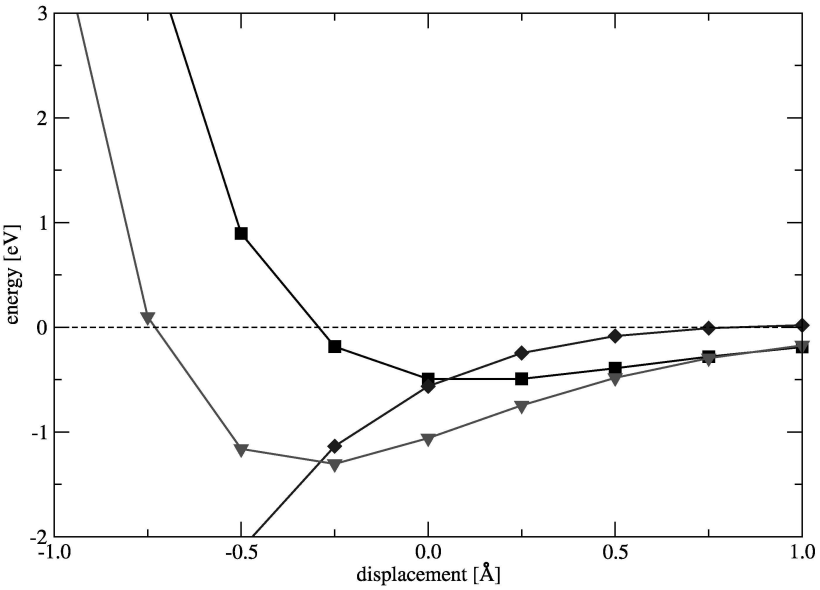

Figure 5.5: Plot of the relative total energy (squares), exchange-correlation energy (diamonds) and kinetic energy (triangles) of adenine adsorbed on graphene calculated as a function of the displacement from their respective equilibrium position.

The binding energy of the system consisting of the nucleic acid base and the graphene sheet is taken as the energy of the equilibrium configuration with reference to the asymptotic limit obtained by varying the distance between the base and the graphene sheet in the z-direction (Table 5.1). Within LDA, adenine, cytosine and thymine were all found to all possess nearly identical binding energies of about 0.49 eV, while guanine with 0.61 eV is bound more strongly, and uracil with 0.44 eV somewhat more weakly.

It is somewhat surprising that guanine and adenine would possess such different

physisorption energies, despite both containing a five- and a six-membered ring and featuring relatively similar molecular structures. A closer analysis of the various contributions to the total energy (Fig. 5.4 and 5.5) reveals that the Kohn-Sham kinetic energy displays a slightly more pronounced minimum for guanine than for adenine, and that the position of that minimum is shifted by about 0.25 Å towards the graphene sheet. The exchange-correlation energy drops off somewhat more rapidly in the case of adenine; however, the difference to the case for guanine is only very small.

For reasons discussed further in the next paragraph, Table 5.1 also includes the polarizabilities of the nucleic acid bases calculated at the MP2 level of theory. The polarizability of a given nucleic acid base [97], which represents the deformability of the electronic charge distribution, is known to arise from the regions associated with the aromatic rings, lone pairs of nitrogen and oxygen atoms. Accordingly, the purine bases guanine and adenine with their five- and six-membered rings possess the largest polarizabilities, whereas the pyrimidine bases with only one six-membered ring exhibit smaller polarizabilities among the five nucleic acid bases. Furthermore, the purine base guanine with its double-bonded oxygen atom and amine group will possess a larger polarizability than the purine base adenine. The MP2 calculations confirm this trend.

A remarkable correlation is found when the molecular polarizabilities of the base

molecules are compared with the binding energies, in particular when the latter are also determined at the MP2 level of theory (Table 5.1). Clearly, the polarizability of a nucleic acid base is the key factor which governs the strength of interaction with the graphene sheet. This behavior is expected for a system that draws its stabilization from vdW dispersion forces, since the vdW energy is proportional to the polarizabilities of the interacting entities. The observed correlation thus strongly suggests that vdW interaction is indeed the dominant source of attraction between graphene and the nucleic acid bases.

The MP2 binding energies are systematically larger than those calculated within the LDA approximation (Table 5.1). This is due to the well established fact that MP2 provides a more accurate treatment of the vdW interaction than LDA. It should be noted that the adsystem consisting of the base and the sheet is not bound at the HF level of theory, which underscores the importance of electron correlation in describing the weak vdW interactions in this system.

In the equilibrium configuration, a redistribution of the total charge density within a given base seems to appear. From an analysis of the Mulliken charges for the MP2 calculations, one also finds a negligible charge transfer ($< 0.02e$) between any of the five nucleic acid bases and patch of nanographene in the equilibrium configuration. Electrostatic interactions in the adsystem are therefore very unlikely to contribute to the interaction energy.

Since graphene can be regarded as a model system for CNTs with negligible surface curvature, these conclusions should therefore also hold for the physisorption of nucleic acid bases on large-diameter CNTs.

5.3.2 Interaction With High Curvature CNT

The initial step in the constrained optimization process resulted in to a configuration of all five nucleic acid bases in which their planes are likewise oriented almost exactly parallel to the CNT surface. Fig 5.6 shows the configuration referred to as the axial configuration. The base molecule-CNT separation was about 3.2 Å, which is a little less than the characteristic distance for π–π stacked systems [95, 96]. The latter does however strictly apply only for planar entities, the high-curvature surface of a tube such as (5,0) allows for the π-orbitals of the nucleic acid base to come closer before the repulsive interaction sets in the system.

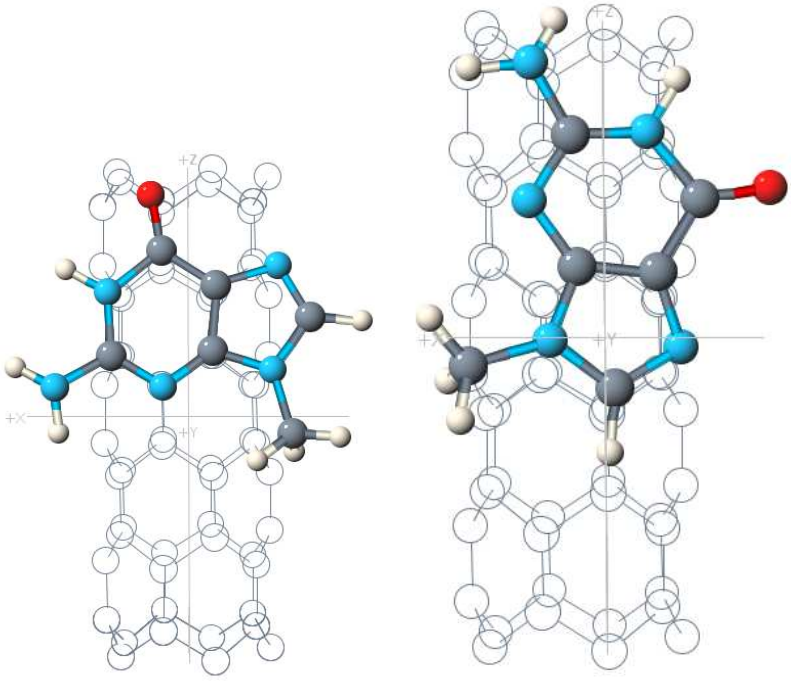

Figure 5.6: The orientations, perpendicular and axial, of guanine with CNT.

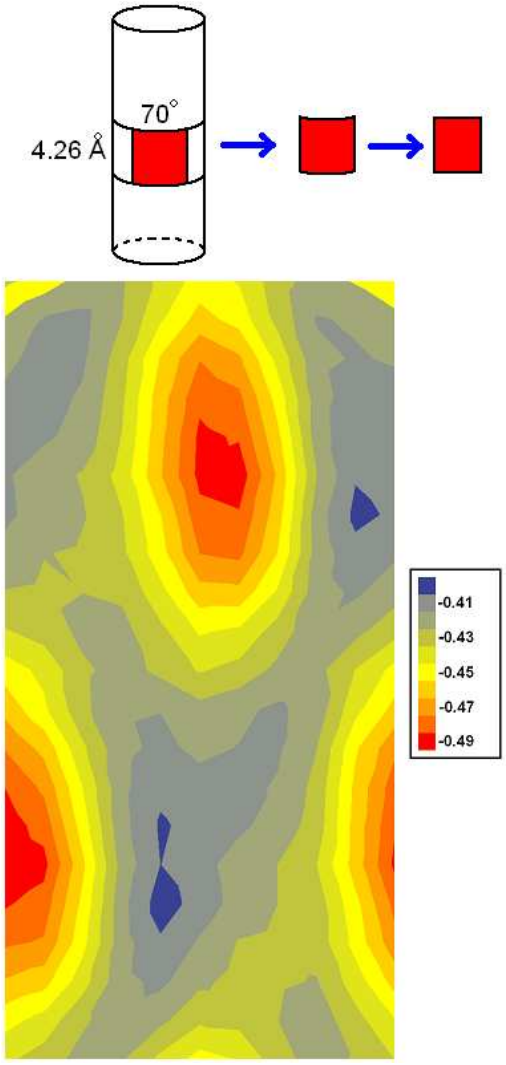

Figure 5.7: Potential energy surface plot (in eV) for guanine with CNT. Approximately a 3 × 3 repetition of the unit cell is shown. The energy range between peak and valley is approximately 0.1 eV. Energy barriers of only about 0.04 eV separate adjacent global minima.

The base was translated both along the CNT axis and around its circumference respectively, maintaining a constant separation of approximately 3.2 Å from the CNT surface, as determined in the previous step. From this translational scan of the energy surface, it is apparent that the energy barriers to lateral movement of a given

base is approximately 0.07 eV (Fig. 5.7), thus considerably affecting the mobility of the adsorbed nucleic acid bases on the CNT surface at room temperature, and constricting their movement to certain directions. The base was then rotated 360°, in the minimum total energy configuration obtained from the previous step. Energy barriers of up to 0.12 eV (Fig. 5.8) were found, resulting in severe hindrance of changes in the orientation of the adsorbed nucleic acid base. Interestingly, we find local minima for special rotations corresponding to 90°, 120°, 180°, and 270° (Fig. 5.8).

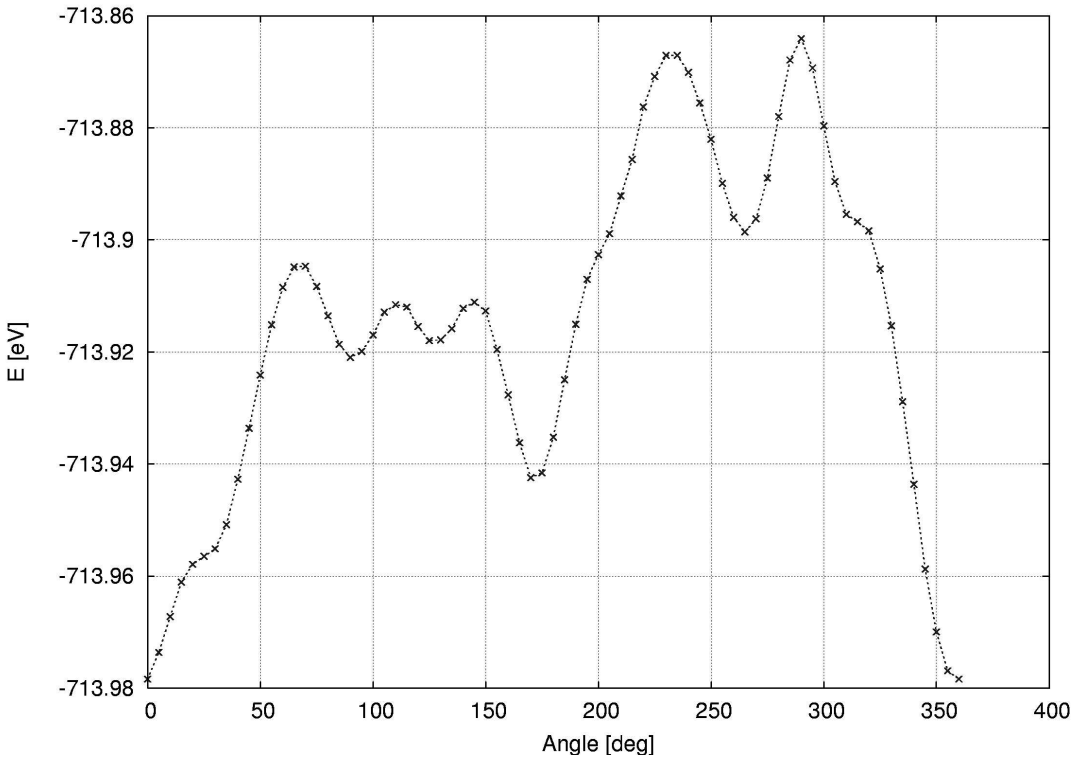

Figure 5.8: Rotational energy scan (in eV) for guanine with CNT.

For all five base molecules, the eventually determined equilibrium configuration was

characterized by a separation between base and CNT surface that was equal to the optimum height chosen in the previous lateral potential energy surface scan.

In their equilibrium configuration, the base molecules A, T and U tend to position themselves on CNT in a configuration reminiscent of the Bernal's AB stacking of two adjacent graphene layers in graphite (Fig. 5.9). The base molecules G and C, on the other hand, showed less degree of resemblance to the AB stacking. The interatomic structure of the nucleic acid bases in their equilibrium configurations underwent virtually no changes when compared to the corresponding gas-phase geometries, as it could be expected for a weakly interacting system.

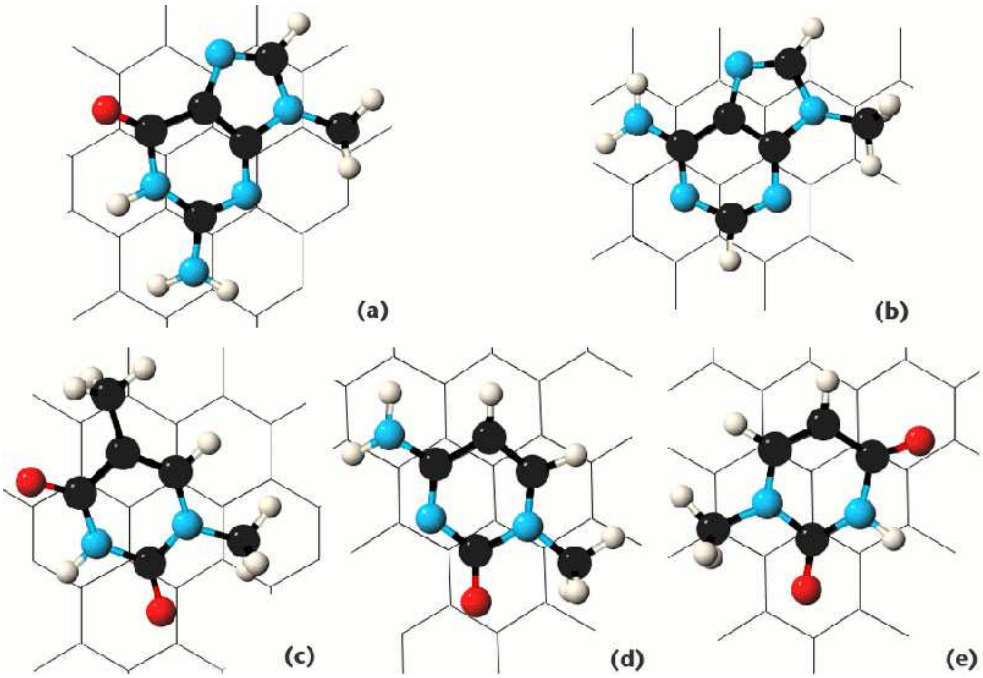

Figure 5.9: Equilibrium geometry of nucleic acid bases on top of CNT: (a) guanine, (b) adenine, (c) thymine, (d) cytosine, and (e) uracil.

Base	E_b^{CNT} (eV)	$E_b^{graphene}$ (eV)	α ($e^2a_0^2E_h^{-1}$)
G	0.49	1.07	131.2
A	0.39	0.94	123.7
T	0.34	0.83	111.4
C	0.29	0.80	108.5
U	0.28	0.74	97.6

Table 5.2: Binding energy E_b of the DNA/RNA nucleic acid bases with a (5,0) CNT and with a flat graphene sheet as calculated within LDA. A close correlation with the nucleic acid bases' polarizabilities α from MP2 calculations can be seen.

The tendency of the π–orbitals of the bases and the graphene-like surface of CNT to minimize their overlap, in order to lower the repulsive interaction, helps us to understand the observed stacking arrangement (Fig. 5.9). The geometry deviates from the perfect AB base-stacking as, unlike graphene, the six- and five-membered rings of the bases possess a heterogeneous electronic structure due to the presence of both nitrogen and carbon in the ring systems. Additionally, there exist different side groups containing CH_3, NH_2, or O, all of which contribute to the deviation from the perfect AB base-stacking as well.

The binding energy of the system consisting of the nucleic acid base and the CNT is taken as the energy of the equilibrium configuration with reference to the asymptotic limit obtained by varying the distance between the base and the CNT surface in the direction perpendicular to both the tube axis and the plane of the base molecule (Table 5.2). G was found to bound most strongly, while the interaction strength for U was weakest.

Table 5.2 also includes the polarizabilities of the base molecules calculated using the HF approach coupled with MP2 perturbation theory as implemented in the GAUSSIAN 03 suite of programs [20]. The polarizability of the base molecule [97], which represents the deformability of the electronic charge distribution, is known to arise from the regions associated with the aromatic rings, lone pairs of nitrogen and oxygen atoms. Accordingly, the purine base G appears to have the largest value, whereas the pyrimidine base U has the smallest value among the five bases. The present calculations confirm this behavior.

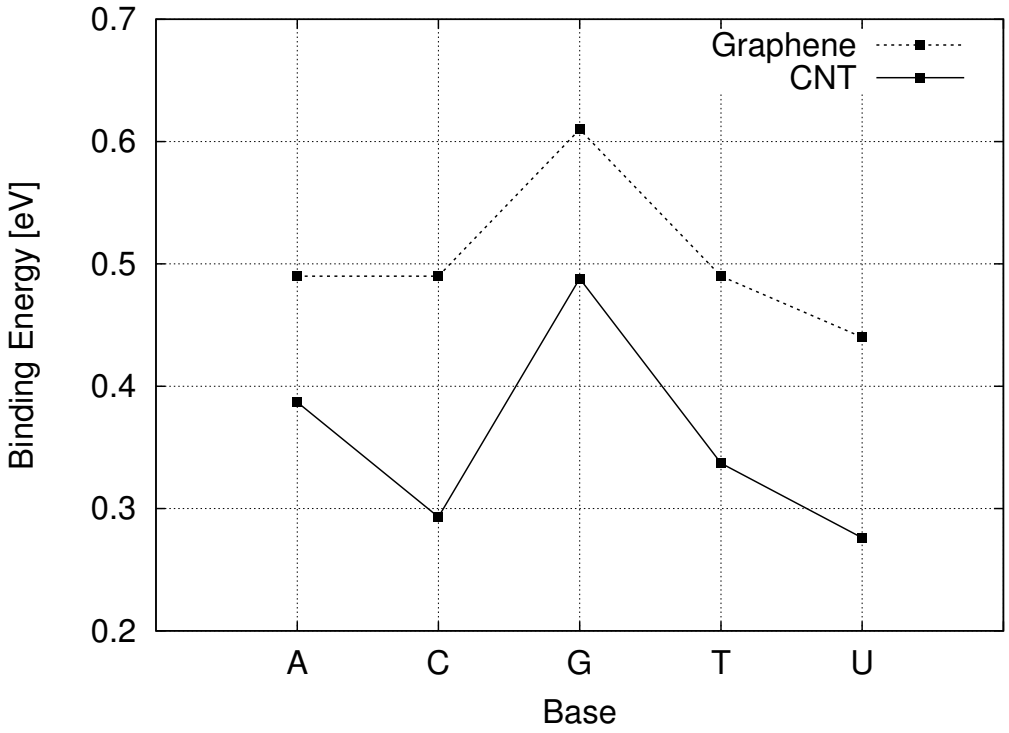

Figure 5.10: Comparison of binding energies of nucleic acid bases with graphene and CNT.

The binding energies and the molecular polarizabilities of the base molecules calcu-

lated using MP2 (Table 5.2) show a correlation. The polarizability of a nucleic acid base plays a key role in governing the strength of interaction with the CNT. This is an expected behavior for a system that draws its stabilization from vdW dispersion forces, since the vdW energy is proportional to the polarizabilities of the interacting entities. The observed correlation thus strongly suggests that vdW interaction is indeed the dominant source of attraction between the CNT and the nucleic acid bases.

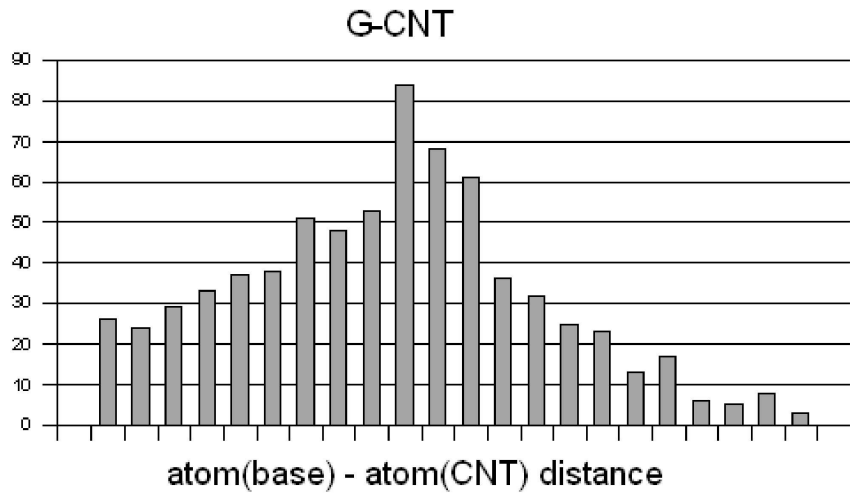

Figure 5.11: Distance distribution of atoms in guanine relative to carbon atoms in (top) CNT and (bottom) graphene.

Comparing these results with the ones obtained for graphene [98], one clearly notes (Table 5.2) that the binding energy of the base molecules is substantially reduced for physisorption on small-diameter CNTs with high curvature. While the curvature allows the nucleic acid base to approach the surface more closely, the majority of the carbon atoms in CNT are actually further removed from the atoms of the bases than

in the corresponding case on a graphene sheet (Fig. 5.11). Since the interaction is clearly dominated by vdW dispersion which falls off as $1/r^6$ with the distance r, the overall interaction is reduced for the case of CNT.

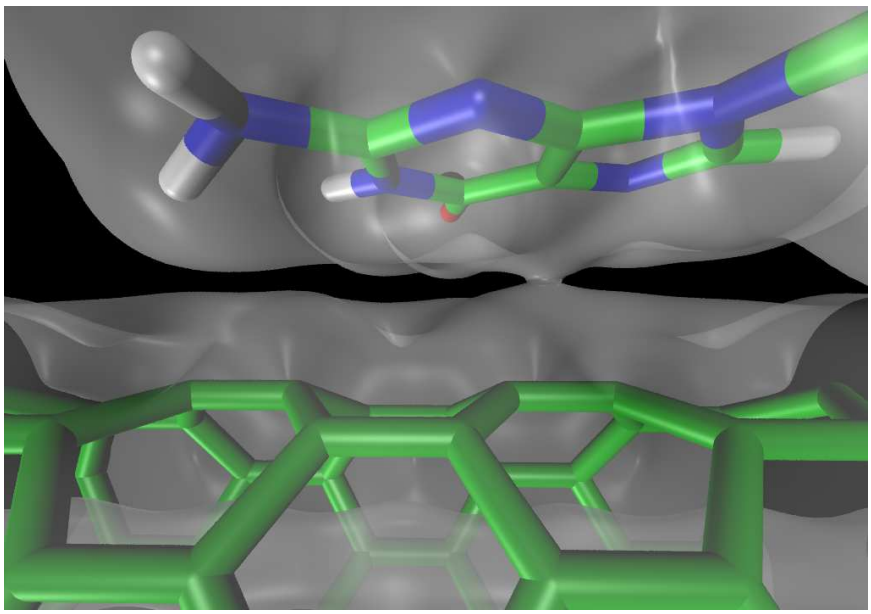

Figure 5.12: Charge density plot for guanine physisorbed on a (5,0) CNT. A small funnel is noticeably connecting the two entities near the C-C bond of guanine where the six- and five-membered rings join in the molecule.

The charge transfer between the bases and the CNT was investigated. For G, it was found from the Bader analysis that the CNT possesses an excess charge of $-0.08e$ and correspondingly a slight depletion of electrons on G by $+0.08e$. For A with CNT, $-0.05e$ were found to have been transferred from the nucleic acid base to the CNT. These results should be compared with the corresponding findings from the interaction of nucleic acid bases with a flat graphene sheet [98], where merely 0.02 e were transferred in the case of G. Thus, the higher curvature of the (5,0) CNT

leads to an increased electronegativity which manifests itself in the larger amount of charge transferred. The different behavior of G and A becomes understandable when one considers that G has a smaller ionization potential than A, and it is thus easier to remove an electron from G than from A. While there are no *whole elementary charges* transferred in this case, but only fractions, it still shows that the CNT is able to get more charge from G than from A. It appears that the charge transfer originates primarily from the C–C bond that joins the six- and five-membered ring (Fig. 5.12).

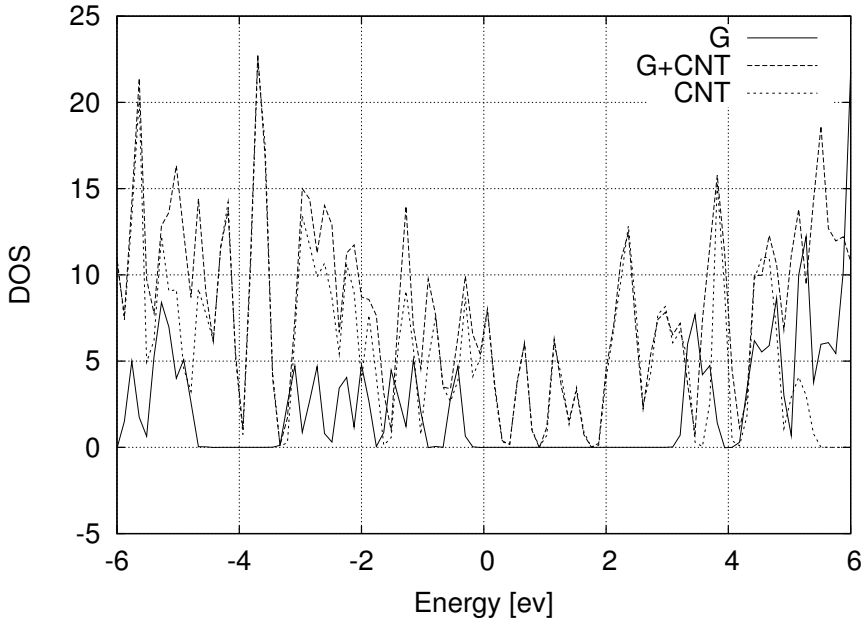

Figure 5.13: Density of States - of guanine, CNT and the combined system.

Finally, the density of states (DOS) for the combined system of base+CNT were analyzed and compared with the corresponding DOS for the individual parts, i.e., CNT and nucleic acid base separated (Fig. 5.13). The DOS of the combined system was found to be almost exactly the superposition of the DOS of the individual parts,

highlighting that the system is interacting rather weakly, and that no significant hybridization between the respective orbitals takes place. This finding is in agreement with a recent tight-binding study of DNA-wrapped CNTs [99].

5.4 Conclusions

From the results of *first-principles* studies on the physisorption of the five DNA/RNA nucleic acid bases on a planar sheet of graphene as well as with a (5,0) zigzag CNT of very high curvature, it can clearly noted that the nucleic acid bases exhibit significantly different interaction strengths when physisorbed on graphene. This finding represents an important step towards a better understanding of experimentally observed sequence-dependent interaction of DNA with CNTs [83, 84]. The calculated trend in the binding energies strongly suggests that the polarizability of the base molecules determines the interaction strength of the nucleic acid bases with graphene.

When comparing the results obtained here for physisorption on the small diameter CNT considered with those from the previous study on graphene [98], one can observe that the interaction strength of nucleic acid bases is smaller for the tube. Thus, these results show that the effect of introducing curvature is to reduce the binding energy. The binding energies for the two extreme cases of negligible curvature (flat graphene sheet) and of very high curvature [the (5,0) CNT studied here] may be considered as upper and lower bounds. Based on the results obtained up to this point, the hierarchy of the binding energies of the nucleic acid bases to the graphene-like surfaces of CNTs appears to be universally valid, as long as the interaction is dominated by van der Waals forces.

Chapter 6

Future Work

As can be seen from discussions in Chapter 2, 3 and 5, the results obtained from the calculations were based on a judicious approximations, choice of hamiltonian along with a combination of basis set and functional forms. This judicious choice was guided by an effort to optimize the quality of results utilizing the available computational resources. As better computational tools and resources become available with time, the accuracy of these results can be improved. Apart from these, following are some directions to extend the scope of projects entailed in this work:

† A systematic study of the structural, electronic and vibrational properties of other group III oxide clusters, In_xO_y being one such system.

† Expanding the current computing platform, enhancing the admin/user interface

for ease of use, understanding and modifying the computational codes to reduce inter nodal communication, adding hitherto unavailable features to codes.

† Study of interaction between the aforementioned biological molecules with carbon nanotubes of varying diameters and chiralities; study of single stranded DNA (four nucleic acid bases held together by sugar phosphate backbone) with such carbon nanotubes; a systematic study of interaction between carbon nanotubes and other biological molecules; study of interaction between these biological molecules with nanotubes made of other elements - Boron and Boron Nitride nanotubes being couple such cases.

List of Publications

† First-Principles Study of Physisorption of Nucleic Acid Bases on Small Diameter Carbon Nanotube

S. Gowtham, R. H. Scheicher, R. Ahuja, R. Pandey, S. P. Karna

Submitted to *Nanotechnology*; Manuscript under review

† Structures, Energetics, and Electronic and Hydration Properties of $Al_3O_{5+n}H^-_{2n}$ (n=0–4) and $Al_{3-x}Si_xO_{5+n}H^-_{2n-x}$ (x=2, 3; n=3, 4) Clusters

R. H. Scheicher, S. Gowtham, R. Pandey, G. S. Groenewold

Submitted for publication; Manuscript under review

† Physisorption of Nucleobases on Graphene: Density Functional Calculations

S. Gowtham, R. H. Scheicher, R. Ahuja, R. Pandey, S. P. Karna

Phys. Rev. **B**, **76**, 33401 (2007)

† Theoretical Study of Sequential Oxidation of Clusters of Gallium Oxide: Ga_3O_n (n: 4-8)

S. Gowtham, A. Costales, R. Pandey

Chem. Phys. Lett., **431**, 358 (2006)

† Geometry, Electronic Properties, and Thermodynamics of Pure and Al-doped Li Clusters

Mal-Soon Lee, S. Gowtham, H. He, K. C. Lau, L. Pan, D. G. Kanhere

Phys. Rev. **B**, *74*, 245412 (2006)

† Structural, Energetic, Electronic, Bonding, and Vibrational Properties of Ga_3O, Ga_3O_2, Ga_3O_3, Ga_2O_3, and GaO_3 Clusters

S. Gowtham, M. D. Deshpande, A. Costales, R. Pandey

J. Phys. Chem. **B**, **109**, 14836 (2005)

† Structure, Energetics, Electronic, and Hydration Properties of Neutral and Anionic Al_3O_6, Al_3O_7, and Al_3O_8 Clusters

S. Gowtham, K. C. Lau, M. D. Deshpande, R. Pandey, A. K. Gianotto, G. S. Groenewold

J. Phys. Chem. **A**, **108**, 5081 (2004)

† Theoretical Study of Neutral and Ionic States of Small Clusters of Ga_mO_n (m, n = 1, 2)

S. Gowtham, A. Costales, R. Pandey

J. Phys. Chem. B, **108**, 17295 (2004)

References

[1] Drexler, E. *Engines of Creation;* Anchor/Doubleday: New York, 1986.

[2] Drexler, E. *Nanosystems: Molecular Machinery, Manufacturing and Computation;* John Wiley: New York, 1992.

[3] http://wikipedia.org/.

[4] http://wikibooks.org/.

[5] Lau, K. C. PhD thesis, Michigan Technological University, **2007**.

[6] Schrödinger, E. *Ann. Phys. (Leipzig)* **1926**, *79*, 361.

[7] Born, M.; Oppenheimer, J. R. *Ann. Physik* **1927**, *84*, 457.

[8] Bohr, N. *Phil. Mag.* **1922**, *9*, 1.

[9] Hartree, D. R. *Proc. Cambridge Phil. Soc.* **1928**, *24*, 89.

[10] Pauli, W. *Phys. Rev.* **1940**, *58*, 716.

[11] Fock, V. *Z. Physik.* **1930**, *61*, 126.

[12] Hohenberg, P.; Kohn, W. *Phys. Rev. B* **1964**, *136*, B864.

[13] Kohn, W.; Sham, L. J. *Phys. Rev.* **1965**, *140*, A1133.

[14] Slater, J. C. *Phys. Rev.* **1930**, *35*, 210.

[15] Boys, S. F. *Proc. R. Soc. (London) A* **1950**, *200*, 542.

[16] Payne, M.; Teter, M.; Allan, D.; Arias, T.; Joannopoulos, J. *Reviews Of Modern Physics* **1992**, *64*, 1045.

[17] Ashcroft, N.; Mermin, N. *Solid State Physics;* Holt Saunders: Philadelphia, 1976.

[18] Szalewicz, K.; Cole, S. J.; Kolos, W.; Bartlett, R. J. *J. Chem. Phys.* **1988**, *89*, 3662.

[19] Frisch, M. J.; Trucks, G. W.; Schlegel, H. B.; Scuseria, G. E.; Robb, M. A.; Cheeseman, J. R.; Zakrzewski, V. G.; Montgomery, J. A.; Stratmann, R. E.; Burant, J. C.; Dapprich, S.; Millam, J. M.; Daniels, A. D.; Kudin, K. N.; Strain, M. C.; Farkas, O.; Tomasi, J.; Barone, V.; Cossi, M.; Cammi, R.; Mennucci, B.; Pomelli, C.; Adamo, C.; Clifford, S.; Ochterski, J.; Petersson, G. A.; Ayala, P. Y.; Cui, Q.; Morokuma, K.; Malick, D. K.; Rabuck, A. D.; Raghavachari, K.; Foresman, J. B.; Cioslowski, J.; Ortiz, J. V.; Stefanov, B. B.; Liu, G.; Liashenko, A.; Piskorz, P.; Komaromi, I.; Gomperts, R.; Martin, R. L.; Fox, D. J.; Keith, T.; Al-Laham, M. A.; Peng, C. Y.; Nanayakkara, A.; Gonzalez, C.; Challacombe,

M.; Gill, P. M. W.; Johnson, B. G.; Chen, W.; Wong, M. W.; Andres, J. L.; Head-Gordon, M.; Replogle, E. S.; Pople, J. A. *Gaussian 98;* 1998.

[20] Frisch, M. J.; Trucks, G. W.; Schlegel, H. B.; Scuseria, G. E.; Robb, M. A.; Cheeseman, J. R.; Montgomery, Jr., J. A.; Vreven, T.; Kudin, K. N.; Burant, J. C.; Millam, J. M.; Iyengar, S. S.; Tomasi, J.; Barone, V.; Mennucci, B.; Cossi, M.; Scalmani, G.; Rega, N.; Petersson, G. A.; Nakatsuji, H.; Hada, M.; Ehara, M.; Toyota, K.; Fukuda, R.; Hasegawa, J.; Ishida, M.; Nakajima, T.; Honda, Y.; Kitao, O.; Nakai, H.; Klene, M.; Li, X.; Knox, J. E.; Hratchian, H. P.; Cross, J. B.; Bakken, V.; Adamo, C.; Jaramillo, J.; Gomperts, R.; Stratmann, R. E.; Yazyev, O.; Austin, A. J.; Cammi, R.; Pomelli, C.; Ochterski, J. W.; Ayala, P. Y.; Morokuma, K.; Voth, G. A.; Salvador, P.; Dannenberg, J. J.; Zakrzewski, V. G.; Dapprich, S.; Daniels, A. D.; Strain, M. C.; Farkas, O.; Malick, D. K.; Rabuck, A. D.; Raghavachari, K.; Foresman, J. B.; Ortiz, J. V.; Cui, Q.; Baboul, A. G.; Clifford, S.; Cioslowski, J.; Stefanov, B. B.; Liu, G.; Liashenko, A.; Piskorz, P.; Komaromi, I.; Martin, R. L.; Fox, D. J.; Keith, T.; Al-Laham, M. A.; Peng, C. Y.; Nanayakkara, A.; Challacombe, M.; Gill, P. M. W.; Johnson, B.; Chen, W.; Wong, M. W.; Gonzalez, C.; Pople, J. A. *Gaussian 03, Revision C.02.*

[21] Kresse, G. PhD thesis, Technische Universität Wien, **1993**.

[22] Kresse, G.; Hafner, J. *Phys. Rev. B* **1993**, *47*, RC558.

[23] Kresse, G.; Furthmüller, J. *Comput. Mater. Sci.* **1996**, *6*, 15.

[24] Kresse, G.; Furthmüller, J. *Phys. Rev. B* **1996**, *54*, 11169.

[25] Vanderbilt, D. *Phys. Rev. B* **1990**, *41*, 7892.

[26] Kresse, G.; Hafner, J. *J. Phys.: Condensed Matter 6*, 8245.

[27] Haberland, H., Ed. *Clusters of Atoms and Molecules I;* Springer-Verlag: Berlin, 1994.

[28] Kandalam, A. PhD thesis, Michigan Technological University, **2002**.

[29] Dietz, T. G.; Duncan, M. A.; Powers, D. E.; Smalley, R. E. *J. Chem. Phys.* **1981**, *74*, 6511.

[30] Zhang, H. Z.; Kong, Y. C.; Wang, Y. Z.; Du, Z.; Bai, Z. G.; Wang, J. J.; Yu, D. P.; Ding, Y.; Hang, Q. L.; Feng, S. Q. *Solid State Commun.* **1999**, *109*, 677.

[31] Choi, Y. C.; Kim, W. S.; Park, Y. S.; Lee, S. M.; Bae, D. J.; Lee, Y. H.; Park, G. S.; Choi, W. B.; Lee, N. S.; Kun, J. M. *Adv. Mater.* **2000**, *12*, 746.

[32] Park, G. S.; Choi, W. B.; Kim, J. M.; Choi, Y. C.; Lee, Y. H.; Lim, C. B. *J. Cryst. Growth* **2000**, *220*, 494.

[33] Sharma, S.; Sunkara, M. K. *J. Amer. Chem. Soc.* **2002**, *124*, 12288.

[34] Huber, K. P.; Herzberg, G. *Constants of Diatomic Molecules;* Van Nostrand: New York, 1979.

[35] Zehe, M. J.; Lynch, D. A. J.; Kelsall, B. J.; Carlson, K. D. *J. Phys. Chem.* **1979**, *83*, 656.

[36] Cabot, P. L.; Illas, F.; Ricart, J. M.; Rubio, J. *J. Phys. Chem.* **1986**, *90*, 33.

[37] Burkholder, T. R.; Yustein, J. T.; Andrews, L. *J. Phys. Chem.* **1992**, *96*, 10189.

[38] Rambidi, N. G.; Tolmachev, S. M. *Teplofiz. Vys. Temp.* **1965**, *3*, 487.

[39] Rambidi, N. G.; Ezhov, Y. S. *Zh. Strukt. Khim.* **1968**, *9*, 363.

[40] Malt́sev, A. A.; Shevelḱov, V. F. *Teplofiz. Vys. Temp.* **1964**, *2*, 650.

[41] Hinchcliffe, A. J.; Ogden, J. S. *Chem. Commun.* **1969**, page 1033.

[42] Makowiecki, D. M.; Lynch, D. A. J.; Carlson, K. D. *J. Phys. Chem.* **1971**, *75*, 1963.

[43] Hinchcliffe, A. J.; Ogden, J. S. *J. Phys. Chem.* **1971**, *75*, 3908.

[44] Hinchcliffe, A. J.; Ogden, J. S. *J. Phys. Chem.* **1973**, *77*, 2537.

[45] Cai, M.; Canter, C. C.; Miller, T. A.; Bondybey, V. E. *J. Chem. Phys.* **1991**, *95*, 73.

[46] Leszcźynski, J.; Kwiatkowski, K. S. *J. Phys. Chem.* **1992**, *96*, 4148.

[47] Becke, A. D. *J. Chem. Phys.* **1993**, *98*, 5468.

[48] Lee, C.; Yang, W.; Parr, R. G. *Phys. Rev. B* **1988**, *37*, 375.

[49] Bader, R. F. W. *Atoms in Molecules;* Oxford University Press: Oxford, 1990.

[50] Keith, T. A.; Laidig, K. E.; Krug, P.; Cheeseman, J. R.; Bone, R. G. A.; Biegler-König, F. W.; Duke, J. A.; Tang, T.; Bader, R. F. W. *The* AIMPAC95 *programs;* 1995.

[51] Jones, R.; Öberg, S. *Phys. Rev. Lett.* **1992**, *69*, 136.

[52] Nemukhin, A. V.; Weinhold, F. *J. Chem. Phys.* **1992**, *97*, 3420.

[53] Masip, J.; Clotet, A.; Ricat, J. M.; Illas, F.; Rubio, J. *Chem. Phys. Lett.* **1998**, *144*, 373.

[54] Bencivenni, L.; Pelino, M.; Ramondo, F. *J. Mol. Struct. (Theochem)* **1992**, *253*, 109.

[55] Zaitsevskii, A. V.; Serebrennikov, G. V. C.; Stepanov, N. F. *J. Mol. Struct. (Theochem)* **1993**, *280*, 291.

[56] Archibong, E. F.; Sullivan, R. *J. Phys. Chem.* **1995**, *99*, 15830.

[57] Costales, A.; Blanco, M. A.; Martín Pendás, A.; Mori-Sánchez, P.; Luaña, V. *J. Phys. Chem. A* **2004**, *108*, 2794.

[58] Cassam-Chenai, P.; Jayatilaka, D. *Theo. Chim. Acta.* **2001**, *105*, 213.

[59] Rienstra-Kiracofe, J. C.; Tschumper, G. S.; Schaefer III, H. F. *Chem. Rev.* **2002**, *102*, 231.

[60] Desai, S. R.; Wu, H.; Rohlfing, C. M.; Wang, L. *J. Chem. Phys.* **1997**, *106*, 1309.

[61] Wu, H.; Li, X.; Wang, X. B.; Ding, C. F.; Wang, L. S. *J. Chem. Phys.* **1998**, *109*, 449.

[62] Ghanty, T. K.; Davidson, E. R. *J. Phys. Chem. A* **1999**, *103*, 2867.

[63] Martínez, A.; Tenorio, F.; Ortiz, J. V. *J. Phys. Chem. A* **2001**, *105*, 8787.

[64] Martínez, A.; Sansores, L. E.; Salcedo, R.; Tenorio, F.; Ortiz, J. V. *J. Phys. Chem. A* **2002**, *106*, 10630.

[65] Zhao, Y.; Xu, W.; Li, Q.; Xie, Y.; Schaefer III, H. F. *J. Phys. Chem. A* **2004**, *108*, 7448.

[66] Pearson, R. G. *Chemical Hardness;* Wiley-VCH Verlag: Germany, 1997.

[67] Gowtham, S.; Lau, K. C.; Deshpande, M. D.; Pandey, R.; Gionotto, A. K.; Groenewold, G. S. *J. Phys. Chem. A* **2004**, *108*, 5081.

[68] Martinez, A.; Tenorio, F. J.; Ortiz, J. V. *J. Phys. Chem. A* **2003**, *107*, 2589.

[69] Gowtham, S.; Deshpande, M. D.; Costales, A.; Pandey, R. *J. Phys. Chem. B* **2005**, *109*, 14836.

[70] Papadopoulos, P. M.; Katz, M. J.; Bruno, G. *IEEE Cluster* **2001**.

[71] Saunders, V.; Dovesi, R.; Roetti, C.; Orlando, R.; Zicovich-Wilson, C.; Harrison,

N.; Doll, K.; Civalleri, B.; Bush, I.; D'Arco, P.; Llunell, M. *CRYSTAL 03 User's Manual;* 2003.

[72] *DMol User Guide;* Molecular Simulations and Inc., 1995.

[73] Soler, J. M.; Artacho, E.; Gale, J. D.; Garcia, A.; Junquera, J.; Ordejón, P.; Sánchez-Portal, D. *J. Phys. Condens. Matter* **2002**, *14*, 2745.

[74] Rocha, A. R.; Garcia-Suarez, V.; Bailey, S. W.; Lambert, C. J.; Ferrer, J.; Sanvito, S. *Nat. Mater.* **2005**, *4*, 335.

[75] Rocha, A. R.; Garcia-Suarez, V.; Bailey, S. W.; Lambert, C. J.; Ferrer, J.; Sanvito, S. *Phys. Rev. B* **2006**, *73*, 085414.

[76] Rocha, A. R. *Theoretical and Computational Aspects of Electronic Transport at the Nanoscale;* 2007.

[77] Gowtham, S. *Design, Development & Maintenance of a Parallel Computational Facililty - Administrator's Guide;* 2007.

[78] Watson, J. D.; Crick, F. H. C. *Nature* **1953**, *171*, 737.

[79] Stent, G. S. *The Double Helix;* W. W. Norton & Co.: New York, 1980.

[80] Clark, D. P.; Russel, L. D. *Molecular Biology - Made Simple and Fun;* Cache River Press: St. Louis, 2005.

[81] Nakashima, N.; Okuzono, S.; Murakami, H.; Nakai, T.; Yoshikawa, K. *Chem. Lett.* **2003**, *32*, 456.

[82] Zheng, M.; Jagota, A.; Semke, E. D.; Diner, B. A.; Mclean, R. S.; Lustig, S. R.; Richardson, R. E.; Tassi, N. G. *Nature Mater.* **2003**, *2*, 338.

[83] Zheng, M.; Jagota, A.; Strano, M. S.; Santos, A. P.; Barone, P.; Chou, S. G.; Diner, B. A.; Dresselhaus, M. S.; Mclean, R. S.; Onoa, G. B.; Samsonidze, G. G.; Semke, E. D.; Usrey, M.; Walls, D. J. *Science* **2003**, *302*, 1545.

[84] Staii, C.; Johnson, A. T.; Chen, M.; Gelperin, A. *Nano Lett.* **2005**, *5*, 1774.

[85] Heller, D. A.; Jeng, E. S.; Yeung, T. K.; Martinez, B. M.; Moll, A. E.; Gastala, J. B.; Strano, M. S. *Science* **2006**, *311*, 508.

[86] Perdew, J. P.; Zunger, A. *Phys. Rev. B* **1981**, *23*, 5048.

[87] Perdew, J. P.; Chevary, J. A.; Vosko, S. H.; Jackson, K. A.; Pederson, M. R.; Singh, D. J.; Fiolhais, C. *Phys. Rev. B* **1992**, *46*, 6671.

[88] Simeoni, M.; Luca, C. D.; Picozzi, S.; Santucci, S.; Delley, B. *J. Chem. Phys.* **2005**, *122*, 214710.

[89] Tournus, F.; Latil, S.; Heggie, M. I.; Charlier, J. C. *Phys. Rev. B* **2005**, *72*, 075431.

[90] Ortmann, F.; Schmidt, W. G.; Bechstedt, F. *Phys. Rev. Lett.* **2005**, *95*, 186101.

[91] London, F. *Z. Phys.* **1930**, *63*, 245.

[92] Monkhorst, H. J.; Pack, J. D. *Phys. Rev. B* **1976**, *13*, 5188.

[93] Shibayama, Y.; Sato, H.; Enoki, T.; Endo, M. *Phys. Rev. Lett.* **2000**, *84*, 1744.

[94] Harigaya, K.; Enoki, T. *Chem. Phys. Lett.* **2002**, *351*, 128.

[95] Klein, C.; Jr., C. S. H. *Manual of Mineralogy* **1985**.

[96] Watson, J. D.; Baker, T. A.; Bell, S. P.; Gann, A.; Levine, M.; Losick, R. *Molecular Biology of the Gene. 5th ed* **2004**.

[97] Seela, F.; Jawalekar, A. M.; Münster, I. *Helevetica Chimica Acta* **2005**, *88*, 751.

[98] Gowtham, S.; Scheicher, R. H.; Ahuja, R.; Pandey, R.; Karna, S. P. *Phys. Rev. B* **2007**, *76*, 033401.

[99] Enyashin, A. N.; Gemming, S.; Seifert, G. *Nanotechnology* **2007**, *18*, 245702.

Index